TECNOLOGIA BARREIRO
ESCOLA SUPERIOR
POLITÉCNICO SETÚBAL

IGOR BENTO PEDRA

RESIDUAL BIOMASS BIOCHAR FOR EFFECTIVE WASTEWATER TREATMENT OF TEXTILE DYE POLLUTANTS

Thesis to obtain the Master's Degree in
Biological and Chemical Engineering

SUPERVISORS

Doctor Maria de Lurdes de Figueiredo Gameiro

Doctor Ana Paula Vieira Soares Pereira Dias

September 2024

IGOR BENTO PEDRA

RESIDUAL BIOMASS BIOCHAR FOR EFFECTIVE WASTEWATER TREATMENT OF TEXTILE DYE POLLUTANTS

BOARD OF EXAMINERS

Chairperson: Doctor Ana Cláudia Cavaco de Sousa Coelho, Escola Superior de Tecnologia do Barreiro, Instituto Politécnico de Setúbal

Supervisor: Doctor Ana Paula Vieira Soares Pereira Dias, Instituto Superior Técnico, Universidade de Lisboa

Member of the Board: Doctor Bruna Alexandra Canuto Rijo, Instituto Politécnico de Portalegre

September 2024

Agradecimentos

Em primeiro lugar, gostaria de expressar o meu sincero agradecimento à Tinamar pela generosa colaboração, ao disponibilizar os seus corantes industriais, para a investigação conduzida para a minha tese de mestrado.

Gostaria de expressar uma profunda gratidão à minha supervisora, a Prof.ª Dr.ª Ana Paula Soares Dias, por toda a orientação, paciência e incentivo ao longo de todo o processo de desenvolvimento desta tese, bem como de toda a disponibilidade e ajuda, que demonstrou desde o primeiro dia no seu laboratório. Os seus conselhos foram fundamentais para a conclusão deste trabalho. É uma referência a nível profissional que nunca irei esquecer.

À Prof.ª Dr.ª Maria de Lurdes Gameiro gostaria de agradecer pela sua simpatia, ajuda, e orientação não só ao longo da elaboração deste trabalho, mas sim, ao longo de todo o curso. A sua ética de trabalho e maneira de ser fizeram com que tivesse sido um gosto frequentar as suas aulas; bem como ter reunido para discutir assuntos relacionados com a tese. De todos os anos de ensino que frequentei foi sem dúvida alguma a Professora por quem mais apreço tenho. São pessoas como a Prof.ª Lurdes que fazem a diferença no ensino.

Aos meus pais, e à minha avó Albertina, agradeço profundamente por todo o apoio, compreensão, motivação ao longo de todos estes anos, sem eles a conclusão desta etapa da minha vida não teria sido possível, sendo que dessa forma estarei eternamente grato, poderia ter tido melhor apoio da minha família. Com um especial agradecimento para a minha avó e mãe por tudo!

À minha melhor amiga e namorada, gostaria de expressar o meu maior agradecimento, por me motivar, diariamente, especialmente nos momentos mais difíceis. Foi, é, e será o meu maior pilar, tendo dessa forma sido essencial ao longo do meu percurso académico, sendo que em parte, o meu sucesso a nível académico também a ela se deve. Foi um prazer ter partilhado este percurso com ela, bem como um crescimento a nível pessoal e profissional.

Ao grande amigo que esta instituição me deu, Pedro agradeço por tudo, desde a sua boa disposição, diária, aos seus conselhos, ajuda e paciência. É de facto alguém que tornou o ambiente académico leve, proporcionando momentos de boa disposição constantes, que fizeram com que o tempo “voasse”.

Agradeço também a todos os colegas de laboratório, mais especificamente ao Pedro, ao Francisco, à Nawik, ao Tiago, e à Joana por toda a ajuda, simpatia, motivação, e conselhos que foram fundamentais para a realização do meu trabalho no laboratório.

Por fim, agradeço a todos que, de alguma forma, contribuíram para a realização deste trabalho e tornaram este caminho mais agradável e possível.

Resumo

A necessidade de desenvolver métodos sustentáveis e de baixo custo para o tratamento de águas residuais, particularmente na indústria têxtil, que é um dos principais contribuintes para a poluição da água, é de extrema relevância, visto que os métodos tradicionais para remover corantes dos efluentes apresentam, frequentemente, um elevado custo, produzem poluentes secundários e apresentam uma menor eficácia. Assim, os biocarvões oferecem uma alternativa promissora devido à abundância de matérias-primas disponíveis, ao seu baixo custo, e ao potencial de serem ajustados em função da aplicação pretendida. Dessa forma, foram desenvolvidas diferentes amostras de biocarvões, derivadas de diferentes resíduos agrícolas, como cascas de arroz, folhas de abacate, cascas de amendoim, e misturas de macroalgas. As amostras de biocarvões foram produzidas através de pirólise a 350°C, sendo que a caracterização dessas amostras envolveu técnicas avançadas, como a Difração de Raios X (XRD), Espectroscopia Raman e Análise Termogravimétrica (TGA). Essas análises revelaram informações sobre a morfologia, grupos funcionais na superfície e estabilidade térmica dos biocarvões, fatores cruciais que determinam a eficácia de cada amostra, como adsorventes. Entre as amostras produzidas, o biocarvão de casca de arroz (BRH) foi o que apresentou um desempenho superior no que toca à remoção de corantes, alcançando uma capacidade de remoção de 99,2% para o corante Bezaktiv Blue HP-R, 81,4% para o Bezaktiv Red HP-R e 76,4% para o Bezaktiv Yellow HP-R. Para as misturas de corantes, o BRH removeu 94,8% da mistura de corante verde e 100% da mistura de corante roxo. O biocarvão de folhas de abacate (BAL) também demonstrou uma elevada capacidade, especialmente na remoção de Bezaktiv Blue HP-R (94,8%) e Red HP-R (83,6%). O biocarvão de casca de amendoim (BPS) apresentou desempenho variável, com a maior eficiência para Bezaktiv Yellow HP-R (94%), mas com resultados inferiores para outros corantes. Já o biocarvão de mistura de macroalgas (BMM) apresentou a menor capacidade de remoção, particularmente para o corante Bezaktiv Yellow HP-R (58,2%) e o Bezaktiv Red HP-R (69,1%). O bom desempenho do biocarvão derivado de cascas de arroz (BRH), e do proveniente de folhas de abacate (BAL), pode estar relacionado com a sua área de superfície, e com as interações que essas superfícies promovem. A amostra BRH, com um alto teor de sílica e uma estrutura microporosa bem desenvolvida, oferece uma elevada área de superfície e volume de poros, proporcionando dessa forma a capacidade de adsorver moléculas de corantes, por intermédio de mecanismos como o preenchimento de poros, ou através de interações eletrostáticas. A amostra BAL, por outro lado, é rica em grupos funcionais fenólicos e álcoois, que contribuem para fortes interações de ligação de hidrogénio e interações π-π com as moléculas dos corantes. Esses grupos funcionais, juntamente com as estruturas aromáticas presentes no BAL, facilitam a formação de complexos estáveis com os corantes, resultando em alta eficiência de adsorção.

Palavras-chave: Biocarvão; Adsorção; Tratamento de águas residuais; Corantes reativos; Sustentabilidade.

Abstract

The study is motivated by the urgent need for sustainable and cost-effective methods for wastewater treatment, particularly in the textile industry, which is a major contributor to water pollution. Traditional methods for removing dyes from effluents are often costly, generate secondary pollutants, and are less effective. Thus, biochar offers a promising alternative due to its abundant raw materials, cost-effectiveness, and potential to be tailored for specific applications. For that reason, distinct biochar samples were developed, derived from various agricultural wastes—namely rice husk, avocado leaves, peanut shells, and mixed macroalgae—as efficient sorbents for removing reactive dyes from wastewater. Biochar samples were produced via pyrolysis at 350°C, a process known to influence the physicochemical properties of the resulting material. The characterization of these biochars involved advanced techniques such as X-ray Diffraction (XRD), Raman Spectroscopy, and Thermogravimetric Analysis (TGA). These analyses revealed critical insights into the morphology, elemental composition, surface functional groups, and thermal stability of the biochars, which are crucial factors determining their effectiveness as adsorbents. Among the biochar samples, rice husk biochar (BRH) exhibited superior performance in dye removal, achieving removal efficiencies of 99.2% for Bezaktiv Blue HP-R, 81.4% for Bezaktiv Red HP-R, and 76.4% for Bezaktiv Yellow HP-R. For mixed dyes, BRH removed 94.8% of the Green dye mixture and 100% of the Purple dye mixture. Avocado leaves biochar (BAL) also demonstrated high efficiency, particularly in removing Bezaktiv Blue HP-R (94.8%) and Red HP-R (83.6%). Peanut shell biochar (BPS) showed a varied performance, with the highest efficiency for Bezaktiv Yellow HP-R (94%) but lower results for other dyes. Mixed macroalgae biochar (BMM) consistently displayed the lowest removal efficiency, particularly for Bezaktiv Yellow HP-R (58.2%) and Bezaktiv Red HP-R (69.1%). The superior adsorption performance of biochar derived from rice husk (BRH) and avocado leaves (BAL) can be attributed to their distinct surface properties and the specific interactions these surfaces promote. BRH, with its high silica content and well-developed microporous structure, provides extensive surface area and pore volume, enhancing its ability to adsorb dye molecules through mechanisms such as pore-filling and electrostatic interactions. Additionally, the alkaline nature of BRH due to its ash content likely increases the adsorption of anionic dyes by enhancing electrostatic attraction. BAL, on the other hand, is rich in phenolic and alcoholic functional groups, which contribute to strong hydrogen bonding and π-π interactions with the dye molecules. These functional groups, along with the aromatic structures present in BAL, facilitate the formation of stable complexes with dyes, leading to high adsorption efficiency.

Keywords: Biochar; Adsorption; Wastewater treatment; Reactive Dyes; Sustainability.

Table of contents

List of Figures

List of Tables

List of Abbreviations

- **AOP** - Advanced Oxidation Processes
- **ASC** - Aamla Seed Carbon
- **ATR** - Attenuated Total Reflectance
- **BAL** - Biochar derived from Avocado Leaves
- **BMM** - Biochar derived from Mixed Macroalgae
- **BPS** - Biochar derived from Peanut Shells
- **BRH** - Biochar derived from Rice Husk
- **CEC** - Cation exchange capacity
- **EDS** - Energy Dispersive X-ray Spectroscopy
- **EF** – Efficient
- **FLP** – Flash Pyrolysis
- **FP** – Fast Pyrolysis
- **FTIR** - Fourier Transform Infrared Spectroscopy
- **HC** – High cost
- **HT** – Heating time
- **HTT** - Highest treatment temperature
- **HYC** – Hydrothermal Carbonization
- **IDC** - Initial dye concentration
- **INSO** - Insoluble
- **MF** – Microfiltration
- **NIR** – Near infra-red
- **NF** – Nanofiltration
- **PRC** – Pyrolysis reaction time
- **PS** - Particle size
- **RBDS** – Reactive Blue Dye Solution
- **RD** – Reactive Dye
- **RDS** - Reactive Dye Solutions
- **RO** - Reverse Osmosis
- **RRDS** – Reactive Red Dye Solution
- **RYDS** – Reactive Yellow Dye Solution
- **SA** – Surface area
- **SEM** - Scanning Electron Microscopy
- **SNC** - Soapnut Carbon
- **SOL** – Soluble
- **SP** – Slow Pyrolysis
- **TGA** - Thermogravimetric Analysis
- **TSC** - Tamarind Seed Carbon
- **UF** - Ultrafiltration
- **UV** - Ultraviolet
- **XRD** - X-ray Diffraction

1. Introduction

1.1. Scope and motivation

The increasing awareness of environmental pollution has led to a growing interest in the development of sustainable and eco-friendly technologies for wastewater treatment [1]. One of the major contributors to water pollution is the textile industry, as illustrated in Figure 1, which generates massive quantities of dye-containing effluents, that consequently can cause significant environmental and health hazards if not properly treated [2]. For that reason, there has been a drastic upsurge in the number of research articles published on dye adsorption, as shown in Figure 2.

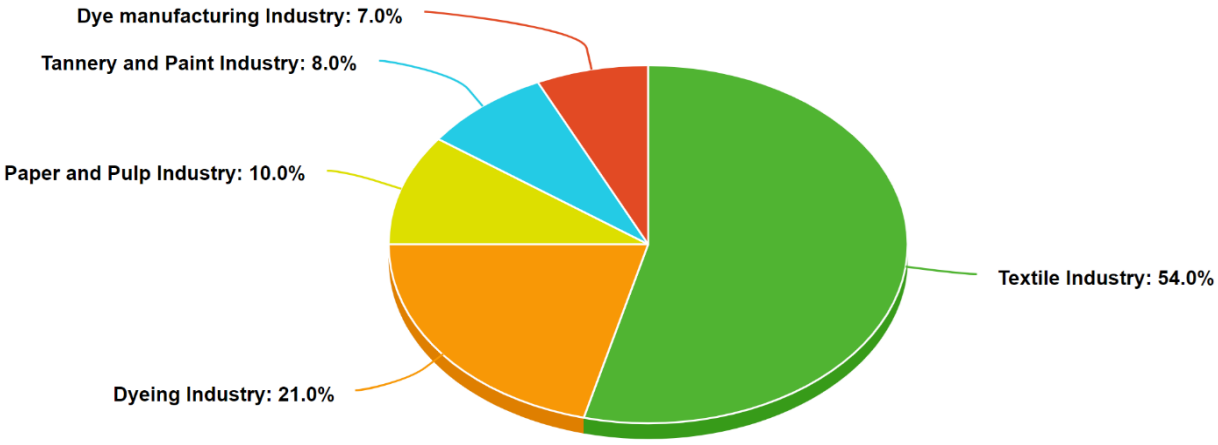

Figure 1 - Major contributors to the water pollution by industries (adapted from [2])

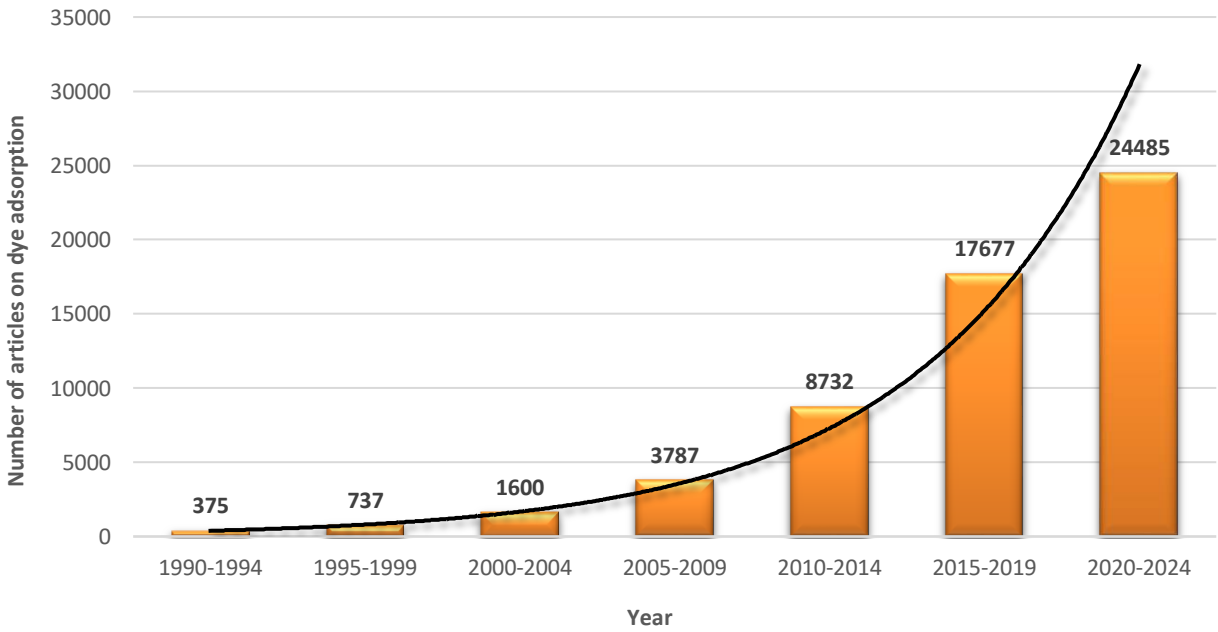

Figure 2 - Trend in the number of published papers on dye adsorption over the past three decades (adapted from [3])

Conventional methods for the remotion of pollutants such as dyes from wastewater effluents can range from membrane technologies, and electrochemical processes, to biological treatments and reactions, however, these have several limitations, including high operational and maintenance costs, the production of a toxic sludge, and limited efficiency [4,5,6].

In recent years, biochar-based sorbents have emerged as a promising alternative for dye removal from wastewater effluents [7]. Moreover, the use of residual feedstocks as precursors for biochar production offers a sustainable and cost-effective solution for wastewater treatment [7].

The purpose of this study is to investigate the development of biochar-based sorbents from residual feedstocks like rice husks, avocado leaves, and peanut shells for the removal of dyes from wastewater effluents. The motivation behind this research is to provide a sustainable and eco-friendly alternative solution for the adsorption of dye contamination, to help reduce the environmental impact of wastewater effluents while also promoting the valorization of agricultural waste.

The disposal of wastewater effluents, contaminated with dyes, into natural water presents an adverse effect on the photosynthetic activity in aquatic ecosystems and consequently can produce negative effects on aquatic organisms due to the existence of toxic materials, such as metals, while also presenting toxic effects on human health (e.g., carcinogenic, and allergic effect) [8,9,10,11]. Figure 3 demonstrates the distinct routes for environmental pollution, caused by a vast variety of dyes while enhancing the different industries that contribute to this contamination.

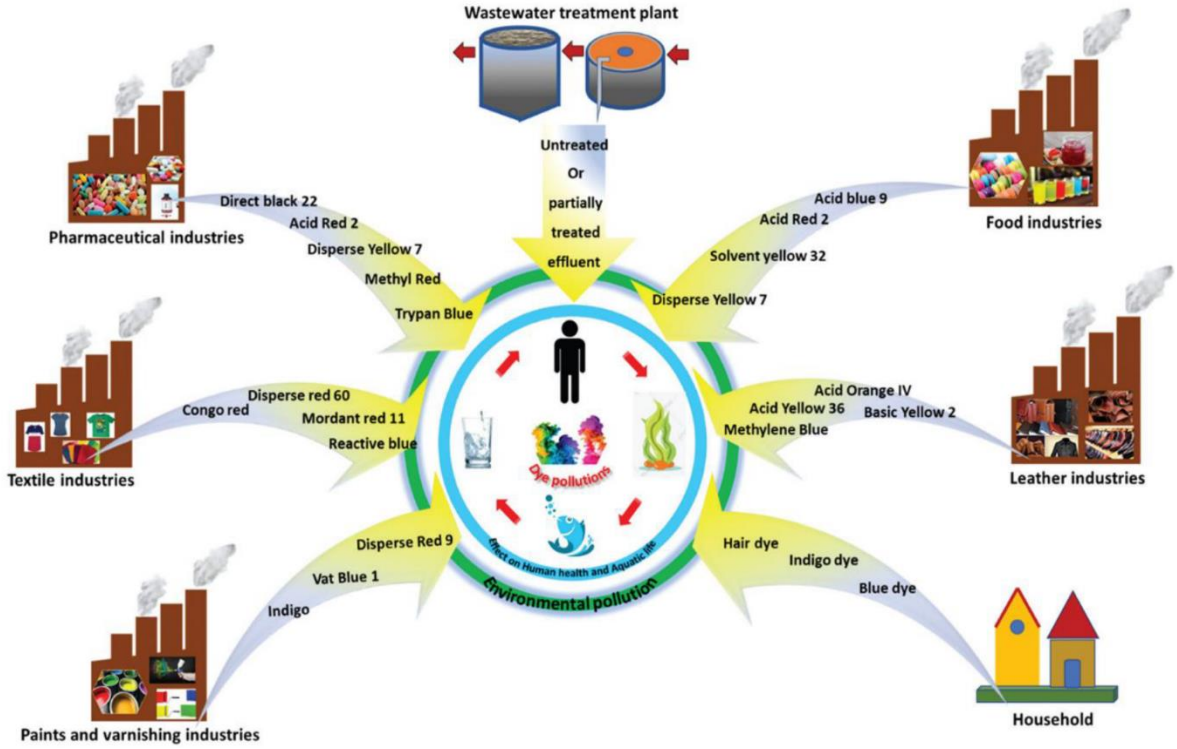

Figure 3 - Main sources of contamination by dye type (adapted from [8])

2. State of the art

2.1. Life cycle analysis of Biochar

2.1.1. Biochar definition and feedstocks

Biochar is a term derived from carbonaceous materials, which can have multiple applications such as for the production of sustainable fuels, soil remediation, and carbon sequestration. In other terms, biochar is defined as charcoal and a carbon-rich material produced by partial oxidation of carbonaceous organic sources from a diverse range of biomass feedstocks, excluding fossil fuel products [12,13,14].

The source of biomass can play a significant role in the physical and chemical properties of biochar products produced from it, which can be classified into lignocellulosic and non-lignocellulosic biomass based on cellulose and lignin contents [15]. A lignocellulosic biomass is mainly composed of cellulose, hemicellulose, and lignin [16]. Figure 4 illustrates a representative scheme of a lignocellulosic biomass structure. These three components are characterized as polymeric molecules that contain covalently bonded monomers with a biological origin, in other words also known as biopolymers; Lignin; Hemicellulose; and Cellulose can present different composition percentages according to the source of the biomass, but the ordinary percent of each one on a biomass structure corresponds to lignin (10-25%); hemicellulose (20-35%); and cellulose (35-50%) [17,18].

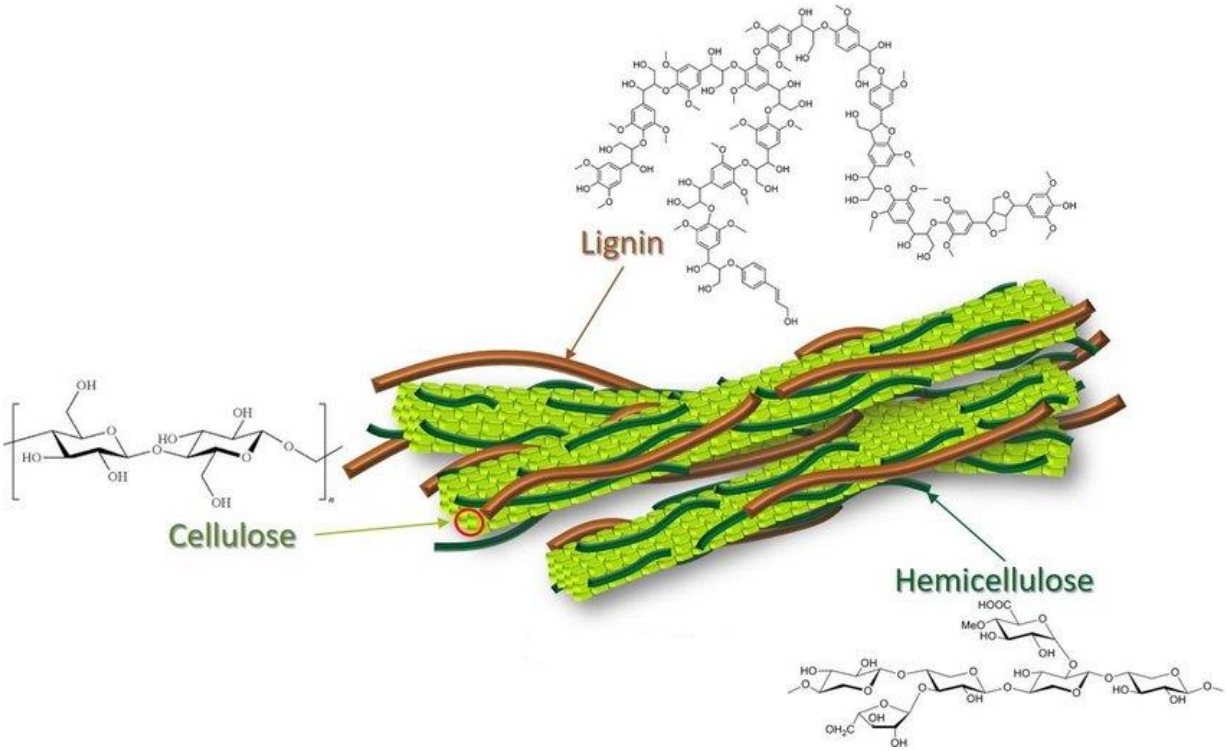

Figure 4 - Biopolymers, cellulose, hemicellulose and lignin, of woody biomass (adapted from [19])

Lignin acts as a binder around and in between the other biomass components, to provide structure to the biomass, and many other characteristics, such as compressive strength; resistance; and water resistance [17]. To enable access to the core components of the lignocellulosic biomass, a hydrolysis process is needed, that will be responsible for the degradation of the lignocellulose material, involving the depolymerization of cellulose and hemicellulose into monomeric sugars, such as glucose; mannose; xylose; arabinose; and also, galacturonic acid, that can be used as an acidifying agent for the food industry [20,21].

The non-lignocellulosic biomass is composed of lipids, proteins, carbohydrates, heavy metals, minerals, and heteroatoms [22]. The source of this type of biomass can assume a broad range of options, like manure; sewage sludge; bone and meat from dead animals; feathers; and algae [22]. From an overall perspective, there is a huge variety of residual biomass feedstocks, that can range from an agricultural waste perspective, which includes crop residues and process residues, to a food waste point of view, with an extent of options like fruit and vegetable peels and roots, to residues from poultry and slaughterhouses such as feathers; eggshells; and meat or bones [23]. Figure 5 displays some of the options of feedstocks previously cited.

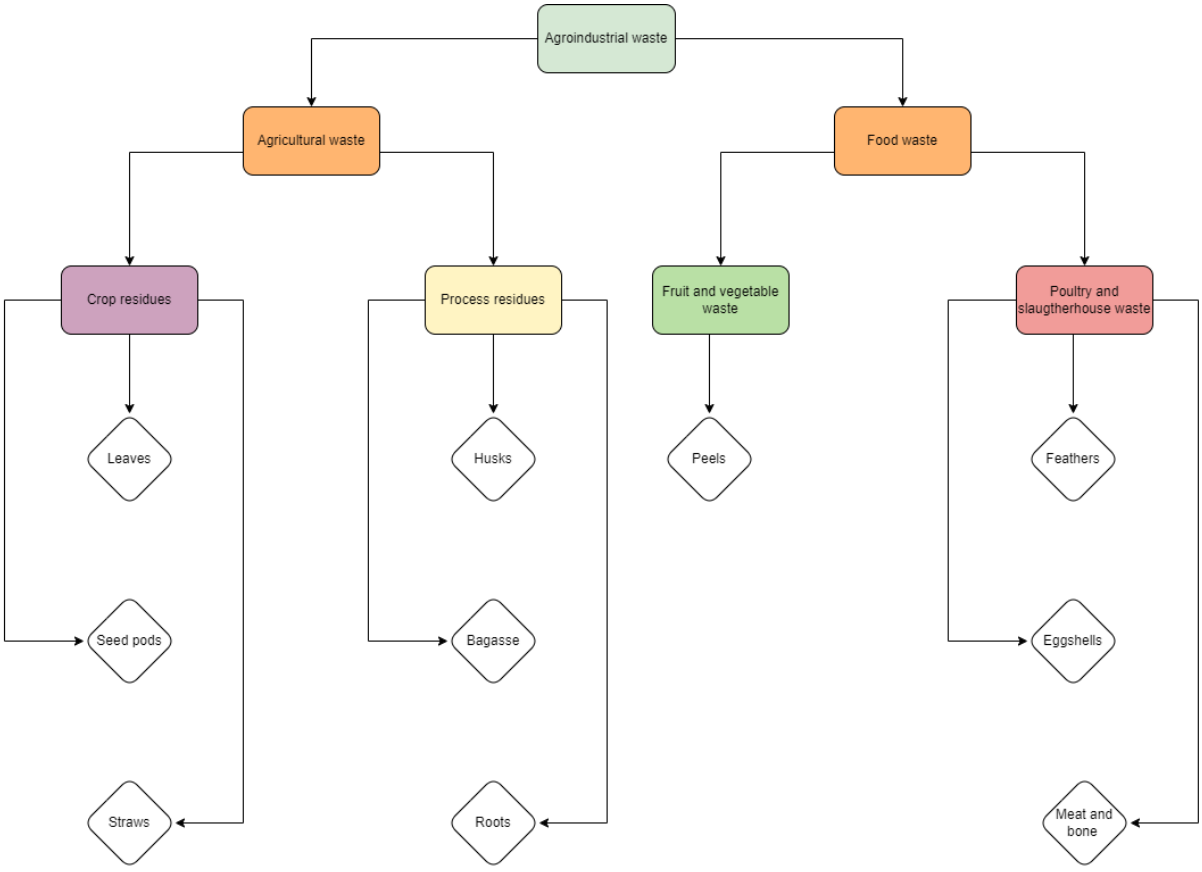

Figure 5 - Different residual sources of biomass from agro-industrial waste (adapted from [23])

Biochar has some similarities with activated carbon since both can be produced from pyrolysis, but the temperature of the reaction influences the specific areas, which can range from medium to high, depending on the temperature of pyrolysis. However, biochar owns a higher number of functional groups and a non-carbonized fraction which could be related to the milder conditions of production [24]. These non-carbonized fractions could potentially interact with soil contaminants, as well as other surface functional groups of the biochar, such as hydroxyl and phenolic groups, that could effectively bind soil contaminants. These properties demonstrate that biochar has huge potential as an environmental sorbent for organic and inorganic contaminants in soil or water [25]. With the differences between a biochar and activated carbon being due to different parameters, it is necessary to select the proper conditions of residence time; feedstock type; pyrolysis temperature; and heating rate, in order to produce a biochar with the specific conditions needed as shown in Table 1 - Characteristics of different types of feedstocks [25].

The high yield found on some of the feedstocks is related to the higher level of inorganic constituents, as indicated by their relatively high ash content [25]. It has been reported that the presence of high levels of inorganic constituents like potassium or zinc, and high contents of lignin, on the feedstock correlate with the high biochar yield [26,27]. The increase in temperature provokes dehydration and depolymerization, of plant-based biomass, into smaller dissociation products of lignin and cellulose, on the other hand, poultry manure and sewage sludge biochars do not undergo depolymerization because of the lack of lignocellulosic compounds [25].

Table 1 - Characteristics of different types of feedstocks (adapted from [25])

Feedstock	Pyrolysis Temperature (°C)	Heating Rate (°C min^{-1})	Yield (%)	Mobile Matter (%)	Fixed Matter (%)	Ash (%)	pH	C (%)	H (%)	O (%)	N (%)	Surface Area (m^2 g^{-1})	Pore Volume (cm^3 g^{-1})
Canola straw	400	20	27.4	-	-	-	-	45.7	-	-	0.19	-	-
Corn cobs	500	-	18.9	-	-	13.3	7.8	77.6	3.05	5.11	0.85	0	-
Corn stover	500	-	17	-	-	32.8	7.2	57.29	2.86	5.45	1.47	3.1	-
Orange peel	500	-	26.9	-	-	4.3	-	71.4	2.25	20.3	1.83	42.4	0.019
Peanut shell	300	7	36.9	60.5	37	1.2	7.8	68.27	3.85	25.89	1.91	3.1	-
Peanut shell	700	7	21.9	32.7	58.1	8.9	10.6	83.76	1.75	13.34	1.14	448.2	0.2
Pine needles	400	-	30	-	-	2.3	-	77.85	2.95	18.04	1.16	112.4	0.044
Pine needles	500	-	26.1	-	-	2.8	-	81.67	2.26	14.96	1.11	236.4	0.095
Poultry manure	400	7	54	8.2	63.8	28	10.6	51.04	3.15	39.35	5.41	11.6	0.027
Rapeseed plant	400	5	39.4	27.1	60.7	12.2	-	71.34	3.93	10.84	1.43	16	1.244
Rapeseed plant	500	5	35.6	17.5	69.6	12.9	-	75.03	2.62	7.79	1.41	15.7	1.15
Rice husk	500	-	-	-	-	42.2	-	42.1	2.2	12.1	0.5	34.4	0.028
Tire rubber	400	10	59.3	-	-	15.4	-	77.7	3.56	3.34	-	24.2	0.08
Tire rubber	600	10	54.5	-	-	15.6	-	81.3	1.67	1.43	-	51.5	0.12
Wheat straw	400	8	34	-	-	9.7	-	65.7	4.05	-	1.05	4.8	-
Wheat straw	460	8	-	-	-	12	8.7	72.4	3.15	-	1.07	2.8	-

For the previously stated parameters, a van Krevelen diagram, a diagram based on the molar ratio between hydrogen and carbon and the molar ratio of oxygen and carbon, is required, to enable a full understandability of the influence of pyrolysis temperature on the biochar properties [28,29]. Figure 6 illustrates a van Krevelen diagram for some of the biomass feedstocks previously stated.

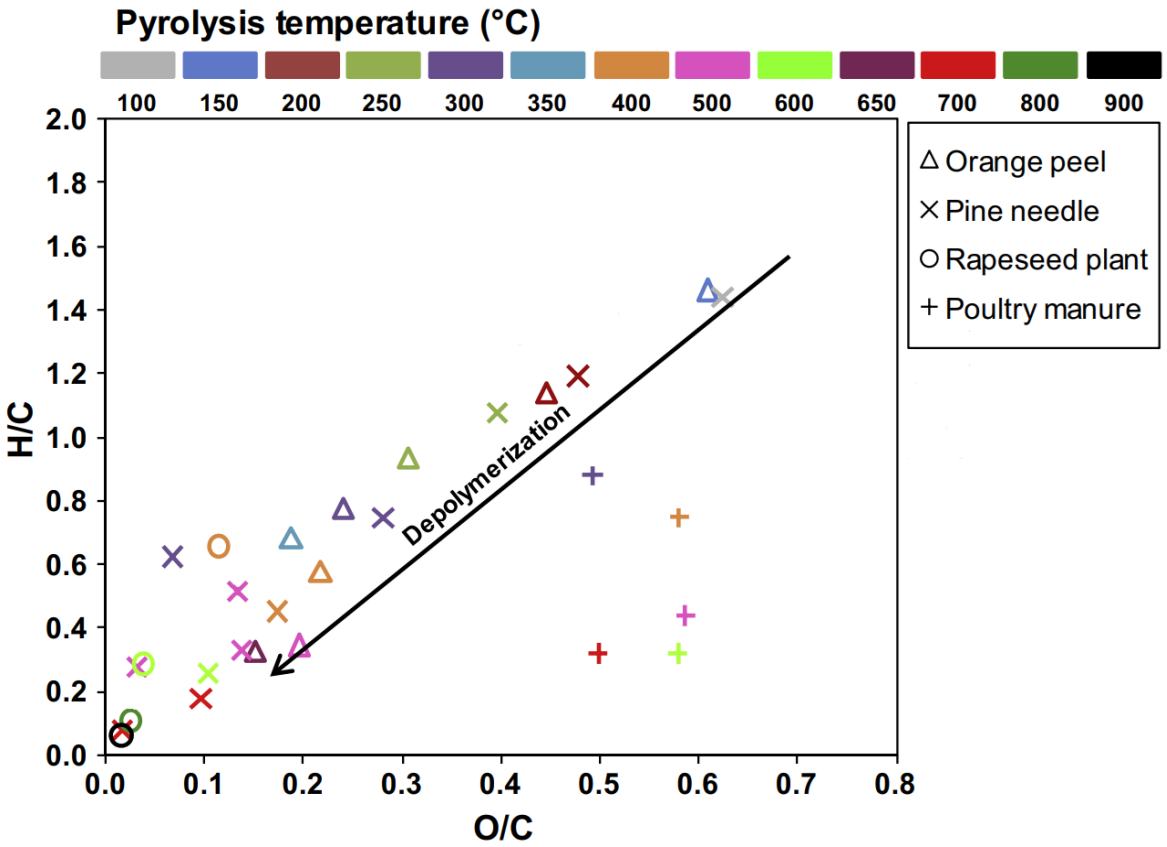

Figure 6 - Van Krevelen diagram illustrating the evolution of H/C and O/C ratios in biochar produced from various biomasses at different pyrolysis temperature (adapted from [25])

The lower values of H/C and O/C demonstrate a higher degree of carbonization of the biomass samples that suffered pyrolysis [29]. Thus, the lower molar ratios of hydrogen/carbon and oxygen/carbon were related to a higher presence of aromatic compounds and a lower polarity of biochar derived from pine needles [30]. The lack of lignocellulosic compounds is easily evidenced in the poultry manure data of Figure 6 since the non-lignocellulosic feedstock does not show the tendency of depolymerization with an increase in temperature, as previously stated.

2.1.2. Biochar production methods and characterization techniques

There are numerous thermochemical conversion techniques to convert biomass into solid, liquid, and gaseous products. Thermal decomposition is a standard process for biochar production, including methods like pyrolysis; hydrothermal carbonization; gasification, and torrefaction [31,32]. It is important to choose the method of production according to the biomass characteristics and desired application since variables such as heating rate; temperature; and residence time can influence the physicochemical properties of the biochar [32].

Not only the characteristics of the biochar, but also the yield can be influenced by the pyrolysis method (e.g. slow pyrolysis method without oxygen boosts the percentage of biochar produced) while the increase of residence time and temperature, implies a decrease in the percentage of solid product, and an increase on the percentage of liquid product [31]. Table 2 demonstrates some different techniques for the processing of biomass samples.

Table 2 - Characteristics of different biochar production techniques (adapted from [31])

Technique	Temperature (°C)	Residence time (s)	Heating rate (°C/s)	Biochar (%)	Bio-oil (%)	Syngas (%)
Slow pyrolysis	300 to 550	hours to days	1 to 10	35	30	35
Fast pyrolysis	450 to 600	<2	10 to 1000	12	75	13
Flash Pyrolysis	750 to 1000	0.5	<1	-	-	-
Gasification	>800	10 to 20	0.8 to 1	10	5	85
Torrefaction	450 to 550	<2h	-	75	20	5
Hydrothermal Carbonization	<200	3600 to 57600	<1	35	30	35

Pyrolysis can be classified into diverse types [33]. Slow pyrolysis (SP) is defined by relatively low heat, slow heating rates, and a prolonged contact time which favors biochar formation [31,34]. Also, SP maximizes the biochar yield by triggering secondary reactions, due to extending the vapor residence time [35].

Fast pyrolysis (FP) is a process that is preferred when bio-oil is the desired product since the production rates of biochar and pygas are relatively low [31]. In FP, secondary decomposition is limited, since the vapors generated by rapid decomposition are quickly swept out of the reactor [36]. Flash pyrolysis (FLP) produces mainly identical products as FP but with the focus of its process aiming for the optimization of bio-oil production. FLP is defined by elevated temperatures, high heating rates, and contact times inferior to a second [31].

Gasification is the thermochemical transformation process of biomass at remarkably elevated temperatures under a specific amount of oxygen, which produces a combustible gas known as syngas, mainly composed of hydrogen; carbon monoxide; and methane [31,37].

The gasification thermochemical process exposes biomass to a thermal treatment at relatively low temperatures, as it happens in slow pyrolysis, but the main difference from that process is the low concentration of oxygen in this case [38].

Hydrothermal carbonization is usually performed at relatively low temperatures when compared to other pyrolysis methods, which makes it less energy-intensive [39]. Because of that, the residence times are prolonged to enable efficient carbonization, and as happens in SP, the variety of products is equal, since in HC the rate of solid; liquid; and gaseous products are identical [31].

After the preparation of the biochar, from the different array of methods addressed, it is imperative to analyze the composition of the product produced, to check if it has the desired characteristics for the applications needed. That characterization is based on the structure of the biochar, on physical and chemical characteristics, on the surface functional groups, and the elemental analysis of the char [40]. Figure 7 illustrates the methods used to analyze distinct characteristics of the biochar, as well as some of the chemical and physical properties, which must be well known, to fully understand the potential and the best applications for a biochar sample produced.

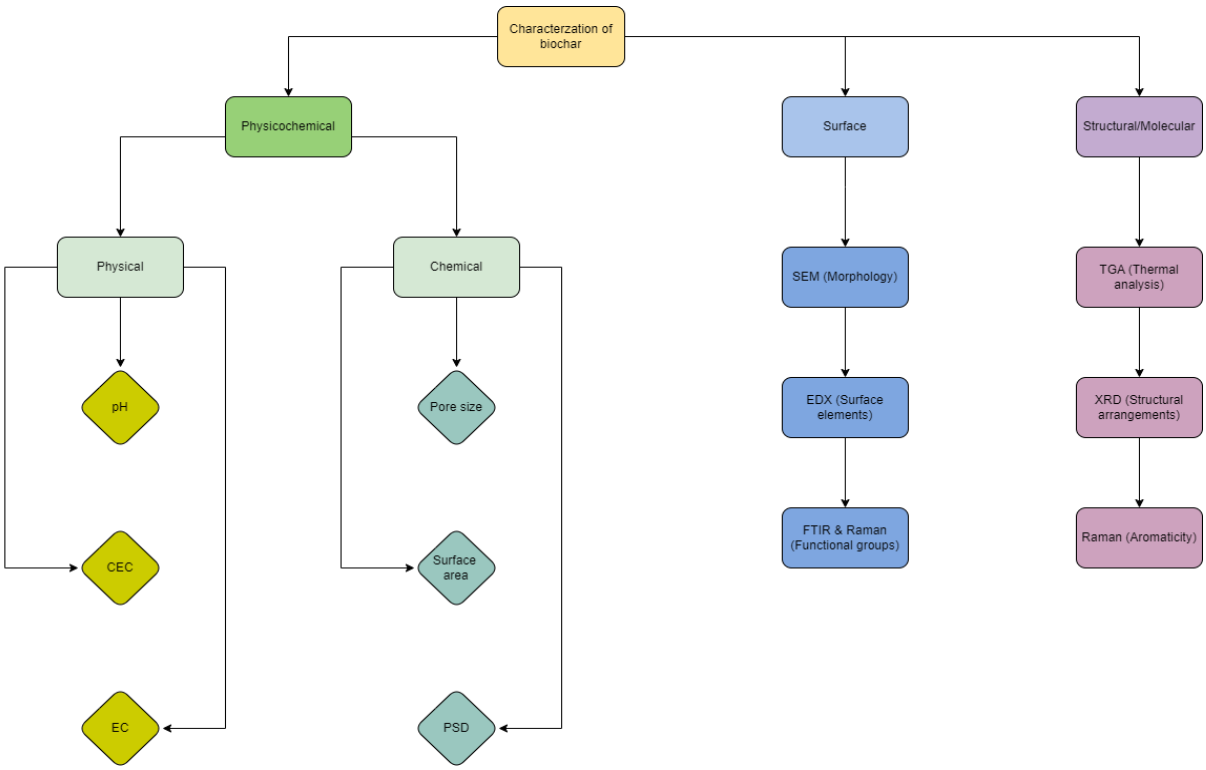

Figure 7 - Parameters and techniques used to study the characteristics of the biochar samples (adapted from [40])

There are some essential functional groups on the surface of biochar that increase the sorption properties including carboxylic (-COOH), hydroxyl (-OH), amine ($-NH_2$), amide ($-CONH_2$), and lactonic groups [41]. Characteristics like pH, surface area, and porosity might reduce biochar functional groups when increased [41]. Biochar pH levels are extremely important since they can influence the pH of soils, in cases where biochar's used to remove contaminants, and consequently provide micronutrient deficiencies and yield reductions in crops [42]. Apart from that, pH is related to the ash content of samples, with woody feedstocks having lower ash values, which implicates an inferior pH than the ones produced from other feedstocks [43]. Not only does the ash content influence the pH of the biochar, but also the temperatures of carbonization, since it has been stated that temperatures above 400°C expected to have higher pH than ones produced at temperature below 400°C [42,44].

The pH of the biochar analysis involves the use of a glass electrode-calomel electrode system, and a solution (usually deionized water), but besides that, some parameters might influence the values obtained from the electrode system since it can be affected by the position of the electrode on the suspension; the shaking time needed between the solution and the biochar; and the ratio of biochar and solution [42,45].

The cation exchange capacity (CEC) of the biochar, is extremely important if the desired application is for soil remediation since biochar is emerging as an alternative for remediation in soil and water of heavy metals [45]. CEC analysis is based on the displacement of an ammonium cation (NH_4^+) by KCl, after a step of washing with an organic solvent (isopropanol or ethanol). By applying this method for the CEC determination, it is possible to avoid hydrolysis problems of non-neutral salts and use low-cost reagents [46]. Foremost it allows the comparison of distinct biochar samples at a neutral pH, which is of extreme importance since pH depends on the CEC and the high variability in surface properties of biochar [47,48].

To fully characterize a biochar, it is necessary to analyze its surface, which includes studying the morphology, functional groups, and surface elements [40]. As illustrated in Figure 7, there are several methods for that, such as Scanning Electron Microscopy (SEM); Energy Dispersive X-ray (EDX); Fourier Transform Infrared Spectroscopy (FTIR); and Raman [40].

From all the methods listed, one of the most applied is, SEM, which is utilized for the analysis of microstructural adsorbent materials, to present an image of a specific adsorbent material and observe its features (e.g., morphology, pore size, and arrangement) or to observe modifications after surface functionalization [49,50].

EDX is usually coupled with the SEM method, since it can provide both semiquantitative and semiqualitative information, on the elements present on the surface of a sample, enabling an elemental analysis and chemical configuration [51]. The data obtained from the analyses of EDX are represented as a plot of E (Energy) vs I (Intensity). Each metal present on a sample surface emits X-rays that are known to have a specific identity (e.g., the same wavelength and energy for the same position on an EDX spectrum) [51]. Many other element peaks can be observed through this method, such as N; C; O; S; and P, which can establish evidence of the adhesion of the compound on the metal [51].

FTIR is a method used to determine the functional groups at the surface of the biochar [40]. The method is based on the excitation of a molecule by IR radiation, resulting in vibrations of its molecular bonds for the different values of wavenumber, with shifts in band intensity indicating that the respective functional groups have been involved in the adsorption process [49]. Every single specific bond has different absorption bands, which are related to the bending and stretching vibrations, which occur at different wavenumbers, and that enable specific surface functional group identification [49]. Also, FTIR is extremely practical to identify if an adsorbate has effectively been adsorbed by the functional groups present at the biochar surface [49].

Not only is important to analyze the surface of the biochar, but also the structure and molecular composition of it, and for that case, there are several methods, like Thermogravimetric Analysis (TGA); X-ray diffraction (XRD); and Raman [40].

TGA is a method that submits the sample to different values of controlled temperature, in a specific atmosphere, to rate the thermal stability of biochar and characterize its structure, by obtaining information about the yield of carbonization for different temperatures; for the moisture content; for the distinct structural components of the biomass feedstock; and the inorganic content of biochar [49].

XRD is an analytical technique based on the diffraction of X-rays by matter, characterized as elastic scattering used to evaluate the structure and molecular characteristics of the biochar, more precisely to determine the crystalline and structure of biochar [40]. This technique can also evaluate the ratio between the crystalline and the amorphous phases, as the large X-ray diffraction peaks indicate amorphous structure, while sharp peaks evidence crystalline arrangements [49,50]. XRD is a nondestructive sample analysis method, used on solid materials to determine the crystalline phases, and provide information on structures, crystal orientations, and other structural parameters such as crystalline, tension, and crystal defects [52].

Raman is characterized as a rapid, non-destructive technique that uses a visible or infra-red laser (532 nm – green light; 785, 830, or 1064 nm – near infra-red (NIR) light) for analyzing the chemical structure of a sample, which makes it a very valuable technique for studying a big variety of carbon-rich materials including graphites, coals, carbon fibers, and amorphous carbons [49,53,54,55]. The technique can determine the degree of biochar carbonization, also known as aromaticity, because of its high sensitivity, and low interference [40]. The spectrum also known as Raman scattered light is composed of diverse bands that indicate specific biochar structures [49].

2.1.3. Biochar applications

Biochar can have numerous applications, as listed in Figure 8, that can range from the incorporation as a catalyst in chemical reactions; to its utilization for soil and water remediation; to producing several types of biofuels from distinct processes [56].

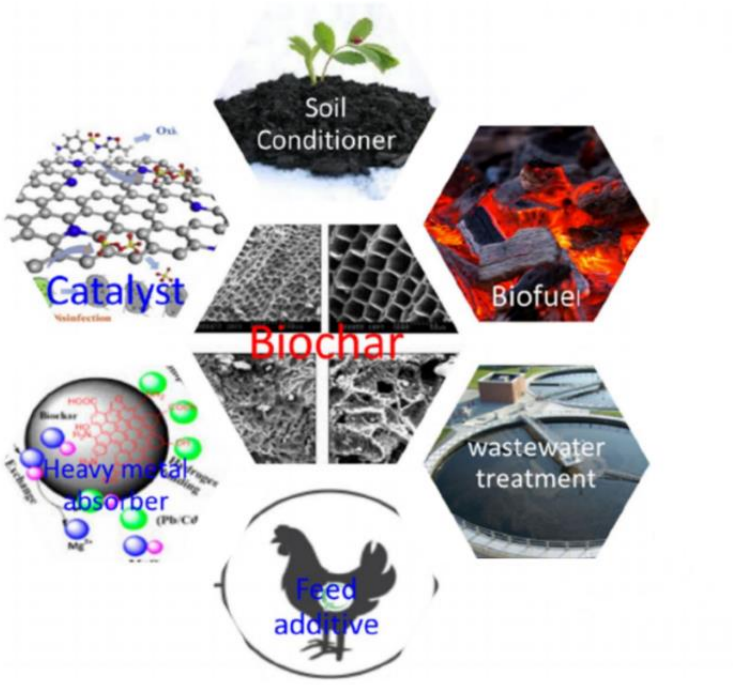

Figure 8 - Biochar applications (adapted from [45])

The final applications of the biochar produced depend on the process chosen to treat the vast array of biomass feedstocks. If the process chosen is based on biochemical processes (fermentation or anaerobic digestion), the biomass can be transformed into bioethanol or biogas, respectively [56]. Bioethanol (C_2H_5OH), also known as ethanol, is an alcohol produced from microbial fermentation of sugars present on biomass, followed by a distillation [57]. Bioethanol is used as an additive to gasoline, being incorporated in blends that usually have 10% bioethanol (B10), and that can already be used by most conventional gasoline engines, without any necessity of any modifications, with a possibility of a slight improvement to their performance [58]. Despite bioethanol, there is another biofuel, previously stated, that can be produced from biochar, biogas, which is obtained by an anaerobic digestion process, based on the breaking of the biomass by bacterial hydrolysis, followed by the conversion of sugar and amino acids by acidogenic bacteria, into carbon dioxide (CO_2); hydrogen (H_2); ammonia (NH_3); and methane (CH_4) [59]. Biogas's main applications consist of providing heat and electricity [60].

Besides the biofuel application, biochar can be used for wastewater treatment which enables the remotion of contaminants present in the water effluents, while also having the ability to seize and retain valuable nutrients and organic matter, which can be recycled and utilized in agriculture or energy production [61]. Biochar has been reported as an effective adsorbent for phenols in wastewater effluents, which makes it a valuable product to treat the current concerns of organic contaminants, such as phenols and dyes, in aqueous solutions [62,63,64]. It has been stated that cationic dyes are more highly adsorbed than anionic dyes, due to the small molecular weight molecules; favorable electrostatic properties, and strong π-π interaction with biochar surface [62]. Current studies state that adsorption for biochar'-s prepared at 900°C, had a better adsorption rate, than those prepared at 600°C, due to the significantly enhanced surface area, from the high temperatures of preparation of samples [62]. It has recently been stated that biochars have an unprecedented ability to remove inorganic pollutants such as heavy metals from wastewater, due to the abundance of functional groups on their surface such as phenolic, hydroxyl, and carboxyl groups, and due to their porous structure and its large surface area [62,65,66]. Since biochar can be used to adsorb a vast variety of contaminants from soil and water, as previously stated, it is important to know that there are distinct mechanisms depending on the type of contaminant, as can be seen in Figure 9.

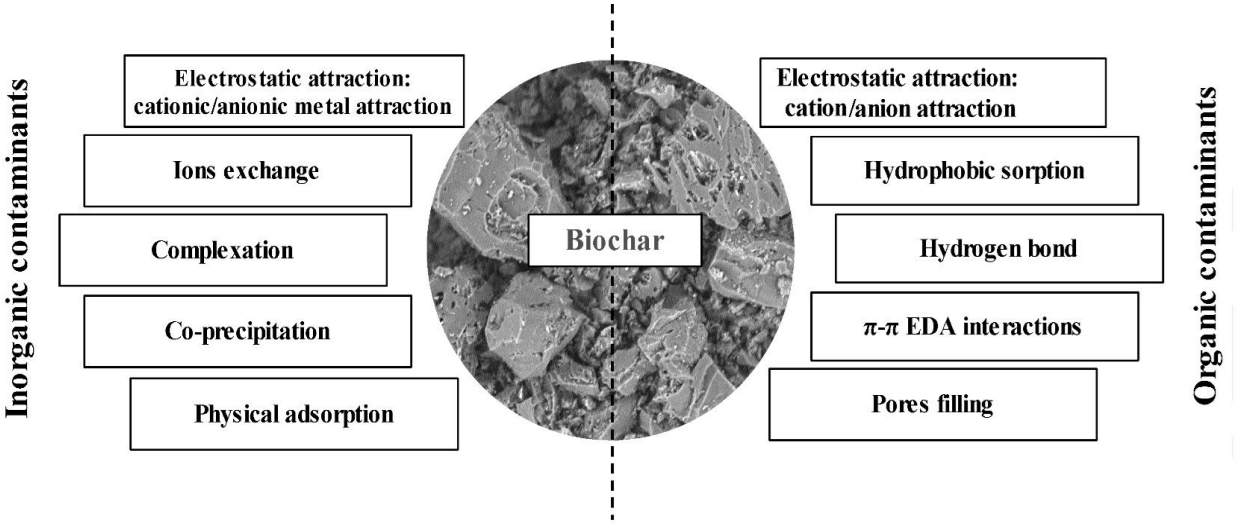

Figure 8 - Mechanisms of adsorption of biochar to remove different types of contaminants (adapted from [62])

If the pollutants to remove are organic, the mechanism of adsorption is promoted by electrostatic attraction; pore-filling; π-π electron-donor acceptor interaction; hydrogen-bonding; complexes adsorption; and hydrophobic interactions [62]. The surface of biochar is normally presented as negatively charged, due to the dissociation of oxygen-containing functional groups, which causes electrostatic attraction between biochar and the positively charged molecules [62,25]. For samples of biochar prepared at elevated temperatures, the loss of oxygen-containing and hydrogen-containing functional groups makes them less polar and more aromatic, which is less appropriate for polar organic contaminants removal [62]. However, the adsorption could occur by hydrogen bonding developed as a result of the electrostatic repulsion, between anionic organic compounds, and the biochar. If the pollutants to remove are inorganic, such as heavy metals, mechanisms including surface precipitation under alkaline conditions, ion exchange, and complexation, cationic and anionic electrostatic attraction are more indicated [62].

Apart from all the important biochar applications, formerly cited, its implementation as a feed additive is of major importance due to the chemical and physical properties of biochar, which have been linked to the possibility of reducing nitrogen content in manure, decreasing the risk of pathogens, and strengthening the immune system of livestock and poultry [67]. There are innumerable benefits of implementing biochar as a food additive for livestock and poultry; from an animal welfare perspective, its implementation can decrease the mortality rates of the animals, paired with a strengthening of the immune system of livestock, and also an increase associated with nutrient digestibility [67]. About the environmental impacts, the incorporation of biochar in animal food enables the reduction of odorous emissions in manure and methane in ruminants [67].

As a catalyst, biochar can arrange more active sites for reactions of catalytic degradation and contribute to the stabilization and dispersion of nanoparticles. As a heterogeneous catalyst, biochar offers many advantages due to its large surface area, lower cost, and a specific functional group that can be tailored to the properties needed, making it extremely appealing for catalytic reactions [68,69]. Biochar can be incorporated into biodiesel production reactions and the production of chemical products. The biochar-based catalysts have some characteristics that make them a viable alternative to solid-based catalysts (e.g. biodegradable; reusable; low cost) [68,70]. The potential of biochars is immense, with a vast range of applications. Besides the ones stated, biochar can also contribute to plant disease suppression; increase plant crop production; contribute to carbon sequestration; enhance composting efficiency; and improve anaerobic digestion efficiency [71].

Also, biochar is a great alternative to traditional electrodes, for the production of highly efficient microbial fuel cells, due to its exceptional qualities, such as a large surface area, and high porosity, which are hugely beneficial for electrodes in those types of fuel cells [72,73]. Since the cost of traditional electrodes represents a significantly high cost on the microbial fuel cells, with rates centered between 40%-50% of the total cost, biochar represents an inexpensive replacement anode material for granular activated carbon and graphite granules [72].

2.2. Textile industry wastewater

2.2.1. Wastewater characteristics

Wastewater term refers to the stormwater and urban runoff effluents, including all the sewage or liquid waste, coming from institutions; hospitals; industries; and domestic houses [74]. The main objective of the treatment of wastewater effluents is to minimize the load of harmful compounds, before the process of discharge returns to the environment, and subsequently cause harm to aquatic and wildlife species, and eventually lead to the contamination of drinking-water distribution systems [74]. Textile wastewater typically contains a complex mixture of organic and inorganic chemicals and is usually polluted with hazardous organics, such as dyes, surfactants, metals, salts, and persistent organic pollutants [75,76].

2.2.2. Types of dyes present in textile industries effluents

Wastewater contains diverse residual dyes [77]. There are many different types of dyes, most resistant to biodegradation, present in wastewater effluents (e.g. azo dyes; anthraquinones; phthalocyanines), and inorganic compounds such as metals [78]. Textile dyes are defined as organic compounds, with the capacity to absorb light radiation in the visible range of the spectrum, reflect or diffuse complementary radiation, and dye a substance [78,79]. Dyes are composed of three essential chromophoric groups: the chromophore; the auxochromes; and the matrix [80]. Thus, the distinct groups on each dye have specific and independent properties (e.g., the color; and ability to be fixed on a textile fabric) [78]. The active site of the dye is located in the chromophore group, and it can summarize the location of the atoms absorbing light energy [80,81]. The chromophore consists of many different groups of atoms, such as nitro (–NO2), azo (–N=N–), nitrous (–N=O), thiocarbonyl (–C=S), carbonyl (–C=O), and alkenes (–C=C–) [80]. The mechanism of absorption by electromagnetic waves due to the chromophore groups, is triggered because of the state of excitation by the electrons of a molecule [80]. Table 3 illustrates some classes of dyes and the respective chromophore group and dye example.

Table 3 - Classes of dyes with examples of each type (adapted from [80])

Class	Chromophore	Dye example
Azo	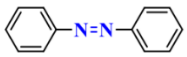	
Cyanine	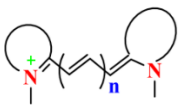	
Anthraquinone	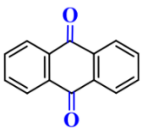	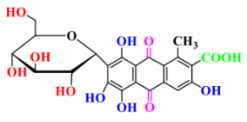
Phthalein	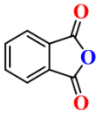	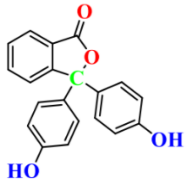

Azo dyes represent 70% of the world's annual production of synthetic dyes and are characterized by at least one or more azo groups (-N=N-), bonded to a (-OH) or a (-NH2) type of group [78]. Azo dye colors are formed inside textile fabrics, in situ, through the reaction of two colorless, or slightly colored, compounds [82]. Some examples of azo dyes are represented in Figure 10, with the respective maximum wavelength.

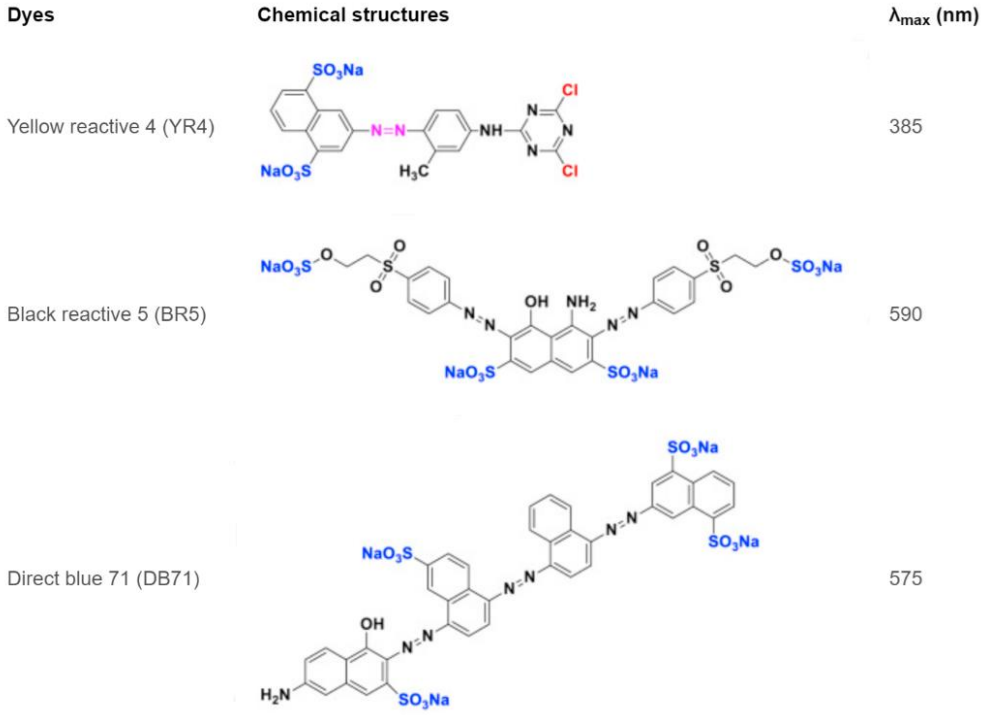

Figure 9 - Examples of azo dyes (adapted from [78])

After the azo dyes, the most notorious class of dyes are the anthraquinones, on which the chromophore group is a quinone nucleus, to where a hydroxyl or amino group can be bonded, giving the dye a good light resistance capacity [83]. Figure 11 illustrates some examples of anthraquinones, with the respective maximum wavelength.

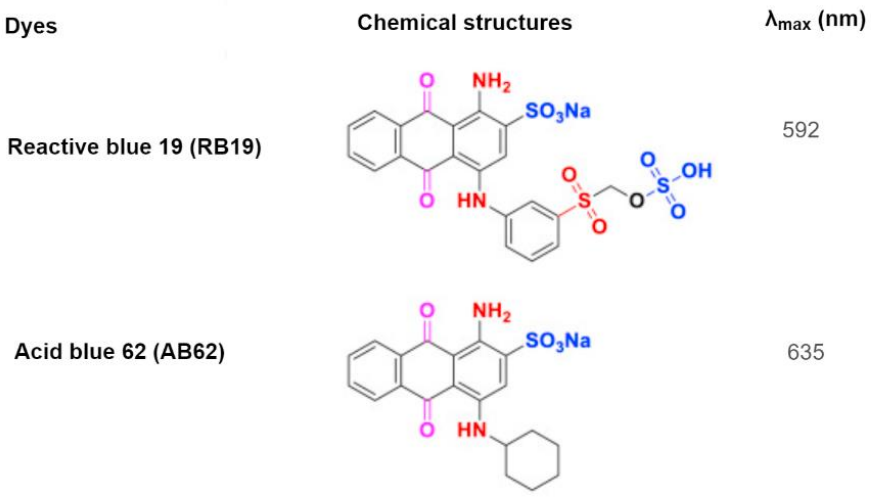

Figure 11 - Examples of anthraquinone dyes (adapted from [78])

Phthalocyanine dyes are produced through the reaction of dicyanobenzene with a variety of metal compounds (e.g., copper, nickel, cobalt, or iron), with the central structure of the molecule allowing the dye to retain its color without fading or washing away, making it an exceptionally durable and long-lasting dye [78]. These dyes are widely used in various industries and applications for their exceptional color retention properties [78]. Figure 12 shows some examples of phthalocyanine dyes with their respective chemical structures and wavelengths.

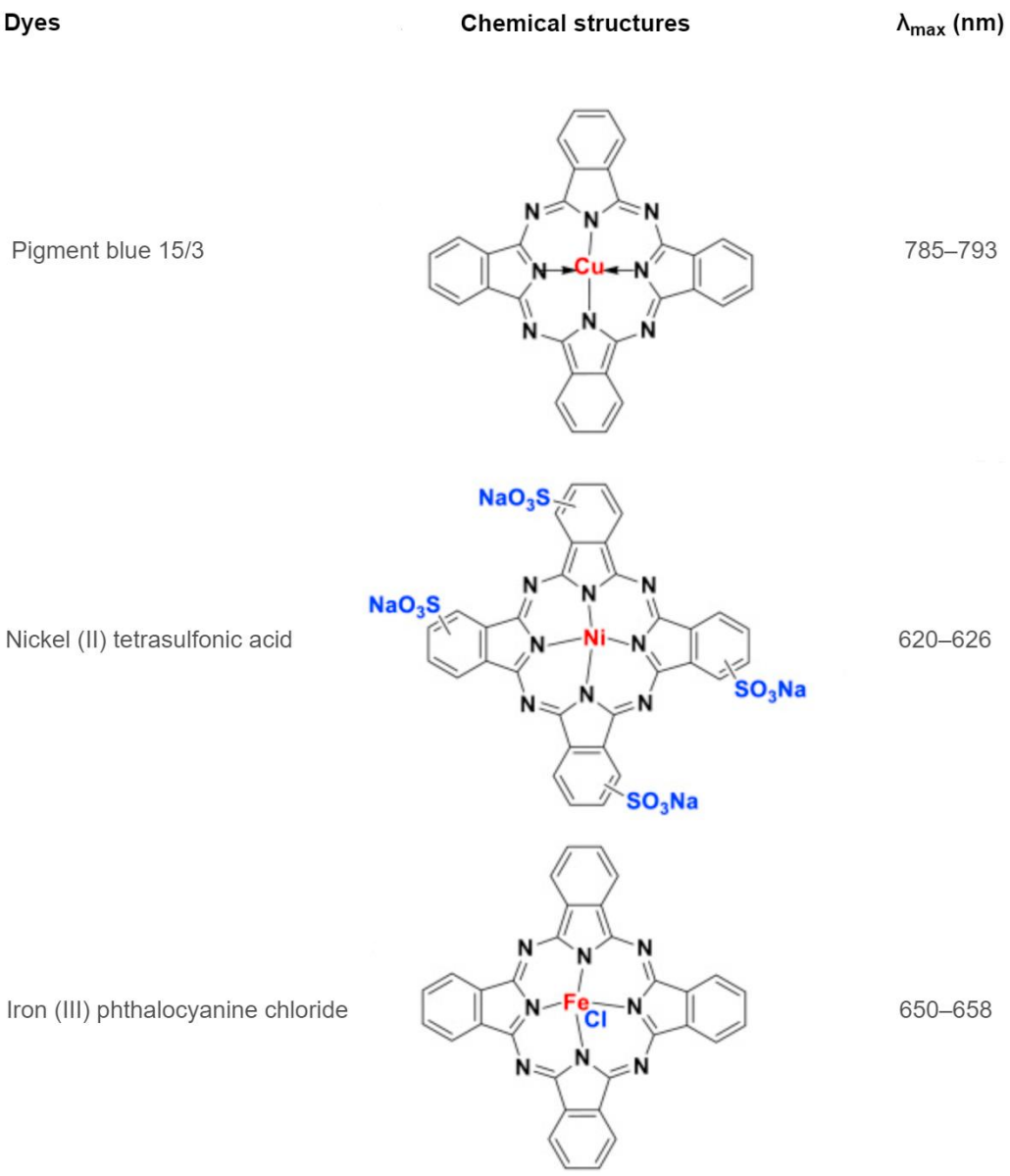

Figure 12 - Examples of phthalocyanine dyes (adapted from [78])

Dye classification is based on the auxochrome chromophoric group, which indicates the dye solubility and its affinity for different fibers, while taking these criteria into account, it is possible to separate the dyes into two different classes, the water-soluble ones, and the water-insoluble ones [78,84]. The soluble types of dyes are divided into anionic; cationic; metalliferous; reactive; or substantive dyes [78]. If insoluble, the types of dyes can be vat; sulphur; dispersible; or pigments [78]. Figure 13 shows the categories of dyes by solubility.

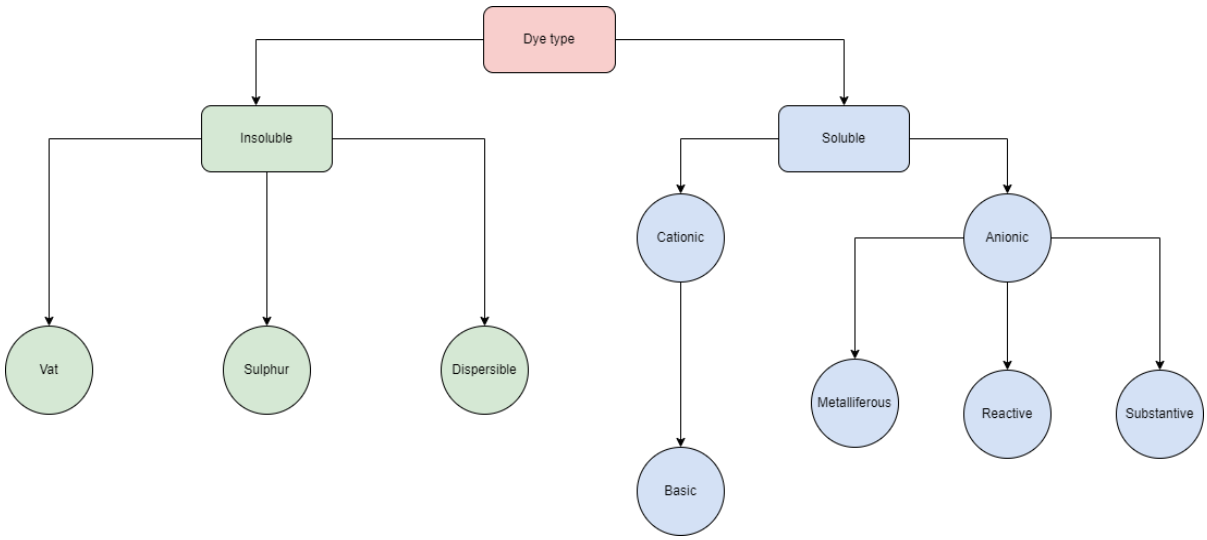

Figure 13 - Classification of dyes through solubility capacity (adapted from [78,85])

The reactive dyes contain chromophoric groups, such as azo, anthraquinone, and phthalocyanine [78,84]. This type of soluble dye, named reactive, denotes the existence of a reactive chemical function type (e.g., vinyl sulfone or triazine), that creates a strong covalent bond with the fibers, to guarantee long-lasting color retention [78,79]. Because of their excellent fastness qualities and simplicity of application, reactive dyes are the most extensively used class of dyes in the textile industry [84,86]. These dyes permanently bind to the fibers, forming a part of the fabric and guaranteeing superior color retention through washing, also RD is the preferred option for dyeing and printing cotton because they provide an extensive spectrum of brilliant colors, excellent brightness, and remarkable fastness [87]. The structures of reactive dyes are simpler, and the absorption spectrum evidences narrower absorption bands, with brighter dyeing, which makes them advantageous over direct dyes [88]. Figure 14 represents two examples of reactive dyes with the corresponding structure and wavelength.

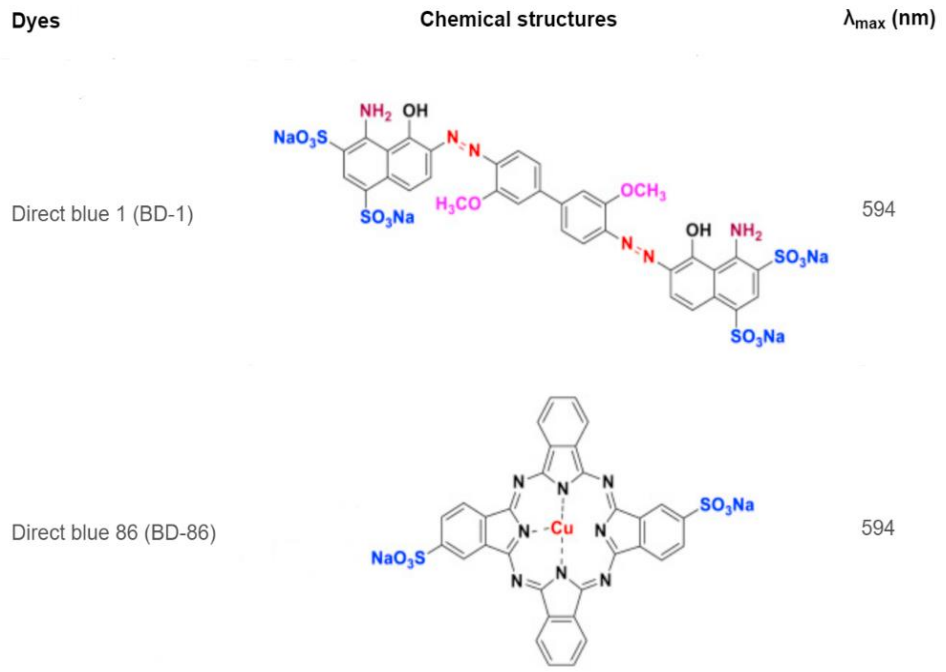

Figure 14 - Examples of reactive dyes (adapted from [78])

2.2.3. Processes involved in the treatment of dye wastewater

Water is an essential natural resource needed for life, while wastewater is also very important, particularly for locations with a shortage of water [89]. Despite being very important, wastewater effluents contain many distinct toxic substances, and for that reason, it is imperative to submit wastewater to treatment, before discharging it back into the environment [89]. With that being said, the treatment of wastewater can be established on two main points: to reestablish the supply of water, and to protect the environment from pollutants [89]. The dye-containing wastewater must be treated effectively so that the protection of the environment and water resources from adverse effects, can be accomplished [89]. Numerous techniques can be used to remove dyes from wastewater effluents, from physical to chemical processes, with advanced oxidation processes (AOP), and also with the use of biological products, supported by bacteria; algae; or yeasts as can be seen in Figure 15.

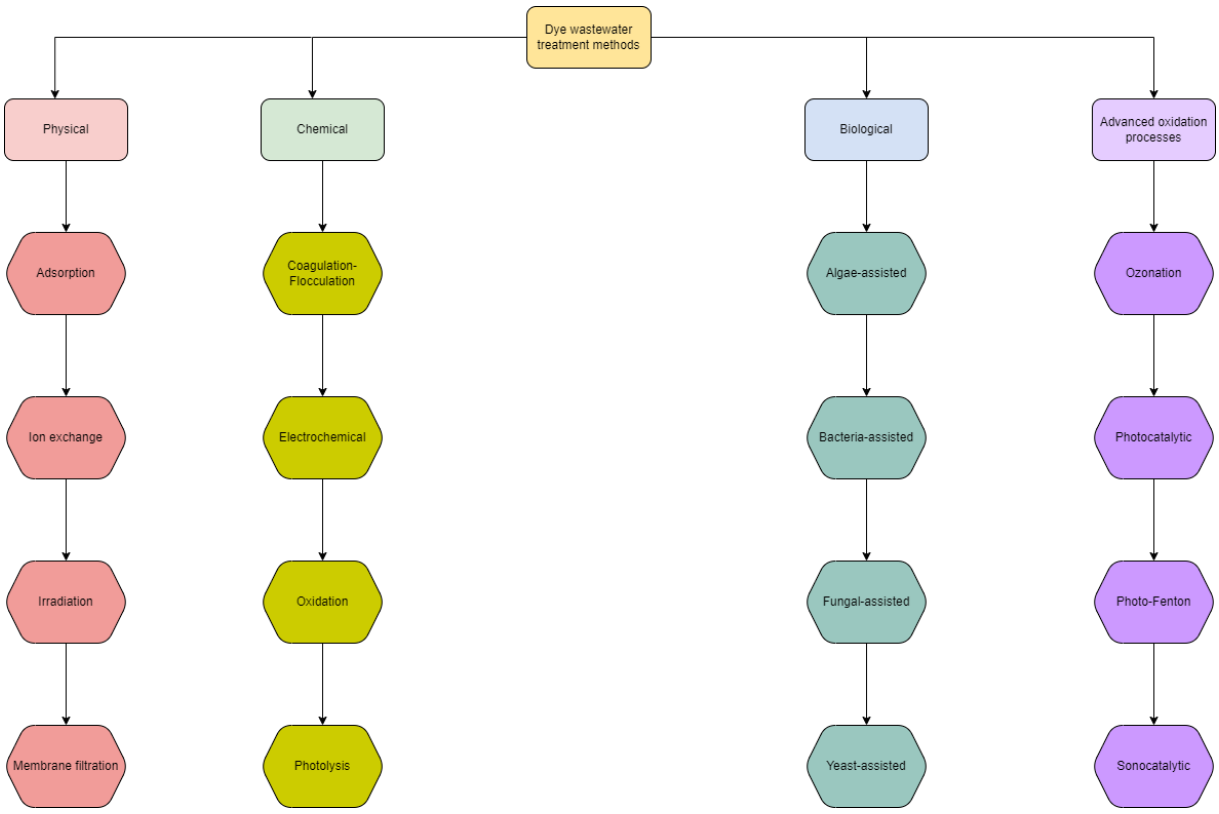

Figure 15 - Distinct techniques for the treatment of wastewater effluents (adapted from [85])

The approach for each method is distinct, for instance, physical processes are usually, simple, and are often based on mechanisms of mass transfer, with the use of membrane filtrations or adsorption processes [90]. These processes are defined as more dependable than biological or chemical processes since it does not include any use of any living beings and/or chemicals [90]. For the chemical processes, there are some important factors to take into consideration, like being more expensive than both physical and biological methods, due to the requirement of high energy; substantial amounts of chemical products; and specific equipment [85]. Furthermore, there are some challenges with these methods, which lie in the production of toxic metabolites and by-products, during the treatment of the effluents of wastewater [91,92,93].

Physical treatment methods incorporate processes such as adsorption; ion exchange; irradiation; and membrane filtration, as reported in Figure 15. Adsorption is the process of atoms, molecules, or ions diffusing and adhering to the surface of solid particles, thus adhesion occurs due, to the not balanced forces between the solid surface, and the impure particles [94]. Ion exchange is a method, usually combined with other physical dye wastewater treatment methods, to improve the efficiency of removal of dyes and contaminants [94]. The method is based on a mechanism where two ions with similar charges are interchanged, between two electrolytes or electrolyte particles [78]. The irradiation method is effective for the remotion of dyes from wastewater effluents, through the use of radiation from a monochromatic ultraviolet lamp, with the requirement of a constant supply of oxygen to ensure that the organic dyes are efficiently removed [95]. The membrane filtration method is based on a molecular sieve that is built into the structure of a film, which can have small pores or a fine mesh to assist in the separation of the particles and molecules [96]. The different membrane filtration methods include nanofiltration (NF); ultrafiltration (UF); microfiltration (MF); and reverse osmosis (RO) [97].

The chemical treatment methods include techniques like oxidation; photolysis; electrochemical, and coagulation/flocculation, described in Figure 15. In the coagulation/flocculation technique, distinct materials (e.g., polymers) are added to the wastewater to destabilize colloidal materials and cause the small particles to agglomerate into larger flocs. [98]. Electrochemical techniques are based on the use of electricity to conduct the treatment process [99]. There are numerous electrochemical techniques, the most common the electrochemical oxidation (utilized for mineralization of organic pollutants; water disinfection; and removal of cyanides); electrochemical reduction (used for metals recovery; and modification of organic compounds into less toxic forms); electrocoagulation (used to remove suspended particles); and electrodialysis (for water desalination) [100]. Photolysis is established on the photodegradation of compounds that absorb light as short wavelengths, through Ultraviolet (UV) light irradiation, to degrade them [101]. The chemical oxidation technique is used to remove colors from dye wastewater effluents, through the use of many different materials (e.g. ozone; hydrogen peroxide; acids) to break down dyes, although oxidized dyes and organic hazard compounds are not removed with this technique, which potentialized the development of AOP [89,102,103].

Despite the chemical and physical methods for the treatment of dye wastewater, there are also biological and advanced oxidation processes, which can be based on distinct technologies. For instance, biological processes can be based on algae; yeast; fungi; or bacteria to biodegrade or adsorb dyes [104]. Advanced Oxidation Processes (AOP) involve distinct effective, and eco-friendly techniques to assist in the remotion of persistent organic contaminants and microbes, while also disinfecting by-products from water, through powerful oxidizing agents (e.g., hydroxyl radicals) in situ [105].

Figure 16 and Figure 17, illustrate some of the numerous advantages and disadvantages inherent to the previously cited, physical and chemical wastewater treatment methods, respectively.

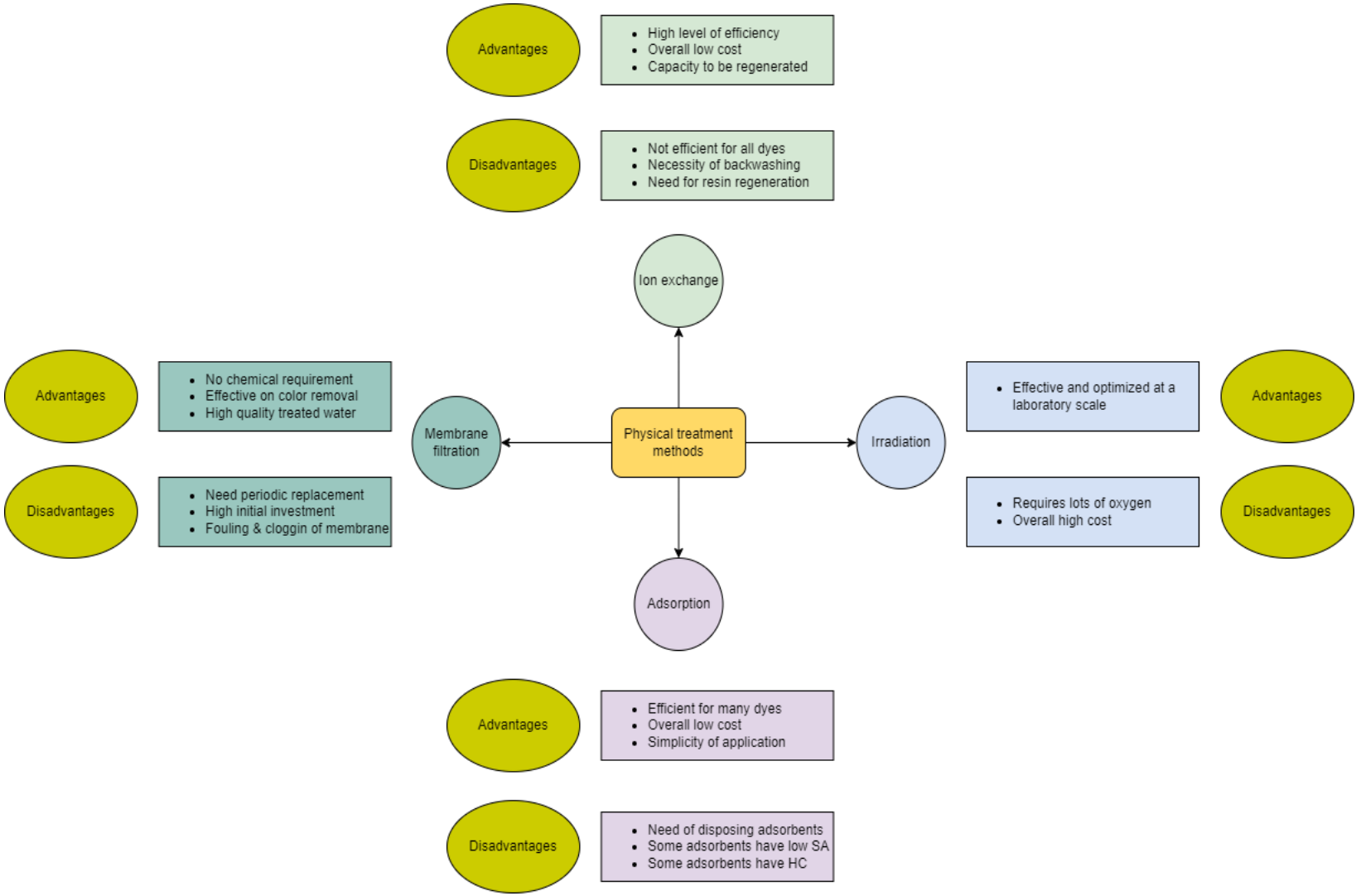

Figure 16 - Illustration of the wastewater physical treatment methods (adapted from [85,90,91,92,106,107])

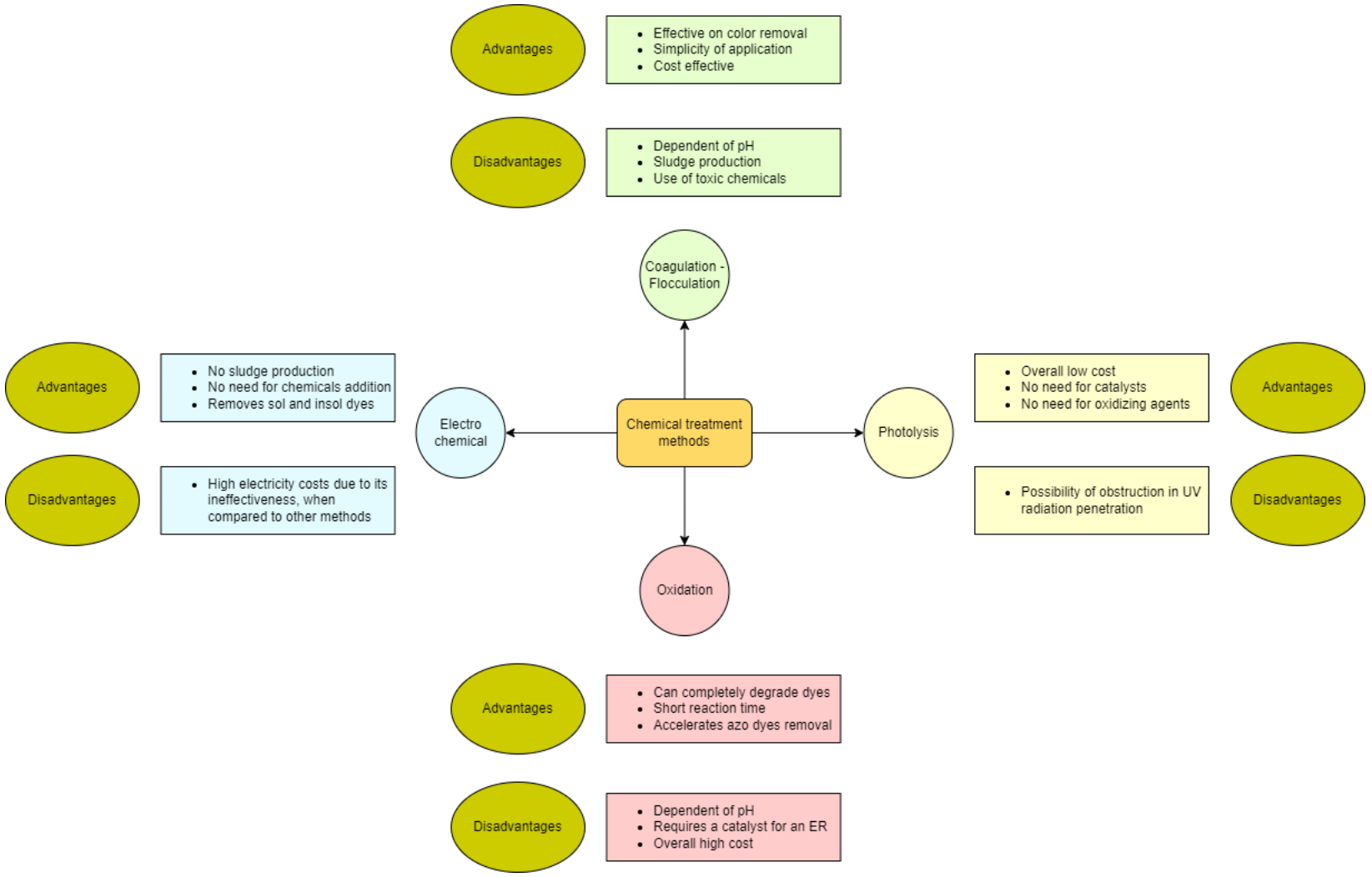

Figure 17 - Illustration of the wastewater chemical treatment methods (adapted from [85,90,91])

2.3. Dye adsorption

2.3.1. The mechanism involved in the dye removal with biochar-based sorbents

Adsorption is defined as the process of adhesion of a liquid; gas; or solid material onto the surface of another material, with the adsorbed material being called adsorbate, and the material that proportionate the adsorption on its surface is defined as adsorbent [108]. Adsorption can be sorted as physisorption or chemisorption, depending on the strength of the interactions, between the adsorbate and the adsorbent. There are distinct mechanisms for the processes of adsorption, based on electrostatic interactions, such as π-π interactions; hydrogen bonding; or pore filling, with each mechanism utilization depending on the properties of each contaminant or dye to be removed [109,110]. Figure 18 summarizes the different mechanisms of adsorption.

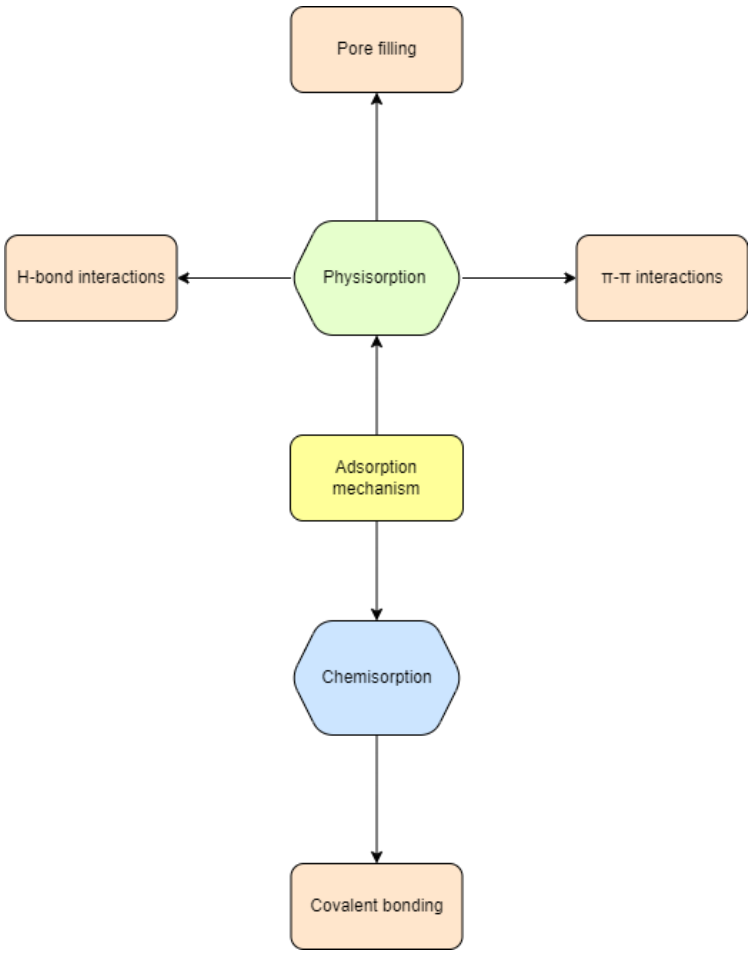

Figure 18 - Mechanisms of adsorption for dye removal (adapted from [109])

There are different physisorption mechanisms, such as the pore-filling process, which is composed of two adsorption steps, while in first place, occurs the external diffusion of the dye molecules, from the boundary layer to the surface of the biochar, and, secondly, the internal diffusion, which consists of the penetration of the dye molecules, into the pores of the biochar [111].

Besides the pore-filling mechanism, there are other physisorption routes such as the H-bond interactions, in which the hydrogen bonding is favored, with materials that contain oxygen groups, since this mechanism is based on interaction from the H-bonds (e.g. −COOH or −OH), that act as a donor of hydrogen to the biochar surface, and the nitrogen or oxygen atoms in dyes (e.g. nitrogen atoms in the Reactive dye molecules) [111].

π-π interactions are another example of physisorption mechanisms [111]. These interactions are defined as a noncovalent interaction between π-acceptors and π-donor molecules [111]. In these reactions, the aromatic rings of the biochar act as π-electron donors and the aromatic rings of the dyes act as π-electron acceptors [111]. Also, molecular structures of cationic dyes possess a cation (e.g. N+), which can end on the binding of cation to the aromatic rings on the biochar surface, forming an π+-π interaction [111]. Figure 19 represents a physical adsorption mechanism based on electrostatic interactions, between a cationic polymer product, called β-Chitosan (CS) and a reactive dye, more precisely reactive blue 221 (RB221) that is an anionic type of dye [112]. The attraction between the two species present on the dye and the chemical adsorbent, is made through the difference between the positive charge of CS protonated amine group ($-NH_3^+$) with the anionic sulfate groups ($-SO_3^-$) of RB221 [112].

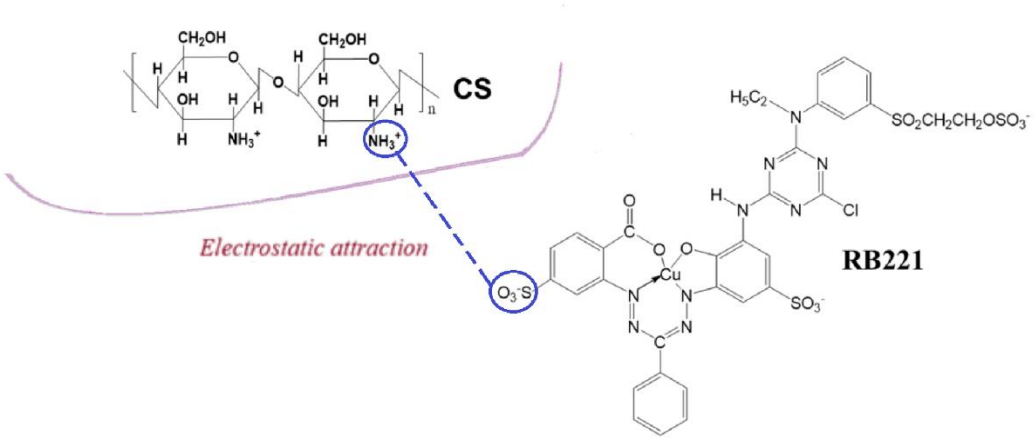

Figure 19 - An example of a physical adsorption mechanism between an adsorbent and a reactive dye (adapted from [111,112])

In alternative to the physical mechanisms, there is also the chemical adsorption route, which consists of the formation of an ionic or covalent chemical bond, between the adsorbent and the adsorbate, with a consequently change in the electronic configuration for both the adsorbate and the adsorbent, with a massive exothermic enthalpy being associated [113]. The bonding between adsorbate and adsorbent is highly site-specific, on chemisorption, since the volumetric number density of the active sites, can inform about the thermodynamic chemisorption models of the adsorbent, in contrast with what happens on the surface adsorption, by physisorption methods [114]. In this type of adsorption, valence forces bind the molecules of the adsorbate, to specific functional groups located on the adsorbent surface [114]. In cases where the adsorbent has defined flat surfaces, the process of chemisorption is limited to a single surface layer [114].

2.3.2. Factors that influence the adsorption process

The adsorption process can be influenced by many different physicochemical factors, which can range from the type of dye and its chemical structure to the properties of the adsorbent utilized to adsorb that dye from wastewater effluents [115]. These important physicochemical factors are the pH of the solution; the temperature; the pressure; the stirring speed; the properties of the adsorbent and dye contaminant, and other parameters, which can be seen in Figure 20.

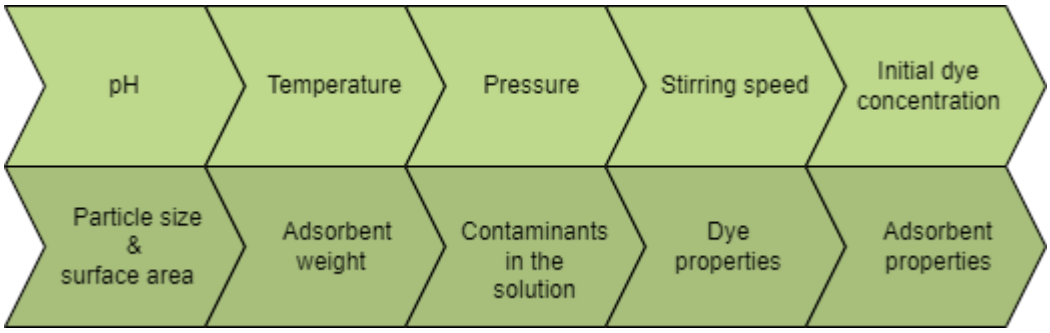

Figure 20 - Range of parameters that affect the adsorption efficiency (adapted from [115])

One of the most important adsorption factors is the pH of the dye solution, which can affect the capacity of the adsorbent and, thus the efficiency of the entire process [115]. This factor can influence the chemistry of the contaminants present in the solution, involving the activity inherent to the functional groups, the surface charge of the adsorbent, and the degree of ionization of the adsorbed ion, while also interfering with the chemical structure of the dye itself [115,116]. It has been reported that anionic dyes can form more efficient bonds with adsorbents in an acidic solution, while cationic dye bonds are more effective in basic solutions [115]. Table 4 summarizes some examples of the influence of pH on the capacity of adsorption of different adsorbents, by distinct nature of dyes. For anionic dyes, it was reported that with an increase in pH, the capacity of adsorption diminishes, while for cationic dyes the capacity of adsorption increased with an increase of the pH levels.

Table 4 - pH influence on the capacity to adsorb reactive dyes (adapted from [115,117,118,119,120])

Dyestuff	Adsorbent	Dyes Ionic Nature	pH	Observations: with the Increase (↑) of pH
Reactive Black 5	spent mushroom waste	anionic	2 to 10	q (mg/g) ↓
Reactive Orange 16	carbon from *Phyllanthus reticulatus*	anionic	2 to 11	q (mg/g) ↓
Malachite Green	almond shell	cationic	2 to 11	q (mg/g) ↑
Methylene Blue	olive stone activated carbons	cationic	2 to 12	q (mg/g) ↑

In addition to the pH parameter, temperature is also of huge importance to the adsorption efficiency, since it can shift the nature of the reaction from endothermic to exothermic [115]. If the reaction is endothermic, with an increase in the temperature levels, there will be an increase in the efficiency of adsorption, linked to an increment in the availability of active sites due to the activation of the adsorbent surface at higher temperatures [115,121].

Contrarily, if the reaction is exothermic, an increase in the temperature will have the inverse effect on the capacity of adsorption, provoking a decrease, since the potential of adsorption between the adsorbate and active sites will become weaker [115,122]. One of the main factors that can influence the adsorption process, is the initial dye concentration (IDC), as it can indirectly affect the efficacy of dye removal, through a decrease or increase in the availability of binding sites on the adsorbent surface [115]. Usually, the percentage of dye removal decreases with an increase in the initial dye concentration, which is correlated to the saturation of the adsorption sites, located on the adsorbent surface [115]. That means that at a low initial dye concentration, the surface area of the adsorbent and consequently the number of adsorption binding sites will be high, making it easier for the dye molecules to bind to the adsorbent surface [115]. However, if there is a high initial dye concentration, the saturation of the adsorption sites will occur, since the number of sites on the adsorbent surface will not be enough to adsorb the full concentration of the dye, which will end in a reduction of the adsorption process efficiency [115]. Adsorption experiments were conducted by Rápó and Tonk (2021) to evaluate the influence of initial dye concentration, with a reactive dye (Reactive Black 5) [115]. The dye concentration varied from 50mg/L to 100mg/L, with a corresponding adsorption capacity of 24.8 mg/g and 6.7 mg/g, respectively, which indicates that an increase of the dye concentration provoked a saturation of the active sites of the experimental adsorbent (pent tea leaves), since the capacity of adsorption could only reach 6.7 mg/g when the concentration of the dye in the solution increases to 100mg/L [115].

Another factor of main influence on the adsorption processes is the particle size (PS) [123]. As it has been reported, it is advantageous to have a reduction of the size of the particles, since the maximum adsorption capacity of the adsorbents increases with a decrease of the PS, which indicates that a smaller particle size is directly correlated to the promotion of larger surface area, to provide a higher availability of active sites [123]. However, the particle size cannot be too small, since it can turn out to be inaccessible to some molecules of dyes that are too large, and for this reason, it is important to find the optimal minimum particle size, to boost the adsorption capacity and not compromise it [123,124]. Figure 21 demonstrates the influence of the particle size of three distinct samples (ASC - aamla seed carbon; TSC - tamarind seed carbon; and SNC - soapnut carbon) on the adsorption capacity, while where it is visible that with an increase in the particle size, there is a decrease in the percentage of removal, indicating that the optimal PS is the lower value illustrated.

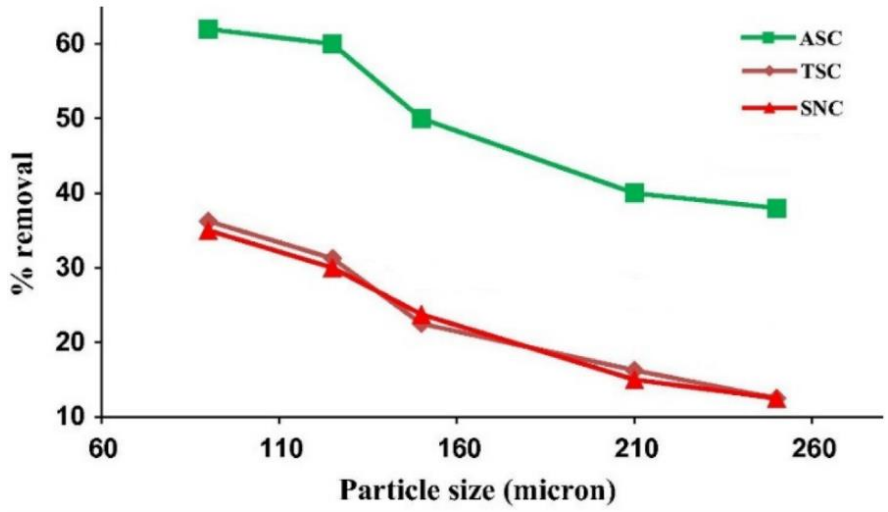

Figure 21 - Influence of the particle size on the adsorption capacity (adapted from [115])

3. Methodology

3.1. Biochar Preparation

Different types of biomass feedstocks were submitted to a pre-treatment step, such as avocado leaves; rice husk; peanut shells; and macroalgae, to prepare the biochar samples via pyrolysis. Some biomass feedstocks were placed in an oven (EHRET BK4029) at 70 °C for 48 hours to reduce water content, while others were already provided dry. The dried biomass was then shredded in a grinder (EDM 07588), to decrease the particle size, and then sieved, with 0.250 mm mesh screens, to minimize impurities and homogenize the biomass powder. After this pre-treatment, the biomass feedstocks were stored in glass containers, to protect them from factors, such as humidity. The production of biochar involved the enclosure of 50g of the pre-treatment biomass in several layers of aluminum foil, with a small aperture for the release of volatiles, then the biomass enclosed in the aluminum was introduced in a muffle (SNOL 13/1100), with the purpose to emulate an oxygen-free pyrolysis reactor, and thereby establishing a non-oxidizing environment. After introducing the biomass in the muffle, slow carbonization was performed, by subjecting the biomass to a heating ramp of approximately 2.5 °C/min until the highest treatment temperature (HTT) of 350 °C was reached. Then, the biomass was kept at that HTT for a further 2 hours, while the cooling was slow in the muffle. Figure 22 illustrates a sample of biomass before being submitted to the muffle, on the left, and after being produced through a thermal process, on the right.

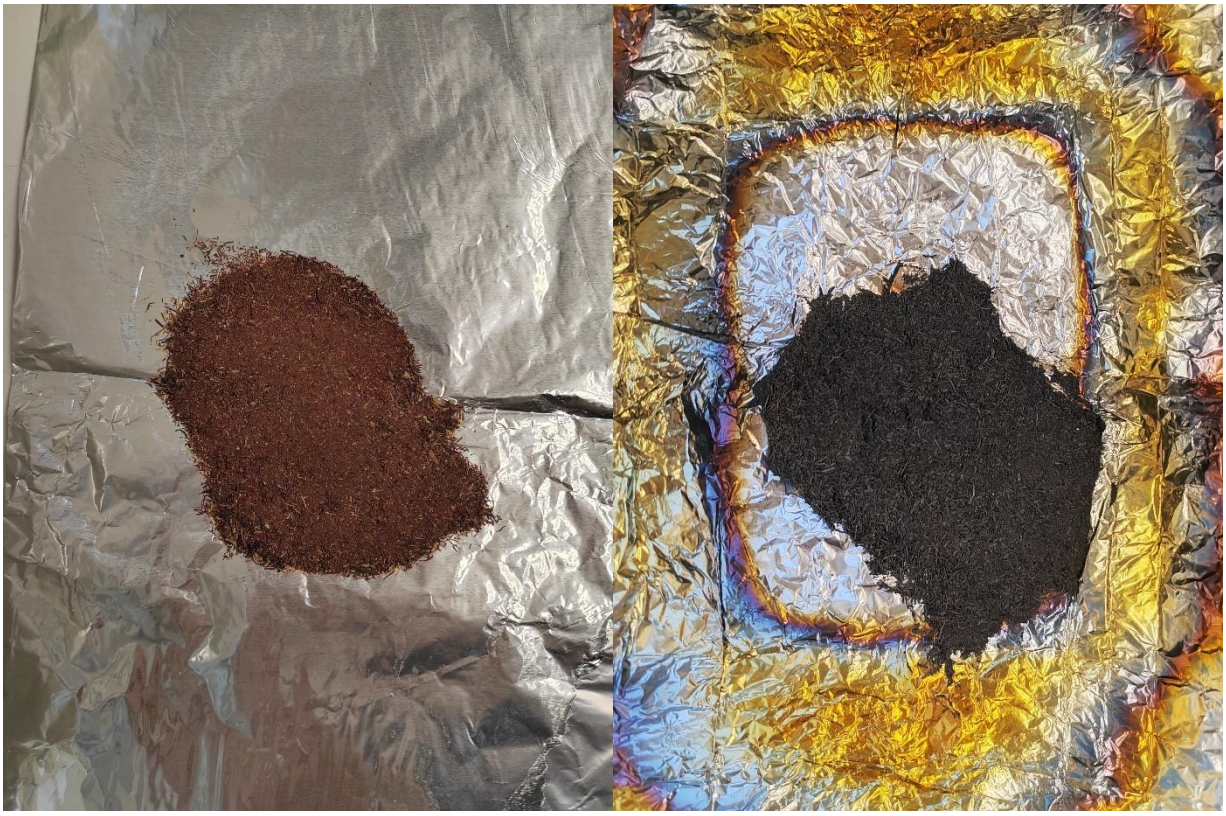

Figure 22 - Biomass sample before and after being submitted to pyrolysis

Following the production of biochar, each sample was weighed, on an analytical balance (Mettler PM460), to determine the corresponding yield. The formula used to calculate the yield is shown in Equation 1, with the mass of biochar produced, denoted as m_f, and the initial mass of the biomass sample defined as m_i [125].

$$Yield\ (\%) = \frac{m_f}{m_i} \times 100 \quad (1)$$

After calculating the yield of each sample produced, it was necessary to grind the biochar samples, with an agate mortar and a pestle, to increase the surface area, and consequently the surface availability to boost the adsorption capacity of each sample [126].

3.2. Biochar Sorbents Characterization

The biochar samples were characterized by a distinct array of methods such as a Scanning electron microscope coupled with X-ray dispersive spectroscopy (SEM-EDS), X-ray diffraction (XRD), Raman spectroscopy, Thermogravimetric analysis (TGA), and Attenuated Total Reflectance-Fourier Transform Infrared spectroscopy (ATR-FTIR).

The Hitachi S-2400 scanning electron microscope (SEM) was used to analyze the morphology and near-surface elemental composition of the sorbents. It was equipped with an Energy Dispersive Spectrometer (EDS) featuring a Bruker SDD light element detector. Digital images were captured using Bruker Esprit 1.9 software at a resolution of 4 nm and an accelerating voltage of 25 kV. The high resolution allowed for a detailed examination of surface structures. This setup ensured precise identification and mapping of elemental distributions across the sorbent surfaces.

The elucidation of phases within biochar was conducted employing an X-ray diffractometer, specifically the Panalytical X'PERT PRO model. This analysis utilized Cu Kα radiation and referenced the Powder Diffraction File™ (PDF2) database from the International Centre for Diffraction Data (ICDD). The parameters for the measurements were meticulously set as follows: a 2θ range from 5° to 70°, with a step size of 0.033° 2θ; the scan was conducted with either 75 or 150-second equivalent step times for extended duration runs. Additionally, the X-ray generator was operated at settings of 35 mA current and 40 kV voltage. The high-resolution data acquisition and precise calibration ensured accurate phase identification and robust analytical results.

Sorbents were meticulously analyzed using Raman spectroscopy to evaluate their degree of graphitization. Raman spectra were acquired with a LabRAM HR 800 Evolution confocal Raman microscope (HORIBA Scientific), employing 532 nm wavelength (green light) radiation and a 50x visible objective. The spectral data were meticulously collected over a range of wavelengths spanning from 2250 to 650 cm^{-1}. To ensure accuracy and clarity, all Raman spectra underwent baseline correction and normalization before further deconvolution analysis.

The analysis of samples utilizing thermogravimetric methods was performed using a NETZSCH STA 409 PC/PG system. This sophisticated instrument facilitates comprehensive thermal characterization by monitoring mass changes as a function of temperature. The thermal analysis was conducted across a range from 30 to 1100°C with a heating rate of 30.0°C/min. The sample measurements were executed under controlled conditions, ensuring precise and reliable data on thermal stability and composition. The system's advanced calibration and high-resolution capabilities provided detailed insights into the material's thermal behavior and decomposition characteristics, thereby enabling a thorough evaluation of the sample's thermal properties.

The surface functional groups of the biochar and its feedstocks were examined using Fourier Transform Infrared Spectroscopy (FTIR) to elucidate the interactions between the dye and the biochar surface. Post-adsorption characterization of various biochars was also performed to illustrate these interactions in detail. Each spectrum was obtained via attenuated total reflectance (ATR) mode, utilizing a PerkinElmer Spectrum Two IR spectrometer, which was outfitted with a Pike ATR accessory featuring a diamond crystal. IR spectra were recorded within the wavenumber range of 4000 to 400 cm^{-1}, employing 64 scans with a resolution of 4 cm^{-1}. This thorough analysis enabled a comprehensive assessment of the chemical interactions and functional group modifications occurring on the biochar surfaces. The results provided insight into the adsorption mechanisms and effectiveness of the biochars in dye removal.

3.3. Conducted adsorption experiments for different dyes

To conduct the adsorption experiments, it was essential to prepare solutions with precise dye concentrations. Initially, a solution of 500 ppm (0.5 g) was formulated using an anionic reactive industrial dye, Bezaktiv Blue HP-R, also known as Reactive Blue 221 [112]. This dye was meticulously dissolved in a 1 L volumetric flask, with distilled water added incrementally until the total volume reached 1 L. Following the preparation, thorough agitation of the mixture was imperative to achieve complete homogenization. Consequently, a dilution of the 500 ppm Bezaktiv Blue HP-R solution was carried out by preparing 1 L of a $6.5x10^{4}$ M acetic acid solution (99% Honeywell), to change the solution of dye to a pH of 4. This choice was made because anionic dyes form more efficient bonds with adsorbents in acidic conditions [115]. Acetic acid was selected for its sustainability, as it can be derived from biomass oxidation or pyrolysis bio-oil, in stark contrast to conventional strong acids, which are generally sourced from non-renewable resources [127,128].

For the dilution, 500 mL of the initial 500 ppm dye solution was mixed with 1000 mL of the acetic acid solution, achieving a 1:3 dilution ratio, which resulted in a final dye concentration of 167 ppm. It is important to note that this preparation process was applied to the three elemental dye colorants included in the study: Bezaktiv Blue HP-R, Bezaktiv Yellow HP-NP, and Bezaktiv Red HP-3B. Each final solution was then transferred to a volumetric flask, wrapped in aluminum foil, and stored in a light-free environment to preserve its stability. Figure 23 demonstrates the coloration of the different solutions prepared with the elemental reactive dyes, previously mentioned. It's important to note that mixtures of reactive dye solutions (RDS) were made through the mixing of an equal mass proportion (1:1), of the elemental colors of RDS, to produce more solution colors, such as green and purple.

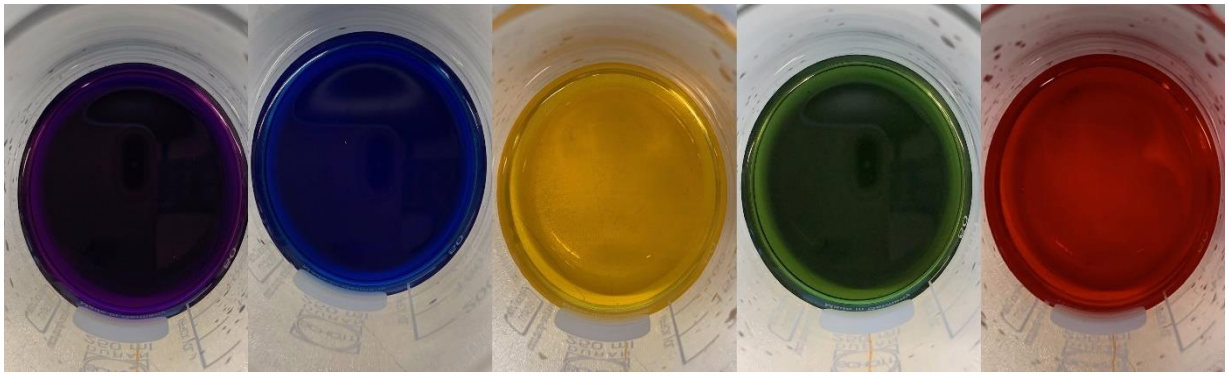

Figure 23 - Distinct solution colorations prepared from Bezaktiv industrial dyes

After meticulously preparing the solutions with a precise dye concentration, experiments were conducted in round-bottom, one-neck glass flasks, which were heated by an electrical resistance apparatus (AGIMAN 7000272) ensuring a controlled temperature environment and consistent agitation. Several adsorption experiments were carried out, each introducing biochar (1g) into the pre-prepared solutions (100 mL) once the desired thermal conditions were attained (40°C) and a pH level of 4. The adsorption system's agitation was facilitated through a magnetic stirring bar (900 rpm), optimizing the contact between the biochar and dye, thereby enhancing the adsorption rate. At predetermined intervals of 15, 30, 45, and 60 min, a 5 mL sample of the solution was carefully extracted using a plastic syringe. This sampling process was conducted to monitor the progress of the adsorption process over time. Upon reaching the predetermined contact duration (60min) between the reactive dye solution (RDS) and the biochar, the sorbent was meticulously separated from the solution via vacuum filtration, employing FILTER-LAB® filter papers characterized by pore apertures of 5-7 µm. Each specific elemental dye concentration in the filtrate was precisely quantified by referencing a calibration curve, obtained for the absorbance at a specific wavelength correlating to the respective reactive dye solution (RDS). This calibration curve was generated using a JASCO V-750 UV-visible spectrophotometer through the analysis of various standard solution concentrations. Figures 24 through 26 elucidate the distinct calibration curves, used for the determination of the adsorption capacity of each sample, for the reactive blue dye solution (RBDS), the reactive red dye solution (RRDS), and the reactive yellow dye solution (RYDS), respectively.

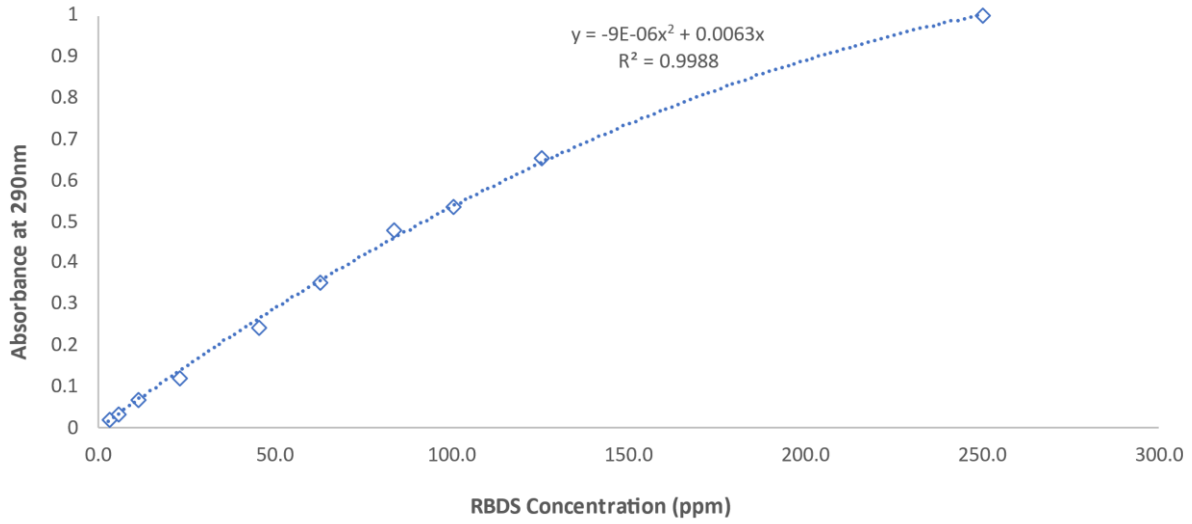

Figure 24 - Calibration curve for obtaining RBDS concentration as a function of absorbance at 290 nm

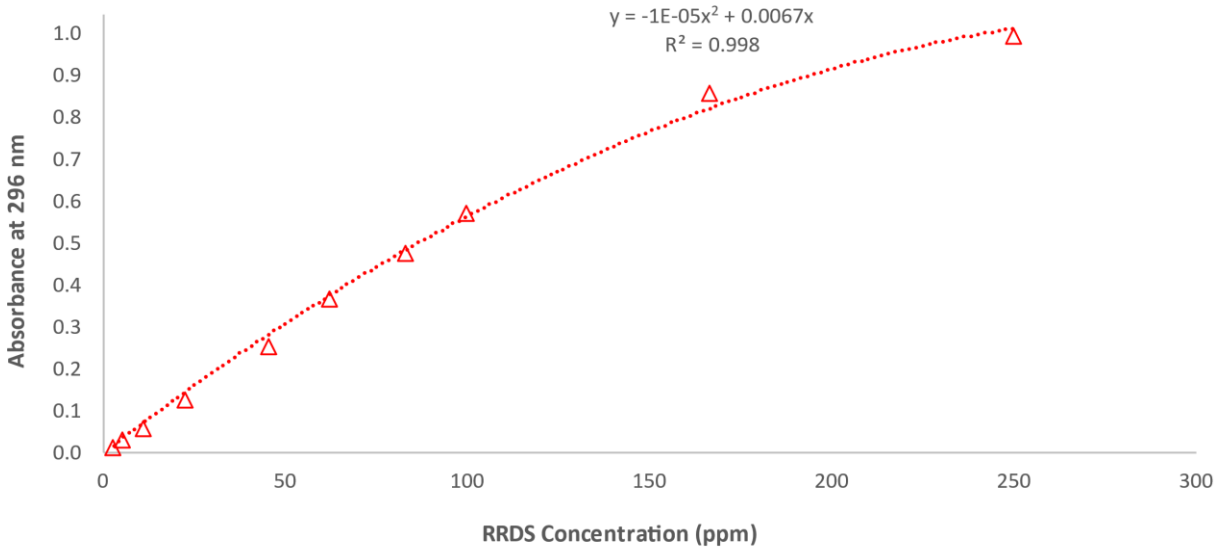

Figure 25 - Calibration curve for obtaining RRDS concentration as a function of absorbance at 290 nm

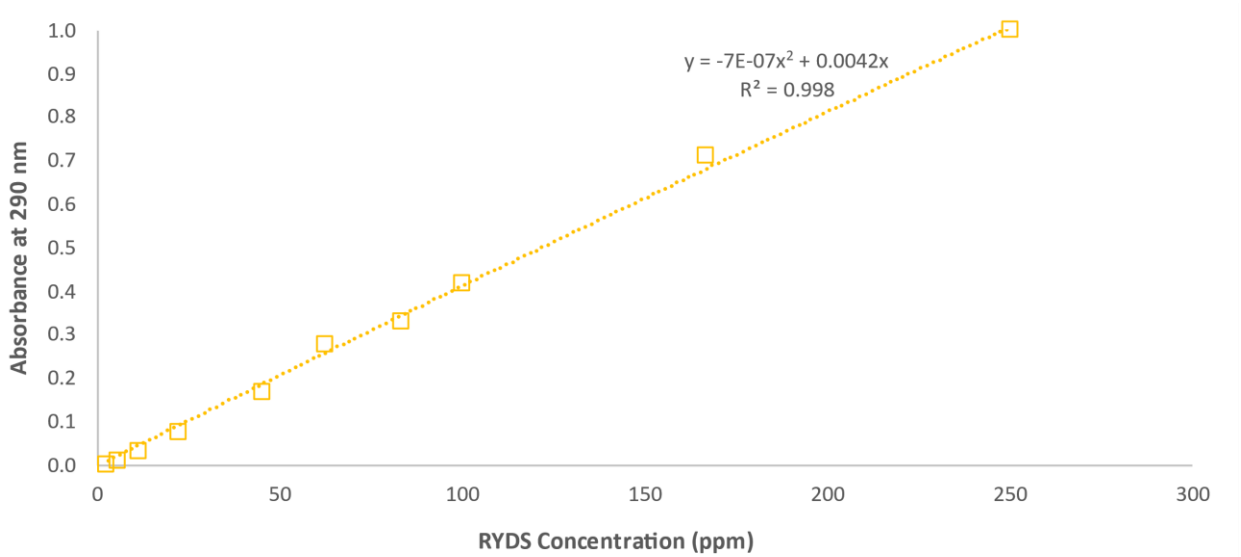

Figure 26 - Calibration curve for obtaining RYDS concentration as a function of absorbance at 290 nm

The removal efficiency percentage of the reactive dye solution (RDS) was ascertained using Equation 2, where C_0 and C_t (mg L^{-1}) represent the initial and residual reactive dye concentrations in the solution after t contact time [129].

$$RDS\ removal\ efficiency\ (\%) = \frac{C_0 - C_t}{C_0} \times 100 \quad (2)$$

The formula provided is essential for calculating the removal efficiency percentage of dye from the reactive dye solution (RDS), making it crucial in assessing how effectively the biochar samples prepared are capable of removing the dye from a solution over time. Further data resembling the influence of concentration in the absorbance levels, is evidenced in the Appendix data, for each sample.

4. Results and Discussion

4.1. **Characterization of Biochar properties**

4.1.1. XRD

The biochar samples were submitted to a XRD analysis in order to study the different crystalline phases of the derived chars produced from different types of biomass feedstocks. Figure 27 to 29 shows the distinct diffractograms of the Mix Macroalgae Biochar (BMM); Avocado Leaves Biochar (BAL); and Rice Husk Biochar (BRH) samples respectively, while the BPS sample was not presented due to the lack of carbonate materials on its spectrum, with the predominant amorphous structures being noted with broad bands.

The BMM sample, illustrated at Figure 27, demonstrates various materials, such as carbonate minerals (e.g., calcite ($CaCO_3$)); chlorides (e.g., sylvite (KCl) and halite (NaCl)); and quartz (SiO_2), due to the fact that some of the crystalline phases present in the macroalgae did not suffered a transformation during the carbonization process, and are of marine origin, with some of the salts being related to the shell remnants in the biomass, or from the evaporation of seaweed moisture [130].

Also, all the sylvite standard bands can be observed, from 2θ=5° to 2θ=70°, with the diffraction peaks of KCl (200; 220; 222) at 2θ=28.3°; 2θ=40.5°; 2θ=50.2°; respectively, being indexed to a cube with a middle face structure [131]. The pattern of peaks and their sharpness indicate well-crystallized phases, while the baseline level and smaller peaks suggest the presence of amorphous or less crystalline components [132]. Macro-nutrients (e.g., nitrogen; phosphorus; potassium; and sulfur) are usually present in the nutritional composition of macroalgae's, which at various temperatures can form mineral phases such as arcanite (K_2SO_4) in biochar samples, with multiple peaks illustrated at Figure 27 [133,134].

Figure 28 represents the BAL sample, with the main observed crystalline phases being correlated to the presence of a chloride (sylvite), since this specific crystalline phase was not transformed through the carbonization, as previously stated [130]. Therefore, calcium oxalate (whewellite) is accumulated in the tissues of the plant corpse and leaves (e.g., avocado leaves) [135]. There is evidence of multiple diffraction standard peaks of this mineral illustrated at the diffractogram in Figure 28, with the higher peaks (100; 021; 040) located at 2θ=14.9°; 2θ=15.3°; 2θ=24.4°, respectively [136].

The BRH sample, illustrated at Figure 29, showed a predominantly mineral presence of quartz (SiO_2) originated from the transformation of amorphous SiO_2 during rice husk pyrolysis [137]. Diffraction peaks of quartz (101; 102; 112) can be seen at 2θ=26.7°; 2θ=39.5°; 2θ=50.2°, while the band fixed between 2θ=18° and 2θ=32° is correlated to the presence of the unreacted SiO_2, characterized as amorphous due to the huge widespread of the band, that indicates the non crystalline nature of the material presented between those values [132,138,139].

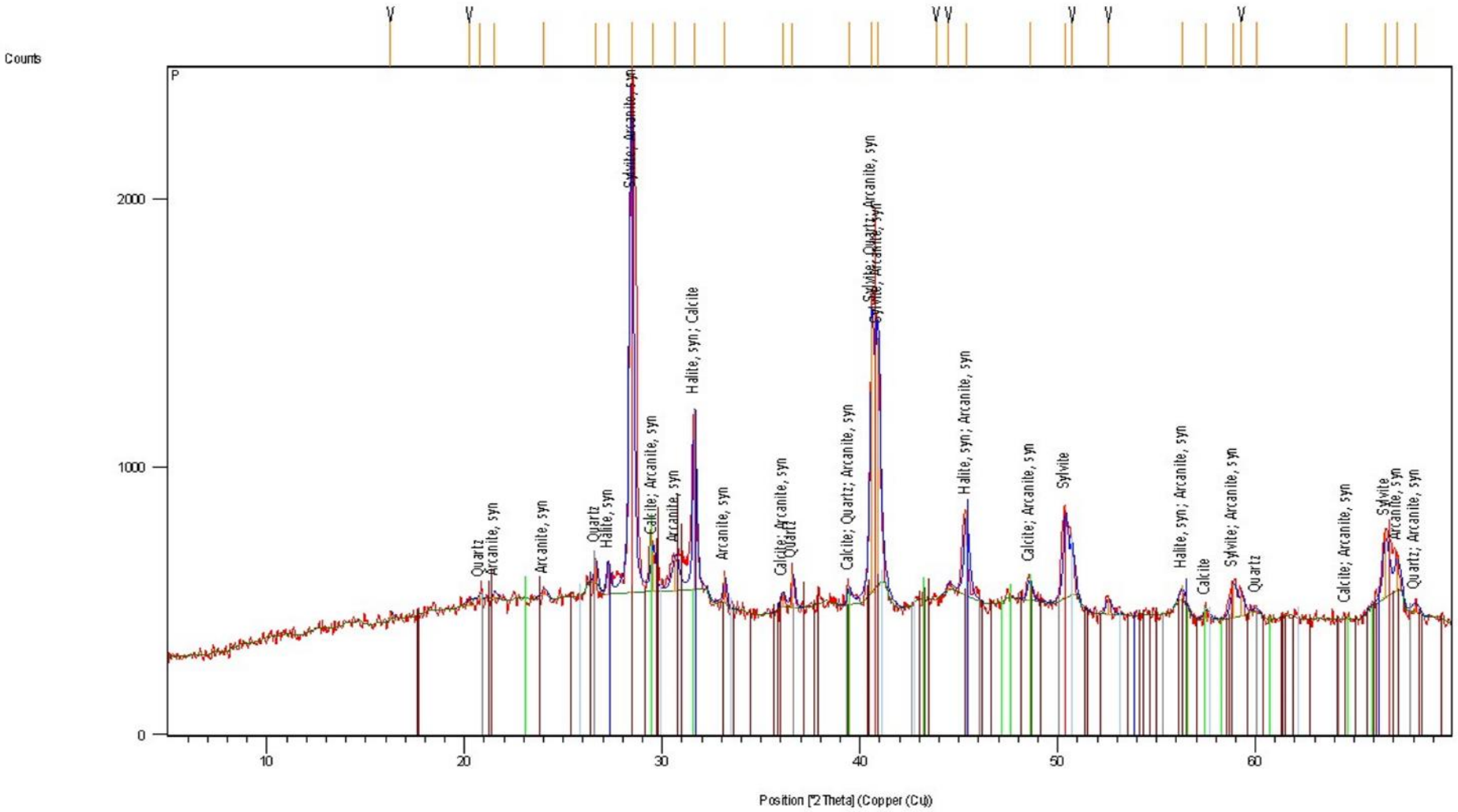

Figure 27 - X-ray diffraction pattern for the BMM sample

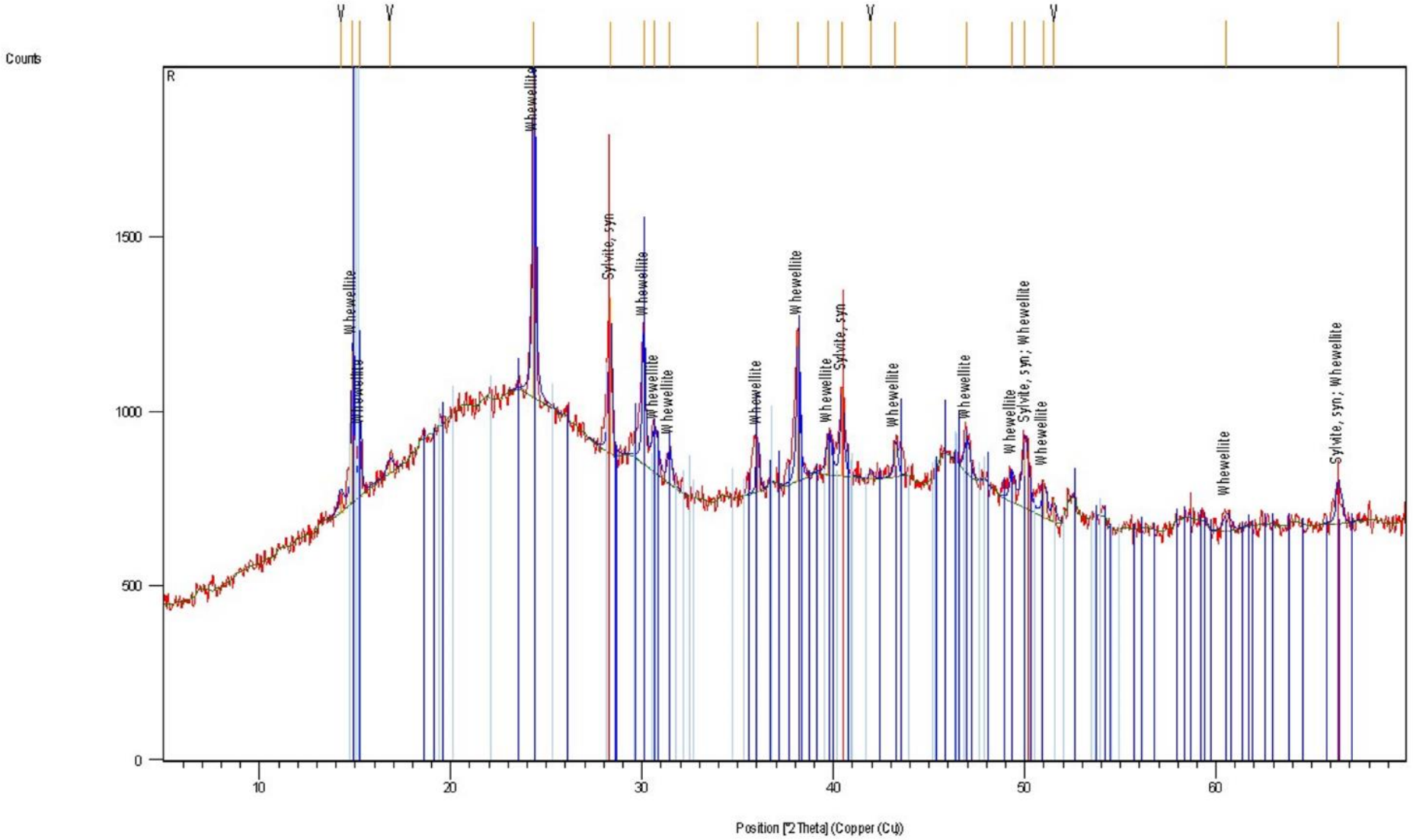

Figure 28 - X-ray diffraction pattern for the BAL sample

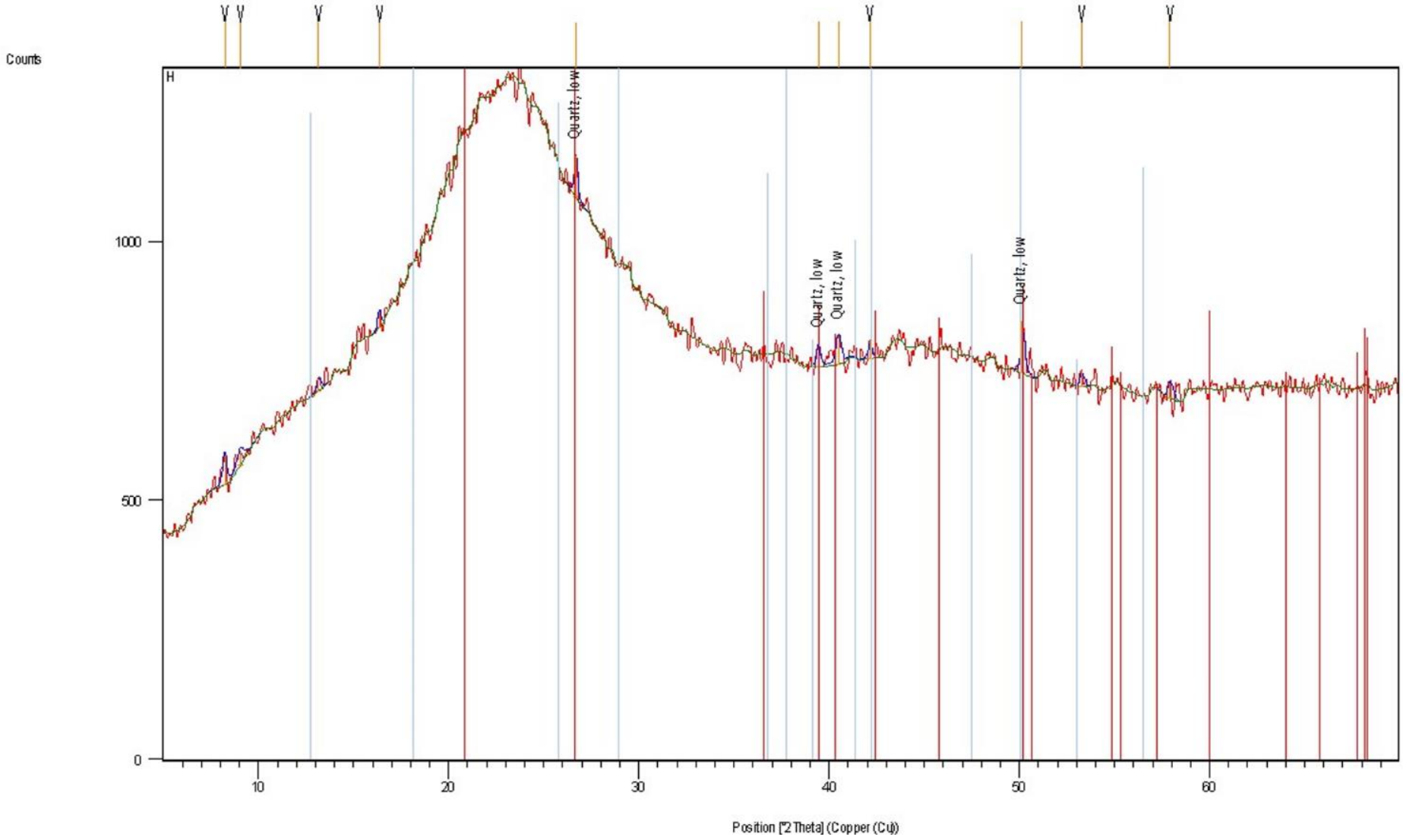

Figure 29 - X-ray diffraction pattern for the BRH sample

4.1.2. ATR-FTIR

Following the identification of the crystalline phases, the samples were further examined using Attenuated Total Reflectance Fourier-Transform Infrared (ATR-FTIR) spectroscopy to observe the functional groups present in each sample. The spectral analysis was conducted across a wavenumber range of 720 to 3600 cm^{-1}, facilitating the identification of specific vibrational bands associated with different chemical bonds and structures, visible in Figure 30.

In the ATR-FTIR spectrum of the BRH sample, distinct peaks were observed, with different molecular vibrations. A minor peak at 800.21 cm^{-1} was attributed to the Si-H stretching vibration [140]. This band is typically associated with silanol groups (Si-H), suggesting that despite the high-temperature pyrolysis process, some residual silanol functionalities remain within the biochar structure [140].

The low intensity of this peak indicates that Si-H bonds are not predominant in the sample, which aligns with the expected transformation of rice husk into biochar, where most silanol groups are likely converted into more stable siloxane (Si-O-Si) structures [140]. A prominent peak at 1069.93 cm^{-1} was identified as corresponding to the Si-O-Si asymmetric stretching vibration [140]. This peak is a hallmark of silica-rich materials, indicating a significant presence of silicon dioxide (SiO_2) in the biochar sample [140].

The high intensity of this band underscores the high silica content, characteristic of biochars derived from rice husk due to the high inorganic content of the precursor material [140]. A slight bump at 1218.32 cm^{-1} indicated the presence of C-O-C stretching vibrations, suggesting that ether-like structures or anhydrides may be present in the biochar, possibly as a result of the partial degradation of cellulose or hemicellulose during pyrolysis, while the presence of these structures implies that some organic components have survived the pyrolysis process, potentially affecting the surface chemistry and reactivity of the biochar [140].

Additionally, the bands observed at 1446.21 cm^{-1} and 1600.02 cm^{-1} were indicative of C=C stretching vibrations within aromatic rings [140]. These peaks are characteristic of the aromatic structures formed during the carbonization process, with the presence of these aromatic vibrations suggesting a high degree of aromaticity in the biochar, which is typical for biochar produced at high temperatures and is associated with their stability and resistance to further thermal degradation [140].

A low-intensity band at 1650.24 cm^{-1} was identified, corresponding to the C=C stretching vibration typical of alkenes, suggesting the presence of unsaturated carbon-carbon bonds in the biochar, which may result from incomplete carbonization of the precursor material [140]. The C=C alkene stretch, though less prominent than the aromatic C=C vibrations, indicates that some degree of unsaturation is retained in the biochar's carbon structure [140].

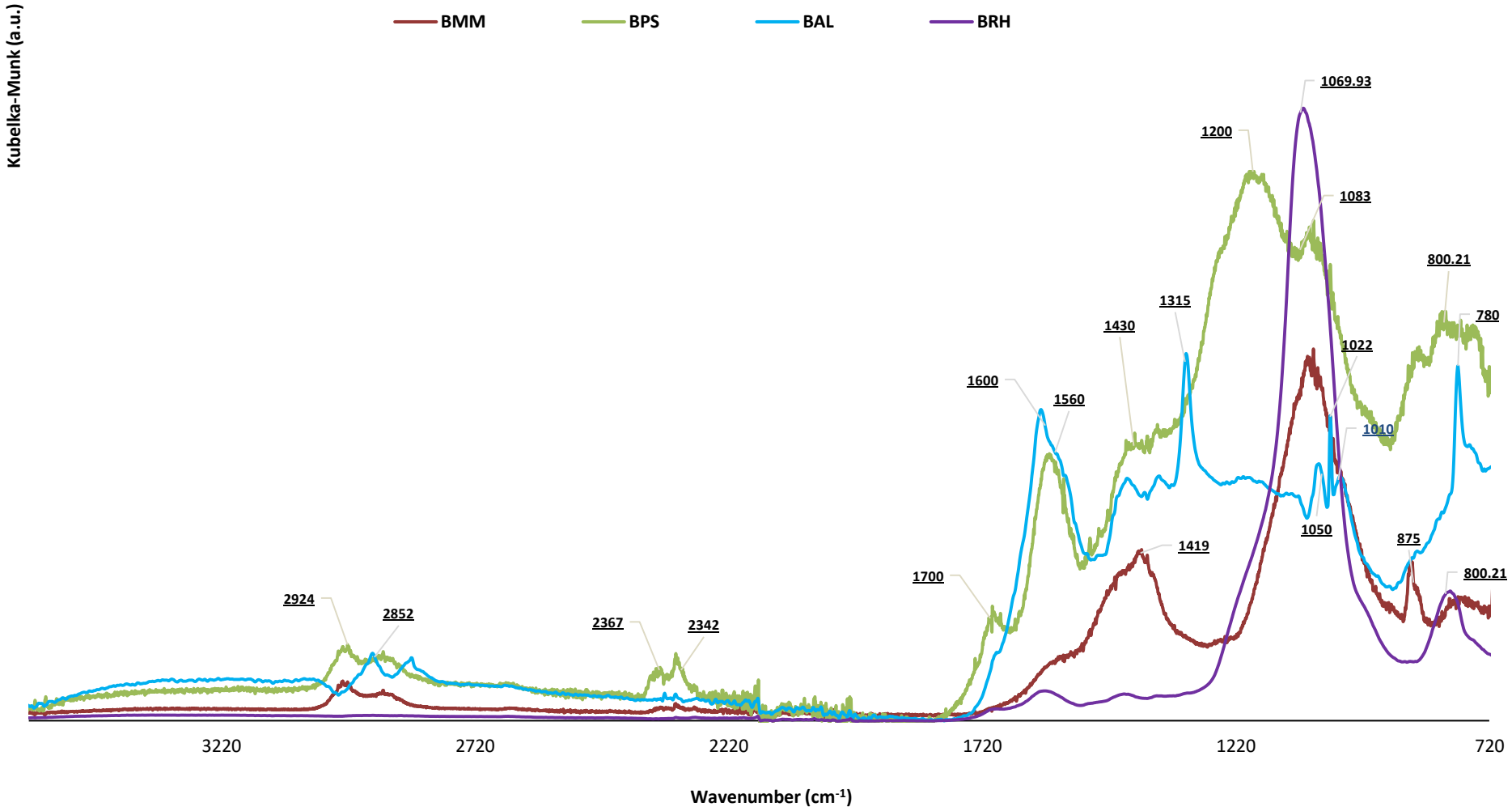

Figure 30 - ATR-FTIR spectra of the BMM; BPS; BAL; and BRH sample between 720 and 3600 cm-1

In the ATR-FTIR spectrum of the BMM sample, several key peaks were observed, each corresponding to distinct molecular vibrations. A band at 875 cm^{-1} was identified, indicative of the presence of carbonate (CO_3^{2-}) minerals [141]. The identification of this carbonate band, along with another prominent carbonate-related band at 1419 cm^{-1}, suggests the presence of calcite ($CaCO_3$) in the biochar, consistent with findings from the X-ray diffraction (XRD) analysis [142]. These bands confirm the retention of inorganic carbonate minerals in the biochar, which could be a result of the original mineral content in the macroalgae precursor material [141,142]. A notable peak centered at 1083 cm^{-1} was attributed to the stretching vibrations of aliphatic amines (C-N) and/or the C-O stretch of phenolic compounds and alcohols [143,144].

The band centered at 1582 cm^{-1} was likely due to the presence of carboxylate (COO^-) groups within the BMM sample, correlating strongly with C=C stretching vibrations in aromatic rings [145]. This peak suggests that the biochar retains some degree of carboxylation, which may be a result of the partial decomposition of polysaccharides and proteins in the macroalgae during pyrolysis [146]. The presence of aromatic C=C stretches indicates a degree of aromaticity, reflecting the formation of stable, conjugated carbon structures in the charred material [145,147]. Furthermore, the presence of aliphatic methylene ($-CH_2$) C-H stretching vibrations was identified at bands centered at 2924 cm^{-1} and 2852 cm^{-1} [148]. These bands are characteristic of long-chain hydrocarbons, which may persist in the biochar due to incomplete pyrolysis of the macroalgae's lipid components [148]. The retention of these aliphatic structures suggests that the biochar has a diverse chemical composition, potentially influencing its hydrophobicity, surface reactivity, and interaction with other organic compounds [148].

In the ATR-FTIR spectrum of the BAL sample, multiple peaks were observed at Figure 30. A narrow band located at 780 cm^{-1} was identified as indicative of an aromatic C-H vibration [149]. This band suggests the presence of aromatic rings within the biochar structure, likely derived from the lignin and other aromatic compounds in the avocado leaves [149]. The sharpness of this band indicates well-defined aromatic structures, which are typically formed during the pyrolysis process as the organic material is converted into stable carbon-rich compounds [149]. Between 1010 and 1050 cm^{-1}, several bands were identified. At 1010 cm^{-1}, the presence of phosphate (PO_4) bonds was detected, likely due to the phosphorus content naturally present in the avocado leaves [150].

Phosphorus is a vital element in plant tissues, and its presence in the biochar could enhance the material's nutrient retention capabilities, making it useful for agricultural applications [150]. The narrow peak at 1022 cm^{-1} corresponds to the stretching vibration of C-O groups, while the band at 1050 cm^{-1} is attributed to the C-OH stretching vibration [151,152]. These bands suggest the presence of oxygen-containing functional groups, such as alcohols and phenolics, which may influence the biochar’s reactivity and adsorption properties [151,152]. A band at 1315 cm^{-1} was identified as corresponding to CH bending vibrations [153]. This band indicates the presence of aliphatic hydrocarbons, which may have survived the pyrolysis process [153]. Additionally, at 1362 cm^{-1}, a C-N stretching vibration for aromatic amines was noted [154]. The presence of these nitrogen-containing functional groups could be significant for the biochar's ability to interact with other organic molecules or serve as a medium for nutrient exchange in soil applications [154].

From 1400 to 1700 cm^{-1}, several peaks were found that are indicative of C=C aromatic stretching vibrations, more precisely, these peaks were observed at 1430 cm^{-1}, 1560 cm^{-1}, 1600 cm^{-1}, and 1695 cm^{-1} [155,156,157]. The presence of multiple bands in this region suggests a high degree of aromaticity within the BAL sample, reflecting the formation of stable, conjugated carbon structures [155,156]. These aromatic C=C stretches indicate the presence of condensed aromatic rings, which are a key feature of biochar's structure and are associated with its long-term stability and resistance to degradation [156,157]. Furthermore, the presence of aliphatic methylene (-CH_2) C-H stretching vibrations was identified at bands centered at 2924 cm^{-1} and 2852 cm^{-1} [148]. These bands are characteristic of long-chain hydrocarbons, as seen in the BMM sample, that may persist in the biochar due to incomplete pyrolysis [148].

For the ATR-FTIR spectrum of the BPS sample, distinct molecular vibrations were observed throughout the different peak regions. A band centered at 800.21 cm^{-1} was identified as indicative of a Si-H stretching vibration [140]. This band suggests the presence of silanol groups within the biochar, likely originating from the silicate content in the peanut shells [140].

The persistence of this Si-H stretch indicates that some silanol groups survived the pyrolysis process, contributing to the inorganic matrix of the biochar [140]. Between 850 and 875 cm^{-1}, a broad band was observed, indicating the presence of carbonate (CO_3^{2-}) minerals, along with C-H asymmetric bending vibrations [141]. The carbonate band suggests the presence of calcite or similar carbonate minerals, which may have been retained from the original biomass or formed during the pyrolysis process [141]. The C-H bending vibrations in this region also indicate the presence of aliphatic or aromatic hydrocarbons, which contribute to the complex organic structure of the biochar [141].

A peak at 1083 cm^{-1} was attributed to the stretching vibrations of aliphatic amines (C-N) [143]. This indicates the presence of nitrogen-containing functional groups within the biochar, likely derived from proteins or other nitrogenous compounds in the peanut shells [143]. These amine groups could play a role in the biochar's potential for nutrient retention or interaction with other organic molecules in environmental applications [143]. The broad band observed around 1200 cm^{-1} was identified as being due to several functional groups, including both inorganic and organic silicon compounds, phosphorus compounds, as well as C-O stretching and sulfate groups [158].

This complex band suggests that the BPS sample contains a mixture of functional groups, which could enhance its chemical reactivity and interaction with various contaminants or nutrients in soil or water environments [158]. A band centered at 1430 cm^{-1} was indicative of C=C stretching vibrations within aromatic rings [155]. The aromaticity of the biochar is further supported by the band at 1582 cm^{-1}, which is attributed to COO^- groups, again associated with C=C stretching in aromatic rings [145]. These aromatic and carboxylate groups indicate that the biochar retains a complex and stable carbon matrix, which is resistant to degradation [145]. At 1700 cm^{-1}, a defined band was correlated with the stretching vibrations of carboxyl (C=O) groups [156].

This band suggests the presence of carboxylic acids or esters within the biochar, which may result from the partial oxidation of organic matter during pyrolysis [156]. The presence of COO^- stretching vibrations was further confirmed by a band at 2342 cm^{-1}, indicating the presence of acetate ions [159]. This band suggests that some organic acids, such as acetic acid, may have survived the pyrolysis process or were formed during the thermal decomposition of the biomass [159]. Additionally, a band at 2367 cm^{-1} was attributed to S-H stretching vibrations, confirming the presence of sulfur-containing groups, possibly in the form of thiols or sulfides [159]. The presence of sulfur in the biochar could influence its reactivity and its ability to interact with heavy metals or other pollutants in environmental applications [159]. As seen in other samples, the presence of aliphatic methylene ($-CH_2$) C-H stretching vibrations was identified at bands centered at 2924 cm^{-1} and 2852 cm^{-1}, due to the incomplete pyrolysis process [148].

4.1.3. Raman

The Raman spectra analysis was made for the biochar samples, that exhibited a better adsorption rate, produced at 350°C from rice husk (BRH), avocado leaves (BAL), and peanut shell (BPS) revealing important insights into their structural properties. Figure 31 display the distinctive bands typical of biochar, with the most prominent peaks occurring between 1350-1370 cm^{-1} and 1580-1600 cm^{-1} [160]. These peaks correspond to the vibrational modes of sp^2-hybridized carbon atoms, where the former peak (D-band) is associated with structural defects, and the latter (G-band) is linked to graphitized carbon structures [160]. The intensity and shape of these bands provide crucial insights into the degree of disorder and graphitization within the biochar samples, while the spectral information is essential for understanding the material's structural properties and potential applications [160].

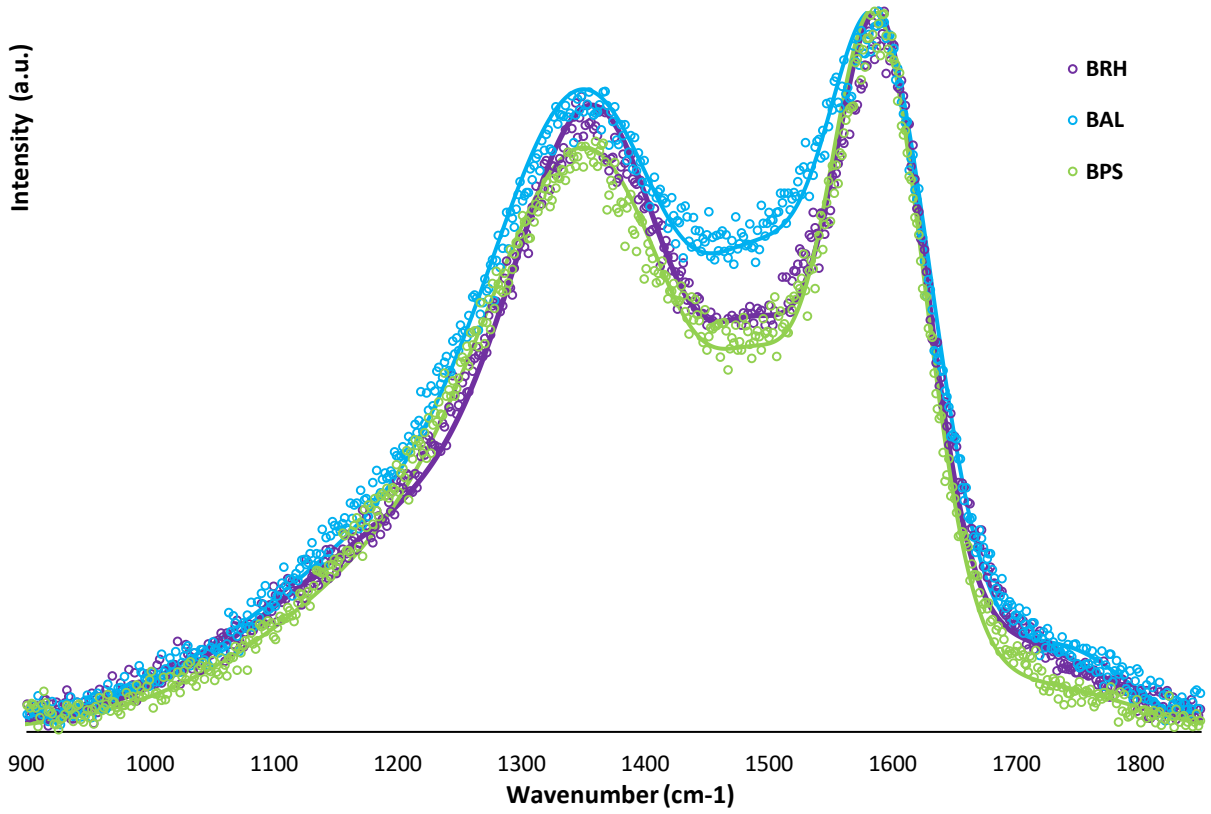

Figure 31 - Raman spectra comparing the D and G band intensity between BRH; BAL; and BPS samples

The D-band areas for BRH, BAL, and BPS are 97.9; 116.9; and 97.8, respectively, while the G-band areas are 86.2; 104.9; and 92.7. These values suggest that BAL exhibits the highest carbon content, as reflected in the largest D-band and G-band areas among the three samples [160].

Table 5 – Graphitization index (I_D/I_G) and the respective band intensity of the BRH; BAL; and BPS samples

Sample	BRH (350°C)	BAL(350°C)	BPS(350°C)
I_{Dband}	97.9	116.9	97.8
I_{Gband}	86.2	104.9	92.7
I_D/I_G	1.11	1.08	1.02

Therefore, the I_D/I_G ratio can predict the biochar graphitization degree, as the lower this ratio is, the closer to non-defective pure graphite is the biochar structure, while also considered a key factor of the amorphous composition of the carbon materials, indicating that a higher ratio is correlated to a lower degree of graphitization [161,162]. The I_D/I_G ratio stands at 1.08 for BAL, 1.11 for BRH, and 1.02 for BPS, which suggests that the BAL sample is relatively more graphitic compared to BRH but slightly less so than BPS [160].

In contrast, BRH, with the highest I_D/I_G ratio of 1.11, shows the greatest degree of disorder, as the larger D-band area relative to the G-band area indicates more defects within its carbon structure [161]. The significant lower values related to the I_D/I_G can be related to the fact that a sample presents a larger particle size and fewer edge defects on its structure, moreover, an increased degree of graphitization can potentially enhance adsorption capacity through π-π interactions, however, this same characteristic might also limit adsorption efficiency due to a reduction in available adsorption sites, often resulting from the diminished presence of heteroatom doping [162,163].

Gao et al. (2022) have reported that the characterization of various biochar samples revealed a correlation between higher doping ratios and a decrease in both the degree of graphitization and surface oxygen (O) content, while surface nitrogen (N) content exhibited an increase [164]. Therefore, it should be noted that the adsorption capacity is positively associated with the surface O content and the degree of graphitization, while negatively associated with the surface N content [164].

4.1.4. TGA

The thermogravimetric analysis (TGA) illustrated at Figure 32 shows the thermal degradation profiles of the three biochar samples: BRH (rice husk biochar), BAL (avocado leaves biochar), and BPS (peanut shell biochar). TGA measures the rate of thermal degradation (in wt.-%/min) as a function of temperature, providing insights into the thermal stability and composition of the materials [165]. The BRH sample exhibits a relatively smooth degradation curve with significant weight loss occurring in two stages, with the first major degradation event occurring between approximately 100°C and 130°C, suggesting that could be related to the evaporation of water adsorbed from moisture [166]. The second degradation stage starts at about 280°C with the completion being observed at, approximately, 460°C which could be attributed to the decomposition of lignin [167].

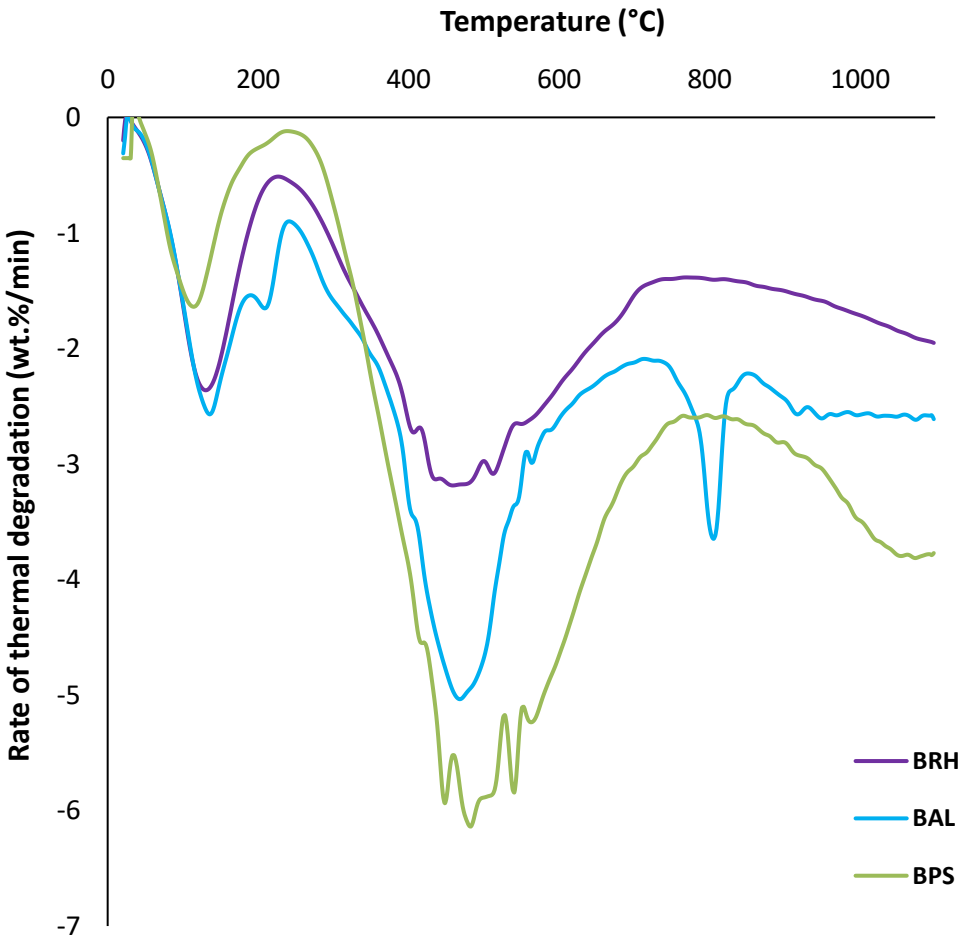

Figure 32 - Thermogram of BRH; BAL; and BPS samples

The BAL sample shows a more complex degradation pattern with multiple stages of weight loss, more precisely between 100°C and 130°C (first stage); at 170°C to 200°C (second stage); at 280°C and 460°C (third stage); and at approximately 800°C (fourth stage). The first degradation stage that occurs is likely due to the release of moisture, as previously seen [166]. The second degradation peak is visible at, approximately, 200°C and indicates the decomposition of organic matter, such as side chains and light molecular compounds [168]. The major degradation event, similar to BRH, occurs between 280°C and 460°C, suggesting the thermal breakdown of lignin [167].

However, the presence of a fourth degradation event, specifically around 750-800°C, is due to the thermal decomposition of whewellite (calcium oxalate monohydrate, $CaC_2O_4 \cdot H_2O$), which corresponds to the decomposition of calcium carbonate ($CaCO_3$), formed as an intermediate product during the decomposition of calcium oxalate, into calcium oxide (CaO) and carbon dioxide (CO_2) [169]. The BPS sample has a similar degradation profile to the BRH sample, with the most prominent weight loss occurring between 280°C and 460°C [166]. However, BPS exhibits a more gradual and extended degradation curve, indicating that it contains a broader range of thermal degradation products, with multiple small peaks in the degradation rate main peak, likely due to the presence of both volatile and stable carbon structures [166].

4.1.5. SEM-EDS

In order to better comprehend the morphology of the samples, previously stated, a SEM analysis was made for each biochar, with a magnification of 160x. Figure 33 illustrates all the four samples surfaces, with the imaging conditions being associated with a 15.0 kV accelerating voltage using a mixture of signals of 50%.

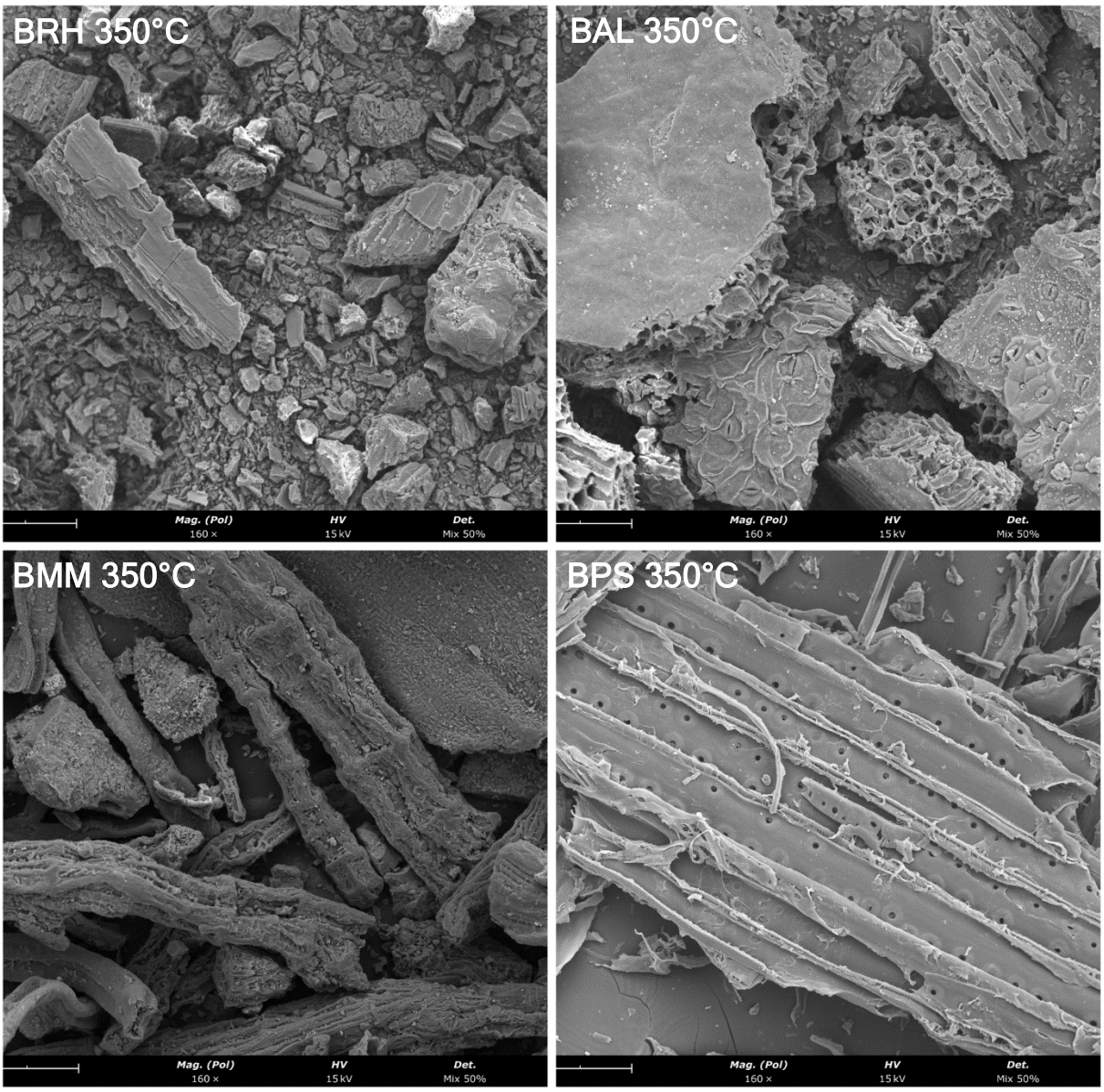

Figure 33 - SEM micrographs of BRH; BAL; BMM; and BPS samples, obtained with a magnification of 160x

By the comparison of the different samples images, it's clear that the BRH sample exhibited rough surfaces and irregular shapes, with many small aggregates inferior to 50 µm. On the other side, samples such as the BAL showed smooth surfaces with larger aggregates, in some cases larger than 200 µm. These differences might be correlated with the nature of the samples, or to the milling intensity. BMM and BPS demonstrated elongated structures with well defined edges. Tables 6 and 7, show the atomic percentage of the different elements found in these samples, by EDS analysis.

Table 6 - Atomic % of carbon and oxygen, and the O/C atomic ratio for the biochar samples, determined by EDS analysis

Atomic % / Sample	C	O	O/C
BRH	61.36	28.69	0.47
BAL	76.22	18.02	0.24
BMM	51.68	9.30	0.18
BPS	84.34	13.53	0.16

Table 7 - Atomic % of inorganic elements for the biochar samples, determined by EDS analysis

Sample / Atomic %	BRH	BAL	BMM	BPS
Mg	0.07	0.26	2.63	---
Si	8.42	---	0.57	---
K	0.85	3.39	9.22	---
Na	---	---	4.17	---
Al	---	---	0.51	---
Cl	---	0.44	9.65	---
Ca	---	0.71	1.31	---

In Table 6, it is clear that the BRH sample got the higher O/C atomic ratio, which can be related to the performance of this sample in terms of adsorption capacity. This ratio is related to the polarity of the biochar samples, in a directly proportional way, which means that the fact that the ratio is higher in this sample, indicates that the polarity for the BRH is also higher [170]. Furthermore, a higher polarity of the adsorption material, favors the adsorption of polar compounds, such as the reactive dyes, desired to remove from the aqueous solutions [171]. The inorganic elements categorized, in Table 7, by each biochar sample, corroborate the previously analysis made, since the BPS does not exhibit any mineral crystallographic structure, as in XRD. The BRH shows a high silica content in it's structure, as also seen by FTIR analysis, while the macroalgae derived biochar got the most inorganic elements, since this biomass is a natural adsorber of minerals [172].

4.2. Reactive dye solution remotion capacity

The data presented in Table 8 shows the efficiency of different biochar samples, in removing reactive dye solutions from water, expressed as a percentage of dye removal. The biochar samples are derived from rice husk (BRH); avocado leaves (BAL); peanut shells (BPS); and mixed macroalgae (BMM). Each biochar was tested into several reactive dyes, such as Bezaktiv Blue HP-R; Bezaktiv Red HP-R; Bezaktiv Yellow HP-R; and combinations such as Bezaktiv Yellow + Blue HP-R (Green); and Bezaktiv Blue + Red HP-R (Purple).

The results show that BRH is the most efficient biochar in removing the coloration from the different solutions, since it exhibits excellent removal for all individual dyes, particularly Bezaktiv Blue HP-R (99.2%) and Bezaktiv Red HP-R (81.4%), while still maintaining high removal for Bezaktiv Yellow HP-R (76.4%). For mixed dyes, BRH shows an outstanding performance, achieving 94.8% removal for the Green dye mixture and complete (100%) removal for the Purple dye mixture. Similarly, BAL performs almost as well, with high removal efficiencies for Bezaktiv Blue HP-R (94.8%) and Red HP-R (83.6%). Although slightly less efficient in removing Yellow HP-R (75.5%), it maintains excellent removal for the Purple dye mixture, reaching nearly 99.9%. In comparison, BPS (Peanut Shell Biochar) performs well in some cases but is generally less effective. While it shows high removal for Bezaktiv Yellow HP-R (94%), its removal efficiency for Bezaktiv Red HP-R (70.7%) Green (78%) and Purple (91.2%) mixtures is lower than that of BRH and BAL. Finally, BMM consistently shows the lowest performance, particularly for Bezaktiv Yellow HP-R (58.2%) and Bezaktiv Red HP-R (69.1%). The superior performance of BRH and BAL can be attributed to their chemical and physical properties, which make them more effective adsorbents compared to the other biochar samples since rice husk and avocado leaves are rich in lignocellulosic materials, which upon pyrolysis, produce biochar with a high surface area and porous structure [173,174,175].

Rice husk has a high silica content and a well-developed microporous structure after pyrolysis, which increases its surface area and improves the adsorption capacity [176]. The presence of oxygen-containing functional groups (such as hydroxyl, and carbonyl groups) on the biochar surface increases the chemical interaction with dye molecules, enhancing the adsorption process [177]. Additionally, the ash content in rice husk can increase the pH of the solution, promoting electrostatic interactions between the negatively charged dye molecules and the positively charged biochar surface [178]. Avocado leaves, on the other hand, contain various phytochemicals that might contribute to higher adsorption efficiency after conversion into biochar, since the presence of functional groups like phenols and alcohols in the avocado leaves may form complex interactions with the dye molecules, enhancing removal efficiency [179]. In contrast, BPS and BMM have different compositions that may explain their relatively lower adsorption capacities, thus peanut shells contain higher levels of lipids and proteins, which produce a less porous biochar structure after pyrolysis, potentially leading to lower surface areas and fewer adsorption sites [180,181]. Moreover, the high performance of some samples in the remotion of mixed solutions could be related to the interplay between the sample's surface properties and the complex structure of the dyes, since mixed dye solutions can contain multiple functional groups, such as anionic or cationic, that can interact with the biochar surface in different ways, which makes BRH and BAL, with distinct surface functional groups, better suited for the effective remotion of these mixtures [182].

Table 8 - Performance of different biochar samples on the remotion of reactive dye solutions expressed in percentage

Biochar sample	Bezaktiv Blue HP-R (removal %)	Bezaktiv Red HP-R (removal %)	Bezaktiv Yellow HP-R (removal %)	Bezaktiv Yellow HP-R + Bezaktiv Blue HP-R (Green) (removal %)	Bezaktiv Blue HP-R + Bezaktiv Red HP-R (Purple) (removal %)
BRH (Biochar of Rice Husk)	99.2	81.4	76.4	94.8	100
BAL (Biochar of Avocado Leaves)	94.8	83.6	75.5	80.8	99.9
BPS (Biochar of Peanut Shell)	90.9	70.7	94	78	91.2
BMM (Biochar of Mix Macroalgae)	92	69.1	58.2	---	---

5. Conclusions

This work investigated the properties and efficacy of different biochar samples derived from distinct biomass feedstocks, including rice husk (BRH), avocado leaves (BAL), peanut shells (BPS), and mixed macroalgae (BMM). Through detailed characterization using X-ray diffraction (XRD), Attenuated Total Reflectance Fourier-Transform Infrared (ATR-FTIR) spectroscopy, Raman spectroscopy, and thermogravimetric analysis (TGA), the study provided comprehensive insights into the structural, chemical, and thermal properties of these biochars and their performance in environmental applications, particularly in the removal of reactive dye solutions from water.

The XRD analysis revealed distinct crystalline phases in each biochar sample, reflecting the composition and transformation of the biomass during pyrolysis. For instance, the BRH biochar exhibited significant peaks associated with quartz (SiO_2), particularly at $2\theta=26.7°$ and $2\theta=50.2°$, indicating a high silica content resulting from the pyrolysis of rice husk at 350°C. In contrast, the BAL biochar displayed peaks correlated with calcium oxalate (whewellite), with major peaks at $2\theta=14.9°$ and $2\theta=24.4°$, suggesting a significant presence of this mineral in avocado leaves. These variations in mineral content highlight how different feedstocks lead to the formation of biochars with unique crystalline structures, which in turn influence their adsorption capabilities.

ATR-FTIR analysis further confirmed the presence of various functional groups that contribute to the reactivity and adsorption properties of the biochars. For example, in the BRH biochar, a prominent peak at 1069.93 cm^{-1} was identified as corresponding to the Si-O-Si asymmetric stretching vibration, indicative of high silica content. Additionally, the presence of aromatic C=C stretching vibrations in the BAL biochar, observed at around 1600 cm^{-1}, suggests a high degree of aromaticity, which is associated with the stability and adsorption capacity of these materials.

The thermogravimetric analysis (TGA) provided insights into the thermal stability of the biochars, with BRH and BPS showing significant weight loss between 280°C and 460°C, attributed to the decomposition of lignin. BAL exhibited a more complex thermal degradation pattern, with multiple stages of weight loss, including a notable event at around 750-800°C, likely due to the decomposition of calcium oxalate. The performance of these biochars in removing reactive dye solutions from water was also evaluated, with BRH and BAL biochars demonstrating superior adsorption efficiencies. Specifically, the rice husk biochar achieved an outstanding 99.2% removal efficiency for Bezaktiv Blue HP-R and 100% removal for the Bezaktiv Blue + Red HP-R (Purple) dye mixture. The BAL biochar similarly performed well, with 94.8% removal of Bezaktiv Blue HP-R and 99.9% removal of the Purple dye mixture. These results can be attributed to the high surface area and well-developed microporous structure, as well as the presence of functional groups like hydroxyl and carbonyl, which enhance chemical interactions with dye molecules.

The findings of this study underscore the potential of biochar as a sustainable solution for wastewater treatment, particularly in the removal of organic contaminants like reactive dyes. The superior performance of BRH and BAL biochars suggests that lignocellulosic materials with high silica or aromatic content are ideal feedstocks for producing effective adsorbents.

Future research should focus on optimizing pyrolysis conditions to further enhance the desirable properties of biochar, such as surface area, pore structure, and functional group density. Moreover, exploring the use of biochar in other environmental applications, such as soil amendment or heavy metal remediation, could provide additional avenues for its utilization. The development of biochar-based materials tailored for specific contaminants could significantly improve the efficiency and cost-effectiveness of water treatment processes, contributing to the broader goal of sustainable environmental management.

In conclusion, this study provides a solid foundation for understanding the properties and applications of biochar derived from various biomass sources. The results indicate that with careful selection of feedstock and pyrolysis conditions, biochar can be engineered to serve as an effective and sustainable material for environmental remediation, particularly in the area of wastewater treatment. Continued research and development in this field will be crucial for advancing the practical application of biochar in diverse industrial and environmental contexts.

6. References

[1] Venditti, S., Salmeron, I., Taffala, P., Hobus, I., Kolisch, G., Hansen, J., 2024. Biochar from recovered cellulose as new admixture is constructed wetlands for micropollutant removal: A circular approach. Science of The Total Environment. Volume 927. 172055. https://doi.org/10.1016/j.scitotenv.2024.172055

[2] Katheresan, V., Kansedo, J., Lau, S., 2018. Efficiency of various recent wastewater dye removal methods: A review. Journal of Environmental Chemical Engineering. Volume 6. Pages 4676-4697. Issue 4. https://doi.org/10.1016/j.jece.2018.06.060

[3] Web of Science, 2024. Certain data included herein are derived from Clarivate InCites. © Copyright Clarivate 202_. All rights reserved. Accessed on 4 July 2024: https://www.webofscience.com/wos/woscc/summary/42061997-ebdd-486b-b14c-7f306fbdec47-fc4f3a58/relevance/1

[4] Rajesh, Y., Boricha, H., Suryavanshi, A., Gajare, A., Jain, S., Suresh, K., 2023. Synthesis, characterization and adsorption studies on activated carbon adsorbent synthesized from Kigelia africana for removal of acid blue 113 dye from synthetic solution. Materials Today: Proceedings. https://doi.org/10.1016/j.matpr.2023.11.046

[5] Varghese, A., Paul, S., Latha, M., 2019. Remediation of heavy metals and dyes from wastewater using cellulose-based adsorbents. Environmental Chemistry Letters. Volume 17. Pages 867-877. https://doi.org/10.1007/s10311-018-00843-z

[6] Yang, Z., Hou, J., Miao, L., Wu, J., 2021. Comparison of adsorption behavior studies of methylene blue by microalga residue and its biochars produced at different pyrolytic temperatures. Environmental Science and Pollution Research. Volume 28. Pages 14028-14040. https://doi.org/10.1007/s11356-020-11470-z

[7] Olugbenga, O., Adeleye, P., Oladipupo, S., Adeleye, A., John, K., 2024. Biomass-derived biochar in wastewater treatment- a circular economy approach. Waste Management Bulletin. Volume 1. Pages 1-14. Issue 4. https://doi.org/10.1016/j.wmb.2023.07.007

[8] Dutta, S., Grupta, B., Srivastava, S., Gupta, A., 2021. Recent advances on the removel of dyes from wastewater using various adsorbents: a critical review. Materials Advances. Volume 2. Pages 4497-4531. Issue 14. https://doi.org/10.1039/D1MA00354B

[9] Nasar, A., Mashkoor, F., 2019. Application of polyaniline-based adsorbents for dye removal from water and wastewater–a review. Environmental Science and Pollution Research. Volume 26. Pages 5333-5356. https://doi.org/10.1007/s11356-018-3990-y

[10] Deering, K., Spiegel, E., Quaisser, C., Nowak, D., Rakate, S., Garí, M., O´Reilly, S., 2020. Exposure assessment of toxic metals and organochlorine pesticides among employees of a natural history museum. Environmental Research. Volume 184. 109271. https://doi.org/10.1016/j.envres.2020.109271

[11] Lellis, B., Polonio, C., Pamphile, J., Polonio, J., 2019. Effects of textile dyes on health and the environment and bioremediation potential of living organisms. Biotechnology Research and Innovation. Volume 3. Pages 275.290. Issue 2. https://doi.org/10.1016/j.biori.2019.09.001

[12] Lee, J., Sarmah, A., Kwon, E., 2019. Chapter 1 - Production and Formation of Biochar. Biochar from Biomass and Waste. Pages 3-18. https://doi.org/10.1016/B978-0-12-811729-3.00001-7

[13] Břendová, K., Tlustoš, P., Száková, J., Habart, J., 2012. Biochar properties from different materials of plant origin. Environmental Science, Materials Science European Chemical Bulletin. https://doi.org/10.17628/ECB.2012.1.535-539

[14] Ghodake, G., Shinde, Surendra., Kadam, A., Sarantale, R., Saratale, G., Kumar, M., Palem, R., Shwaiman, H., Elgorban, A., Syed, A., Kim, D., 2021. Review on biomass feedstocks, pyrolysis mechanism and physicochemical properties of biochar: State-of-the-art framework to speed up vision of circular bioeconomy. Journal of Cleaner Production. Volume 297. 126645. https://doi.org/10.1016/j.jclepro.2021.126645

[15] Jafri, N., Wong, W., Doshi, V., Yoon, L., Cheah, K., 2018. A review on production and characterization of biochars for application in direct carbon fuel cells. Process Safety and Environmental Protection. Volume 118. Pages 152-166. https://doi.org/10.1016/j.psep.2018.06.036

[16] Wang, J., Yin, Y., 2021. Clostridium species for fermentative hydrogen production: An overview. International Journal of Hydrogen Energy. Volume 46. Pages 34599-34625. Issue 70. https://doi.org/10.1016/j.ijhydene.2021.08.052

[17] Phanthonh, P., Reubroycharoen, P., Hao, X., Xu, Guangwen., Abudula, A., Guan, G., 2018. Nanocellulose: Extraction and application. Carbon Resources Conversion. Volume 1. Pages 32-43. Issue 1. https://doi.org/10.1016/j.crcon.2018.05.004

[18] Joshi, G., Yadav, K., 2023. Chapter 2 - Applications of bioresins and biopolymers derived from natural resources as composites in drug delivery. Green Sustainable Process for Chemical and Environmental Engineering and Science. Pages 21-34. https://doi.org/10.1016/B978-0-323-95169-2.00007-9

[19] Jensen, C., Guerrero, J., Karatzos, S., Olofsson, G., 2017. Fundamentals of Hydrofaction™: Renewable crude oil from woody biomass. Biomass Conversion and Biorefinery. Volume 7. Pages 495-509. https://doi.org/10.1007/s13399-017-0248-8

[20] Alfenore, S., Jouve, C., 2016. Current status and future prospects of conversion of lignocellulosic resources to biofuels using yeasts and bacteria. Process Biochemistry. Volume 51. Pages 1747-1756. Issue 11. https://doi.org/10.1016/j.procbio.2016.07.028

[21] Bakó, K., 2007. 9 - Enzymatic extraction and fermentation for the recovery of food processing products. Handbook of Waste Management and Co-Product Recovery in Food Processing. Volume 1. Pages 198-216. https://doi.org/10.1533/9781845692520.3.198

[22] Li, De., Jiang, H., 2017. The thermochemical conversion of non-lignocellulosic biomass to form biochar: A review on characterizations and mechanism elucidation. Bioresource Technology. Volume 246. Pages 57-68. https://doi.org/10.1016/j.biortech.2017.07.029

[23] Sharma, V., Tsai, M., Nargotra, P., Chen, C., Kuo, C., Sun, P., Dong, C., 2022. Agro-Industrial Food Waste as a Low-Cost Substrate for Sustainable Production of Industrial Enzymes: A Critical Review. Catalysts. Volume 12. Issue 11. https://doi.org/10.3390/catal12111373

[24] Barquilha, C., Braga, M., 2021. Adsorption of organic and inorganic pollutants onto biochars: Challenges, operating conditions, and mechanisms. Bioresource Technology Reports. Volume 15. 100728. https://doi.org/10.1016/j.biteb.2021.100728

[25] Ahmad, M., Rajapaksha, A., Lim, J., Zhang M., Bolan, N., Mohan, D., Vithanage, M., Lee, S., Ok, Y., 2014. Biochar as a sorbent for contaminant management in soil and water: A review. Chemosphere. Volume 99. Pages 19-33. https://doi.org/10.1016/j.chemosphere.2013.10.071

[26] Raveendran, K., Ganesh, A., Khilar., 1995. Influence of mineral matter on biomass pyrolysis characteristics. Fuel. Volume 74. Pages 1812-1822. Issue 12. https://doi.org/10.1016/0016-2361(95)80013-8

[27] Sohi, S., Krull, E., Capel, E., Bol, R., 2010. Chapter 2 - A Review of Biochar and Its Use and Function in Soil. Advances in Agronomy. Volume 105. Pages 47-82. https://doi.org/10.1016/S0065-2113(10)05002-9

[28] Keiluweit, M., P, Nico., Johnson, M., Kleber, M., 2010. Dynamic molecular structure of plant biomass-derived black carbon (biochar). Environmental Science & Technology. Volume 44. Pages 1247-1253. Issue 4. https://doi.org/10.1021/es9031419

[29] Wood, R., Mašek, O., Erastov, V., 2024. Developing a molecular-level understanding of biochar materials using public characterization data. Cell Reports Physical Science. Volume 5. Issue 7. https://doi.org/10.1016/j.xcrp.2024.102036

[30] Chen, B., Zhou, D., Zhu, L., 2008. Transitional Adsorption and Partition of Nonpolar and Polar Aromatic Contaminants by Biochars of Pine Needles with Different Pyrolytic Temperatures. Environmental Science & Technology. Volume 42. Pages 5137-5143. Issue 14. https://doi.org/10.1021/es8002684

[31] Amalina, F., Razak, A., Krishnan, S., Sulaiman, H., Zularisam, A., Nasrullah., 2022. Biochar production techniques utilizing biomass waste-derived materials and environmental applications - A review. Journal of Hazardous Materials Advances. Volume 7. 100134. https://doi.org/10.1016/j.hazadv.2022.100134

[32] Amalina, F., Razak, A., Krishnan, S., Zularisam, A., Nasrullah, M., 2022. A comprehensive assessment of the method for producing biochar, its characterization, stability, and potential applications in regenerative economic sustainability – A review. Cleaner Materials. Volume 3. 100045. https://doi.org/10.1016/j.clema.2022.100045

[33] Saravanan, A., Hemavathy, R., Sundararaman, T., Jeevanantham, S., Kumar, P., Yaashikaa, P., 2020. 1- Solid waste biorefineries. Refining Biomass Residues for Sustainable Energy and Bioproducts. Pages 3-17. https://doi.org/10.1016/B978-0-12-818996-2.00001-6

[34] H Naggar,A., Lee, S., Rinklebe, J., Farooq, M., Song, H., Sarmah, A., Zimmerman, A., Ahmad, M., Shaheen, S., Ok, Y., 2019. Biochar application to low fertility soils: A review of status, and future prospects. Geoderma. Volume 337. Pages 536-554. https://doi.org/10.1016/j.geoderma.2018.09.034

[35] Das, S., Ghosh, G., Avasthe, R., 2020. Applications of biomass derived biochar in modern science and technology. Environmental Technology & Innovation. Volume 21. 101306. https://doi.org/10.1016/j.eti.2020.101306

[36] Sharma, T., Hakeem, I., Gupta, A., Joshi, J., Shah, K., Vuppaladadiyam, A., Sharma, A., 2024. Parametric influence of process conditions on thermochemical techniques for biochar production: A state-of-the-art review. Journal of the Energy Institute. Volume 113. 101559. https://doi.org/10.1016/j.joei.2024.101559.

[37] Sharma, S., Rana, V., Rana, N., Prasad, H., Sharma, U., Patiyal, V., 2022. Biochar from fruit crops waste and its potential impact on fruit crops. Scientia Horticulturae. Volume 299. 111052. https://doi.org/10.1016/j.scienta.2022.111052

[38] Chew, J., Doshi, V., 2011. Recent advances in biomass pretreatment – Torrefaction fundamentals and technology. Renewable and Sustainable Energy Reviews. Volume 15. Pages 4212-4222. Issue 8. https://doi.org/10.1016/j.rser.2011.09.017

[39] Entwistle, J., Zhang, Li., Zhang, H., Ruiz, N., 2023. 5.09 - Materials synthesis for Na-ion batteries. Comprehensive Inorganic Chemistry III (Third Edition). Pages 199-215. https://doi.org/10.1016/B978-0-12-823144-9.00195-3

[40] Yaashikaa, P., Kumar, P., Varjani, S., Saravanan, A., 2020. A critical review on the biochar production techniques, characterization, stability and applications for circular bioeconomy. Biotechnology Reports. Volume 28. e00570. https://doi.org/10.1016/j.btre.2020.e00570

[41] Li, H., Dong, X., Silva, E., Oliveira, L., Ma, L., 2017. Mechanisms of metal sorption by biochars: Biochar characteristics and modifications. Chemosphere. Volume 178. Pages 466-478. https://doi.org/10.1016/j.chemosphere.2017.03.072

[42] Singh, B., Dolk, M., Shen, Q., Arbestain, M., 2017. Biochar pH, eletrical conductivity and liming potencial. Biochar: A Guide to Analytical Methods. Pages 23-38. https://doi.org/10.1071/9781486305100

[43] Lehmann, J., Rillig, M., Thies, J., Masiello, C., Hockaday, W., Crowley, D., 2011. Biochar effects on soil biota – A review. Soil Biology and Biochemistry. Volume 43. Pages 1812-1836. Issue 9. https://doi.org/10.1016/j.soilbio.2011.04.022

[44] Yuan, J., Xu, R., Zhang, H., 2011. The forms of alkalis in the biochar produced from crop residues at different temperatures. Bioresource Technology. Volume 102. Pages 3488-3497. Issue 3. https://doi.org/10.1016/j.biortech.2010.11.018

[45] Thomas, G., 1996. Chapter 16 – Soil pH and Soil Acidity. Methods of Soil Analysis: Part 3 Chemical Methods. https://doi.org/10.2136/sssabookser5.3.c16

[46] Schollenberger, C., Simon, H., 1945. Determination of Exchange Capacity and Exchangeable Bases in Soil-Ammonium Acetate Method. Soil Science. Volume 59. Pages 13-24. http://dx.doi.org/10.1097/00010694-194501000-00004

[47] Echeverri, J., Martinsen, V., Strand, L., Zivanovic, V., Cornelissen, G., Mulder, J., 2018.Cation exchange capacity of biochar: An urgent method modification. Science of The Total Environment. Volume 642. Pages 190-197. https://doi.org/10.1016/j.scitotenv.2018.06.017

[48] Mukherjee, A., Zimmerman, A., Harris, W., 2011. Surface chemistry variations among a series of laboratory-produced biochars. Geoderma. Volume 163. Pages 247-255. Issue 3-4. https://doi.org/10.1016/j.geoderma.2011.04.021

[49] Pellenz, L., Oliveira, C., Júnior, A., Silva, L., Silva, L., Souza, A., Souza, S., Borba, F., Silva, A., 2023. A comprehensive guide for characterization of adsorbent materials.Separation and Purification Technology. Volume 305. 122435. https://doi.org/10.1016/j.seppur.2022.122435

[50] Zeghioud, H., Fryda, L., Djelal, H., Assadi, A., Kane, A. 2022. A comprehensive review of biochar in removal of organic pollutants from wastewater: Characterization, toxicity, activation/functionalization and influencing treatment factors. Journal of Water Process Engineering. Volume 47. 102801. https://doi.org/10.1016/j.jwpe.2022.102801

[51] Quadri, T., Fayemi, O., Olasunkanmi, L., Ebenso, E., 2023. Chapter 15 - Survey of different electrochemical and analytical techniques for corrosion measurements. Electrochemical and Analytical Techniques for Sustainable Corrosion Monitoring. Pages 293-323. https://doi.org/10.1016/B978-0-443-15783-7.00012-8

[52] Bourakadi, K., Bouhfid, R., Qaiss, A., 2021. Chapter 2 - Characterization techniques for hybrid nanocomposites based on cellulose nanocrystals/nanofibrils and nanoparticles. Cellulose Nanocrystal/Nanoparticles Hybrid Nanocomposites. Pages 27-64. https://doi.org/10.1016/B978-0-12-822906-4.00010-4

[53] Wharry, J., 2021. 2013-2014 Survey of Chars Using Raman Spectroscopy. Journal of Carbon Research. Volume 7. Issue 3. https://doi.org/10.3390/c7030063

[54] Soares, J., Cançado, L., Falcão, N., Ferreira, E., Achete, A., Jorio, A., 2012. The use of Raman spectroscopy to characterize the carbon materials found in Amazonian anthrosoils. Journal of Raman Spectroscopy. Volume 44. Pages 283-289. Issue 2. https://doi.org/10.1002/jrs.4191

[55] Sadezky, A., Muckenhuber, H., Grothe, H., Niessner, R., Pöschl, U., 2005.Raman microspectroscopy of soot and related carbonaceous materials: Spectral analysis and structural information. Carbon. Volume 43. Pages 1731-1742. Issue 8. https://doi.org/10.1016/j.carbon.2005.02.018

[56] Fodah, A., Ghosal, M., Behera, D., 2022. Microwave-assisted pyrolysis of agricultural residues: current scenario, challenges, and future direction. International Journal of Environmental Science and Technology. Volume 19. Pages 2195-2220. https://doi.org/10.1007/s13762-020-03099-9

[57] Chisti, Y., Karimi, K., 2024. Bioethanol Production. Encyclopedia of Sustainable Technologies (Second Edition). Volume 3. Pages 279-294. https://doi.org/10.1016/B978-0-323-90386-8.00017-6

[58] Dahman, Y., Syed, K., Begum, S., Roy, P., Mohtasebi, B., 14 - Biofuels: Their characteristics and analysis. Biomass, Biopolymer-Based Materials, and Bioenergy. Pages 277-325. https://doi.org/10.1016/B978-0-08-102426-3.00014-X

[59] Milano, J., Ong, H., Masjuki, H., Chong, W., Lam, M., Loh, P., Vellayan, V., 2016. Microalgae biofuels as an alternative to fossil fuel for power generation. Renewable and Sustainable Energy Reviews. Volume 58. Pages 180-197. https://doi.org/10.1016/j.rser.2015.12.150

[60] Kaltschmitt, M., Thrän, D., Smith, K., 2003. Renewable Energy from Biomass. Encyclopedia of Physical Science and Technology (Third Edition). Pages 203-228. https://doi.org/10.1016/B0-12-227410-5/00059-4

[61] Hu, Q., Jung, J., Chen, D., Leong, K., Song, S., Li, F., Mohan, B., Yao, Z., Prabhakar, A., Lin, X., Lim, Ee., Zhang, L., Souradeep, G., Ok, Y., Kua, H., Li, S., Tan, H., Dai, Y., Tong, Y., Peng, Y., Joseph, S., Wang, C., 2021. Biochar industry to circular economy. Science of The Total Environment. Volume 757. 143820. https://doi.org/10.1016/j.scitotenv.2020.143820

[62] Enaime, G., Baçaoui, A., Yaacoubi, A., Lübken, M., 2020. Biochar for Wastewater Treatment–Conversion Technologies and Applications. Biochar for the Environmental Wastewater. Volume 10. Issue 10. https://doi.org/10.3390/app10103492

[63] Mohammed, N., Zurayk, R., Hamadneh, I., Dujaili, A., 2018. Phenol adsorption on biochar prepared from the pine fruit shells: Equilibrium, kinetic and thermodynamics studies. Journal of Environmental Management. Volume 226. Pages 377-385. https://doi.org/10.1016/j.jenvman.2018.08.033

[64] Thang, P., Jitae, K., Giang, B., Viet, N., Huong, P., 2019. Potential application of chicken manure biochar towards toxic phenol and 2,4-dinitrophenol in wastewaters. Journal of Environmental Management. Volume 251. 109556. https://doi.org/10.1016/j.jenvman.2019.109556

[65] Tan, C., Yaxin, Z., Hongtao, W., Wenjing, L., Zeyu, Z., Yuancheng, Z., Lulu, R., 2014. Influence of pyrolysis temperature on characteristics and heavy metal adsorptive performance of biochar derived from municipal sewage sludge. Bioresource Technology. Volume 164. Pages 47-54. https://doi.org/10.1016/j.biortech.2014.04.048

[66] Zhao, M., Dai, Y., Zhang, M., Feng, C., Qin, B., Zhang, W., Zhao, N., Li, Y., Ni, Z., Xu, Z., Tsang, D., Qiu, R., 2020. Mechanisms of Pb and/or Zn adsorption by different biochars: Biochar characteristics, stability, and binding energies. Science of The Total Environment. Volume 717. 136894. https://doi.org/10.1016/j.scitotenv.2020.136894

[67] Graves, C., Kolar, P., Shah, S., Grimes, J., Sharara, M., 2022. Can Biochar Improve the Sustainability of Animal Production? Applied Sciences. Volume 12. Issue 10. https://doi.org/10.3390/app12105042

[68] Akpasi, S., Anekwe, I., Adedeji, J., Kiambi, S., 2022. Biochar Development as a Catalyst and Its Application. Biochar - Productive Technologies, Properties and Application. https://doi.org/10.5772/intechopen.105439

[69] Gan, L., Zhong, Q., Geng, A., Wang, L., Song, C., Han, S., Cui, J., Xu, L., 2019. Cellulose derived carbon nanofiber: A promising biochar support to enhance the catalytic performance of CoFe2O4 in activating peroxymonosulfate for recycled dimethyl phthalate degradation. Science of The Total Environment. Volume 694. 133705. https://doi.org/10.1016/j.scitotenv.2019.133705

[70] Guo, F., Peng, K., Liang, S., Jia, X., Jiang, X., Qian, L., 2019. Evaluation of the catalytic performance of different activated biochar catalysts for removal of tar from biomass pyrolysis. Fuel. Volume 258. 116204. https://doi.org/10.1016/j.fuel.2019.116204

[71] Kochanek, J., Soo, R., Martinez, C., Dakuidreketi, A., Mudge, A., 2022. Biochar for intensification of plant-related industries to meet productivity, sustainability and economic goals: A review. Resources, Conservation and Recycling. Volume 179. 106119. https://doi.org/10.1016/j.resconrec.2021.106109

[72] Zhao, S., Wang, X., Wang, Q., Sumpradit, T., Khan, A., Zhou., Salama, E., Li, X., Qu,J., 2023. Application of biochar in microbial fuel cells: Characteristic performances, electron-transfer mechanism, and environmental and economic assessments. Ecotoxicology and Environmental Safety. Volume 267. 115643. https://doi.org/10.1016/j.ecoenv.2023.115643

[73] You, K., Zhou, Z., Gao, C., Yang, Q., 2021. One-Step Preparation of Biochar Electrodes and Their Applications in Sediment Microbial Electrochemical Systems. Catalysts. Volume 11. Issue 4. https://doi.org/10.3390/catal11040508

[74] Smarzewska, S., Morawska, K., 2021. 1 - Wastewater treatment technologies. Handbook of Advanced Approaches Towards Pollution Prevention and Control. Pages 3-32. https://doi.org/10.1016/B978-0-12-822121-1.00001-1

[75] Gisi, S., Notarnicola, M., 2017. Industrial Wastewater Treatment. Encyclopedia of Sustainable Technologies. Pages 23-42. https://doi.org/10.1016/B978-0-12-409548-9.10167-8

[76] Volmajer, J., Marechal, A., Vajnhandl, S., Jeric, T., Simon, E. 2011. Water in the Textile Industry. Volume 4. Pages 685-706. https://doi.org/10.1016/B978-0-444-53199-5.00102-0

[77] Daoud, M., Kecira, Z., Benturki, O., Girods, P., Rogamaume, Y., Fontana, S., 2023. Characterization of novel adsorbents from Phoenix dactylifera rachis. Box-Behnken design, kinetic, and isotherm models for BEZAKTIV Red S-MAX dye adsorption onto the produced carbons. Biomass Conversion and Biorefinery. https://doi.org/10.1007/s13399-023-04359-7

[78] Berradi, M., Hsissou, R., Khudhair, M., Assouag, M., Cherkaoui, O., Bachiri, A., Harfi, A., 2019. Textile finishing dyes and their impact on aquatic environs. Heliyon. Volume 5. Issue 11. https://doi.org/10.1016/j.heliyon.2019.e02711

[79] Lim, S., Chu, W., Phang, S., 2010. Use of Chlorella vulgaris for bioremediation of textile wastewater. Bioresource Technology. Volume 101. Pages 7314-7322. Issue 19. https://doi.org/10.1016/j.biortech.2010.04.092

[80] Benkhaya, S., M' rabet, S., Harfi, A.,2020. A review on classifications, recent synthesis and applications of textile dyes. Inorganic Chemistry Communications Volume 115. 107891. https://doi.org/10.1016/j.inoche.2020.107891

[81] Azzopardi, E., Owens, S., Murison, M., Rees, D., Sawhney, M., Francis, L., Teixeira, R., Clement, M., Conlan, R., Whitaker, I., 2017. Chromophores in operative surgery: Current practice and rationalized development. Journal of Controlled Release. Volume 249. Pages 123-130. https://doi.org/10.1016/j.jconrel.2016.12.044

[82] Chattopadhyay, D., 2011. 19 – Azoic dyeing. Handbook of Textile and Industrial Dyeing. Volume 1. Pages 604-626. https://doi.org/10.1533/9780857093974.2.604

[83] Franciscon, E., Zille, A., Garboggini, F., Silva, I., Paulo, A., Durrant, L., 2009. Microaerophilic-aerobic sequential decolourization/biodegradation of textile azo dyes by a facultative Klebsiella sp. strain VN-31. Process Biochemistry. Volume 44. Pages 446-452. Issue 4. https://doi.org/10.1016/j.procbio.2008.12.009

[84] Siddiqua, U., Ali, S., Iqbal, M., Hussain, T., 2017. Relationship between structure and dyeing properties of reactive dyes for cotton dyeing. Journal of Molecular Liquids. Volume 241. Pages 839-844. https://doi.org/10.1016/j.molliq.2017.04.057

[85] Solayman, H., Hossen, M., Aziz, A., Yahya, N., Leong, K., Sim, L., Monir, M., Zoh, K., 2023. Performance evaluation of dye wastewater treatment technologies: A review. Journal of Environmental Chemical Engineering. Volume 11. Issue 3. https://doi.org/10.1016/j.jece.2023.109610

[86] Lee, Y., Pavlostathis, S., 2004. Decolorization and toxicity of reactive anthraquinone textile dyes under methanogenic conditions. Water Research. Volume 38. Pages 1838-1852. Issue 7. https://doi.org/10.1016/j.watres.2003.12.028

[87] Shang, S., 2013. 13- Process control in dyeing of textiles. Process Control in Textile Manufacturing. Pages 300-338. https://doi.org/10.1533/9780857095633.3.300

[88] Gupta, V., Suhas., 2009. Journal of Environmental Management. Volume 90. Pages 2313-2342. Issue 8. https://doi.org/10.1016/j.jenvman.2008.11.017

[89] Alsukaibi, A., 2022. Various Approaches for the Detoxification of Toxic Dyes in Wastewater. Processes. Volume 10. Issue 10. https://doi.org/10.3390/pr10101968

[90] Nachiyar, C., Rakshi, A., Sandhya, S., Jebasta, N., Nellore, J., 2023. Developments in treatment technologies of dye-containing effluent: A review. Case Studies in Chemical and Environmental Engineering. Volume 7. 100339. https://doi.org/10.1016/j.cscee.2023.100339

[91] Samsami, S., Mohamadizaniani, M., Sarrafzadeh, M., Rene, E., Firoozbahr, M., 2020. Recent advances in the treatment of dye-containing wastewater from textile industries: Overview and perspectives. Process Safety and Environmental Protection. Volume 143. Pages 138-163. https://doi.org/10.1016/j.psep.2020.05.034

[92] Kishor, R., Purchase, D., Saratale, G., Saratale, R., Ferreira, L., Bilal, M., Chandra, R., Bharagava, R., 2021. Ecotoxicological and health concerns of persistent coloring pollutants of textile industry wastewater and treatment approaches for environmental safety. Journal of Environmental Chemical Engineering. Volume 9. Issue 2. https://doi.org/10.1016/j.jece.2020.105012

[93] Wang, A., Wang, H., Cheng, H., Liang, B., Liu, W., Han, J., Zhang, B., Wang, S., 2020. Electrochemistry-stimulated environmental bioremediation: Development of applicable modular electrode and system scale-up. Environmental Science and Ecotechnology. Volume 3. 100050. https://doi.org/10.1016/j.ese.2020.100050

[94] Sharma, S., Saxena, R., Gaur, G., 2014. Study of Removal Techniques for Azo Dyes by Biosorption: A Review. Environmental Science, Chemistry. https://doi.org/10.9790/5736-071010621

[95] Robinson, T., McMullan, G., Marchant, R., Nigam, P., 2001. Remediation of dyes in textile effluent: a critical review on current treatment technologies with a proposed alternative. Bioresource Technology. Volume 77. Pages 247-255. Issue 3. https://doi.org/10.1016/S0960-8524(00)00080-8

[96] Li, C., Sun, W., Lu, Z., Ao, X., Li, S., 2020. Ceramic nanocomposite membranes and membrane fouling: A review. Water Research. Volume 175. 115674. https://doi.org/10.1016/j.watres.2020.115674

[97] Sharma, C., Zhu, Z., Ronen, A., 2024. Membrane Filtration for Wastewater Treatment - Fouling Mitigation. Wastewater Treatment - Past and Future Perspectives. https://doi:10.5772/intechopen.1004566

[98] Amuda, O., Amoo, I., 2007. Coagulation/flocculation process and sludge conditioning in beverage industrial wastewater treatment. Journal of Hazardous Materials. Volume 141. Pages 778-783. Issue 3. https://doi.org/10.1016/j.jhazmat.2006.07.044

[99] Sillanpää, M., Shestakova, M., 2017. Chapter 3 - Emerging and Combined Electrochemical Methods. Electrochemical Water Treatment Methods. Pages 131-225. https://doi.org/10.1016/B978-0-12-811462-9.00003-7

[100] Sillanpää, M., Shestakova, M., 2017. Chapter 2 – Eletrochemical Water Treatment Melhods. Electrochemical Water Treatment Methods. Pages 47-130. https://doi.org/10.1016/B978-0-12-811462-9.00002-5

[101] Khan, S., Yadav, V., 2021. Advanced Oxidation Processes for Wastewater Remediation: An Overview. Removal of Emerging Contaminants Through Microbial Processes. Pages 71-93. https://doi.org/10.1007/978-981-15-5901-3_4

[102] Langhals, H., 2004. Color Chemistry. Synthesis, Properties and Applications of Organic Dyes and Pigments. Angewandte Chemie International Edition. Volume 43. Pages 5291. 5292. Issue 40. https://doi.org/10.1002/anie.200385122

[103] Yargeau, V., 2012. 17 – Water and wastewater treatment chemical processes. Metropolitan Sustainability. Pages 390-405. https://doi.org/10.1533/9780857096463.3.390

[104] Popli, S., Patel, D., 2015. Destruction of azo dyes by anaerobic–aerobic sequential biological treatment: a review. International Journal Environmental Science and Technology. Volume 12. Pages 405–420. https://doi.org/10.1007/s13762-014-0499-x

[105] Gopal, G., Chandrasekaran, N., Mukherjee, A., 2022. Chapter Three - Overview of nanoparticles technology usage for water treatment with an emphasis on the emerging water pollutants. Comprehensive Analytical Chemistry. Volume 99. Pages 87-103. https://doi.org/10.1016/bs.coac.2021.12.002

[106] Ağtaş, M., Yılmaz, Ö., Dilaver, M., Alp, K., Koyuncu, İ., 2020. Hot water recovery and reuse in textile sector with pilot scale ceramic ultrafiltration/nanofiltration membrane system. Journal of Cleaner Production. Volume 256. https://doi.org/10.1016/j.jclepro.2020.120359

[107] Homem, V., Santos, L., 2011. Degradation and removal methods of antibiotics from aqueous matrices – A review. Journal of Environmental Management. Volume 92. Pages 2304-2347. Issue 10. https://doi.org/10.1016/j.jenvman.2011.05.023

[108] Ray, S., Gusain, R., Kumar, N., 2020. Chapter four - Adsorption in the context of water purification. Carbon Nanomaterial-Based Adsorbents for Water Purification. Pages 67-100. https://doi.org/10.1016/B978-0-12-821959-1.00004-0

[109] Agarwala, R., Mulky, L., 2023. Adsorption of Dyes from Wastewater: A Comprehensive Review. ChemBioEng Reviews. Volume 10. Pages 326-335. Issue 3. https://doi.org/10.1002/cben.202200011

[110] Ekman, S., Reis, G., Laisné, E., Thivet, J., Grimm, A., Lima, E., Naushad, M., Dotto, G., 2023. Synthesis, Characterization, and Adsorption Properties of Nitrogen-Doped Nanoporous Biochar: Efficient Removal of Reactive Orange 16 Dye and Colorful Effluents. Nanomaterials. Volume 13. 2045. https://doi.org/10.3390/nano13142045

[111] Phuong, D., Loc, N., Miyanishi, T., 2019. Efficiency of dye adsorption by biochars produced from residues of two rice varieties, Japanese Koshihikari and Vietnamese IR50404. Desalination and Water Treatment. https://doi.org/10.5004/dwt.2019.24496

[112] Chiu, W., Wu, M., Lin, C., Li, J., Huang, C., Soong, Y., Lee, J., Sanchez, W., Lin, H., 2020. Adsorption Performance for Reactive Blue 221 Dye of β-Chitosan/Polyamine Functionalized Graphene Oxide Hybrid Adsorbent with High Acid-Alkali Resistance Stability in Different Acid-Alkaline Environments. Nanomaterials. Volume 10. 748. https://doi.org/10.3390/nano10040748

[113] Agudo, E., Agudo, C., 2024. Geochemical applications of mineral-water interactions. Reference Module in Earth Systems and Environmental Sciences. https://doi.org/10.1016/B978-0-323-99762-1.00051-6

[114] Paso, K., 2022. Chapter 6 - Constructing thermodynamic models of toxic metal biosorption. Microbial Biodegradation and Bioremediation (Second Edition). Pages 109-143. https://doi.org/10.1016/B978-0-323-85455-9.00020-5

[115] Rápó, E., Tonk, S., 2021. Factors Affecting Synthetic Dye Adsorption; Desorption Studies: A Review of Results from the Last Five Years (2017-2021). Molecules. Volume 26. 5419. https://doi.org/10.3390/molecules26175419

[116] Brito, M., Veloso, C., Santos, L., Bonomo, R., Fontan, R., 2018. Adsorption of the textile dye Dianix® royal blue CC onto carbons obtained from yellow mombin fruit stones and activated with KOH and H3PO4: kinetics, adsorption equilibrium and thermodynamic studies. Powder Technology. Volume 339. Pages 334-343. https://doi.org/10.1016/j.powtec.2018.08.017

[117] Kavitha, G., Subhapriya, P., Dhanapal, V., Dineshkumar, G., Venkateswaran, V., 2021. Dye removal kinetics and adsorption studies of activated carbon derived from the stems of Phyllanthus reticulatus. Materials Today: Proceedings. Volume 45. Pages 7934-7938. https://doi.org/10.1016/j.matpr.2020.12.837

[118] Ghouti, M., Absi, R., 2020. Mechanistic understanding of the adsorption and thermodynamic aspects of cationic methylene blue dye onto cellulosic olive stones biomass from wastewater. Scientific Reports. 15928. https://doi.org/10.1038/s41598-020-72996-3

[119] Arfi, R., Karoui, S., Mougin, K., Ghorbal, A., 2017. Adsorptive removal of cationic and anionic dyes from aqueous solution by utilizing almond shell as bioadsorbent. Euro-Mediterranean Journal Environmental Integration. Volume 2. https://doi.org/10.1007/s41207-017-0032-y

[120] Alhujaily, A., Yu, H., Zhang, X., Ma, F., 2020. Adsorptive removal of anionic dyes from aqueous solutions using spent mushroom waste. Applied Water Science. Volume 10. https://doi.org/10.1007/s13201-020-01268-2

[121] Khalaf, I., Sudani, F., AbdulRazak, A., Aldahri, T., Rohani, S., 2021. Optimization of Congo red dye adsorption from wastewater by a modified commercial zeolite catalyst using response surface modeling approach. Water Science & Technology. Volume 83. Pages 1369-1383. Issue 6. https://doi.org/10.2166/wst.2021.078

[122] Abualnaja, K., Alprol, A., Saied, M., Ashour, M., Mansour, A., 2021. Removing of Anionic Dye from Aqueous Solutions by Adsorption Using of Multiwalled Carbon Nanotubes and Poly (Acrylonitrile-styrene) Impregnated with Activated Carbon. Sustainability. Volume 13. 7077. https://doi.org/10.3390/su13137077

[123] Wang, H., Shadman, F., 2012. Effect of particle size on the adsorption and desorption properties of oxide nanoparticles. AIChE Journal. Volume 59. Pages 1502-1510. Issue 5. https://doi.org/10.1002/aic.13936

[124] Hadi, P., Yeung, K., Barford, J., An, K., McKay, G., 2015. Significance of “effective” surface area of activated carbons on elucidating the adsorption mechanism of large dye molecules. Journal of Environmental Chemical Engineering. Volume 3. Pages 1029-1037. Issue 2. https://doi.org/10.1016/j.jece.2015.03.005

[125] Farobie, O. Amrullah, A. Bayu, A. Syaftika, N. Anis, L. Hartulistiyoso, E., 2022. In-depth study of bio-oil and biochar production from macroalgae Sargassum sp. via slow pyrolysis†. RSC Advances. Volume 16. Pages 9567-9578. Issue 16. https://doi.org/10.1039/D2RA00702A

[126] Harindintwali, J. He, C. Xiang, L. Dou, Q. Liu, Y. Wang, M. Wen, X. Fu, Y. Islam, M. Chang, S. Kueppers, S. Shaheen, S. Rinklebe, J. Jian, X. Schaeffer, A. Wang, F., 2023. Effects of ball milling on biochar adsorption of contaminants in water: A meta-analysis. Science of The Total Environment. Volume 882. 163643. https://doi.org/10.1016/j.scitotenv.2023.163643

[127] Chen, Y., Yang, Y., Liu, X., Shi, X., Wang, C., Zhong, H., Jin, F., 2023. Sustainable production of formic acid and acetic acid from biomass. Molecular Catalysis. Volume 545. 113199. https://doi.org/10.1016/j.mcat.2023.113199

[128] Sarchami, T., Batta, N., Berruti, F., 2021. Production and separation of acetic acid from pyrolysis oil of lignocellulosic biomass: a review. Volume 15. Pages 1912-1937. Issue 6. https://doi.org/10.1002/bbb.2273

[129] Yagub, M., Sem, T., Ang, H., 2012. Equilibrium, Kinetics, and Thermodynamics of Methylene Blue Adsorption by Pine Tree Leaves. Water, Air, & Soil Pollution. Volume 223. Pages 5267-5282. https://doi.org/10.1007/s11270-012-1277-3

[130] Vassilev, S., Vassileva, C., 2016. Composition, properties and challenges of algae biomass for biofuel application: An overview. Fuel. Volume 181. Pages 1-33. https://doi.org/10.1016/j.fuel.2016.04.106

[131] Ismail, S., Ali, E., Alwan, B., Abd, A., 2022. Potassium Chloride Nanoparticles: Synthesis, Characterizations, and Study the Antimicrobial Applications. Macromolecular Symposia. Volume 401. Issue 1. 2100312. https://doi.org/10.1002/masy.202100312

[132] Ghahramanifard, F., Fazlolahzadeh, O., Rouhollahi, A., 2018. Electrodeposition of Cu-doped p-type ZnO nanorods; effect of Cu doping on structural, optical and photoelectrocatalytic property of ZnO nanostructure. Superlattices and Microstructures. Volume 114. Pages 1-14. https://doi.org/10.1016/j.spmi.2017.07.019

[133] Ray, A., Kumar, M., Karim, A., Biswas, K., Mohanty, S., Shadangi, K., Kumar, S., Sarkar, B., 2023. Potassium-phosphorus-sulfur augmented biochar production from potentially toxic elements abated gypsum pond wastewater of phosphate fertilizer industry. Journal of Environmental Chemical Engineering. Volume 11. Issue 5. 110404. https://doi.org/10.1016/j.jece.2023.110404

[134] Patel, R., Pandya, K., Jasrai, R., Brahmbhatt, N., 2017. A REVIEW: SCOPE OF UTILIZING SEAWEED AS A BIOFERTILIZER IN AGRICULTURE. International Journal of Advanced Research. Volume 5. Issue 7. 2320-5407. http://dx.doi.org/10.21474/IJAR01/4941

[135] Nakata, P., 2003. Advances in our understanding of calcium oxalate crystal formation and function in plants. Plant Science. Volume 164. Issue 6. Pages 901-909. https://doi.org/10.1016/S0168-9452(03)00120-1

[136] RRUFF. Whewellite 5050240. Accessed on 1 August 2024: https://rruff.info/whewellite/display=default/R050240

[137] Avornyo, V., Manu, A., Laird, D., Thompson, M., 2021. Temperature Effects on Properties of Rice Husk Biochar and Calcinated Burkina Phosphate Rock. Agriculture. Volume 11. Issue 5. https://doi.org/10.3390/agriculture11050432

[138] Islam, T., Peng, C., Ali, I., Li, J., 2020. Synthesis of Rice Husk-Derived Magnetic Biochar Through Liquefaction to Adsorb Anionic and Cationic Dyes from Aqueous Solutions. Arabian Journal for Science and Engineering. Volume 46. Pages 233-246. https://doi.org/10.1007/s13369-020-04537-z

[139] RRUF. Quartz R040031. Accessed on 2 August 2024: https://rruff.info/quartz/display=default/R040031

[140] Amritha, K., Sankar, S., 2021. Surface morphology and Structural characteristics of rice husk, its biochar and vermicompost. Journal of Natural Resource Conservation and Management. Volume 2. Issue 2. Pages 114-119. https://doi.org/10.51396/anrcm.2.2.2021.114-119

[141] Araya, M., Rivas, J., Sepúlveda, G., González, C., Lira, S., Meynard, A., Blanco, E., Escalona, N., Ginocchio, R., Ramírez, E., Porcia, L., 2021. Effect of Pyrolysis Temperature on Copper Aqueous Removal Capability of Biochar Derived from the Kelp Macrocystis pyrifera. Applied Sciences. Volume 11. Issue 19. 9923. https://doi.org/10.3390/app11199223

[142] Szerszen, M., Orzechowski, M., 2018. Infrared spectroscopy methods in reservoir rocks anaylsis - semiquatitative approch for carbonate rocks. NAFTA-GAZ. Volume 11. 802. http://dx.doi.org/10.18668/NG.2018.11.04

[143] Zhang, C., Zhang, L., Gao, J., Zhang, S., Liu, Q., Duan, P., Hu, X., 2020. Evolution of the functional groups/structures of biochar and heteroatoms during the pyrolysis of seaweed. Algal Research. Volume 48. 101900. https://doi.org/10.1016/j.algal.2020.101900

[144] Lyu, H., Gao, B., He, F., Zimmerman, A., Ding, C., Huang, H., Tang, J., 2018. Environmental Pollution. Volume 233. Pages 54-63. https://doi.org/10.1016/j.envpol.2017.10.037

[145] Yuan, R., Dong, Y., Hou, R., Shang, L., Zhang, J., Zhang, S., Chen, X., Song, H., 2023. Structural transformation of porous and diordered carbon during ball-milling. Chemical Engineering Journal. Volume 454. Part 3. 140418. https://doi.org/10.1016/j.cej.2022.140418

[146] Parsa, M., Nourani, M., Baghdadi, M., Hosseinzadeh, M., Pejman, M., 2019. Biochars derived from marine macroalgae as a mesoporous by-product of hydrothermal liquefaction process: Characterization and application in wastewater treatment. Journal of Water Process Engineering. Volume 32. 100942. https://doi.org/10.1016/j.jwpe.2019.100942

[147] Guleç, F., Williams, O., Kostas, E., Samson, A., Stevens, L., Lester, E., 2022. A comprehensive comparative study on methylene blue removal from aqueous solution using biochars produced from rapeseed, whitewood, and seaweed via different thermal conversion technologies. Fuel. Volume 330. 125428. https://doi.org/10.1016/j.fuel.2022.125428

[148] Li, M., Zhang, Y., Cheng, S., Qu, B., Li, A., Meng, F., Ji, G., 2023. The impact of heating rate on the decomposition kinetics and product distribution of algal waste pyrolysis with in-situ weight measurement. Chemical Engineering Journal. Volume 457. 141368. https://doi.org/10.1016/j.cej.2023.141368

[149] Zhang, H., Su, L., Cheng, C., Cheng, H., Chang, M., Liu, F., Liu, N., Oh, K., 2022. A new type of calcium-rich biochars derived from spent mushroom substrates and their efficient adsorption properties for cationic dyes. Front Bioeng Biotechnol. Volume 10. 1007630. https://doi.org/10.3389/fbioe.2022.1007630

[150] Bayartsengel, B., Ochir, N., Battulga, S., Tyeliubek, S., 2021. Characterization of Biochars Produced from Various Biowastes. 5th International Conference on Chemical Investigation and Utilization of Natural Resource (ICCIUNR-2021). https://doi.org/10.2991/ahcps.k.211004.012

[151] Lu, X., Zhao, J., 2024. Adsorption of ciprofloxacin on co-pyrolyzed biochar from fish scale and pine needle. Chinese Journal of Analytical Chemistry. Volume 52. Issue 1. 100350. https://doi.org/10.1016/j.cjac.2023.100350

[152] Luo, X., Du, H., Zhang, X., Yang, Y., 2022. Amine-functionalized magnetic biochars derived from invasive plants Alternanthera philoxeroides for enhanced efficient removal of Cr(VI): performance, kinetics and mechanism studies. Environmental Science and Pollution Research. Volume 29. Issue 51. Pages 1-15. http://dx.doi.org/10.1007/s11356-022-20987-4

[153] Torrisi, A., Cutroneo, M., Torrisi, L., Lavalle, S., 2024. Unveiling the Potential of Vitamin D3 Orodispersible Films: A Comprehensive FTIR and UV-Vis Spectroscopic Study. Molecules. Volume 29. Issue 16. 3762. http://dx.doi.org/10.3390/molecules29163762

[154] Zhang, N., Reguyal, F., Praneeth, S., Sarmah, A., 2023. A green approach of biochar-supported magnetic nanocomposites from white tea waste: Production, characterization and plausible synthesis mechanisms. Science of The Total Environment. Volume 886. 163923. https://doi.org/10.1016/j.scitotenv.2023.163923

[155] Gámiz, B., Velarde, P., Spokas, K., Cox, L., 2022. The Role of Nanoengineered Biochar Activated with Fe for Sulfanilamide Removal from Soils and Water. Molecules. Volume 27. 7418. https://doi.org/10.3390/molecules27217418

[156] Siipola, V., Tamminen, T., Kalli, A., Kupila, R., 2018. Effects of biomass type, carbonization process, and activation method on the properties of bio-based activated carbons. BioResources. Volume 13. Issue 3. 5976-6002. http://dx.doi.org/10.15376/biores.13.3.5976-6002

[157] Younis, U., Rahi, A., Danish, S., Ali, M., Ahmed, N., Datta, R., et al., 2021. Fourier Transform Infrared Spectroscopy vibrational bands study of Spinacia oleracea and Trigonella corniculata under biochar amendment in naturally contaminated soil. PLoS ONE. Volume 16. Issue 6. e0253390. https://doi.org/10.1371%2Fjournal.pone.0272183

[158] Nicholas, H., Mabbet, I., Apsey, H., Robertson, I., 2022. Physico-chemical properties of waste derived biochar from community scale faecal sludge treatment plants. Gates Open Res. Volume 6. https://doi.org/10.12688/gatesopenres.13727.2

[159] Moreno, O., Pérez, R., Portillo, M., Specia, M., 2016. Growth of doped PbS:Co2+ nanocrystals by Chemical Bath. Revista Mexicana de Física. Volume 62. Issue 5. Pages 456-460.

[160] Dias, A., Pedra, I., Salvador, É., Rijo, B., Pereira, M., Serralha, F., Nogueira, I., 2024. Biodiesel Production over Banana Peel Biochar as a Sustainable Catalyst. Catalysts. Volume 14. Issue 4. 266. https://doi.org/10.3390/catal14040266

[161] Yuan, C., Abomohra, A., Wang, S., Liu, Q., Zhao, S., Cao, B., Hu, X., Marrakchi, F., He, Z., Hu, y., 2021. High-grade biofuel production from catalytic pyrolysis of waste clay oil using modified activated seaweed carbon-based catalyst. Journal of Cleaner Production. Volume 313. 127928. https://doi.org/10.1016/j.jclepro.2021.127928

[162] Yang, W., Wang, J., Wu, Y., Chang, H., 2022. Preparatory Conditions Optimization and Characterization of Hierarchical Porous Carbon from Seaweed as Carbon-Precursor Using a Box–Behnken Design for Application of Supercapacitor. Materials. Volume 15. Issue 16. 5748. https://doi.org/10.3390/ma15165748

[163] Chng, C., Ma, X., Abe, Y., Kumagai, S., 2024. Hard carbon/graphite composite anode for durable lithium-ion capacitor. Journal of Energy Storage. Volume 92. 112193. https://doi.org/10.1016/j.est.2024.112193

[164] Gao, W., Lin, Z., Chen, H., Yan, S., Zhu, H., Zhang, H., Sun, H., Zhang, S., Zhan, S., Wu, S., 2022. Roles of graphitization degree and surface functional groups of N-doped activated biochar for phenol adsorption. Journal of Analytical and Applied Pyrolysis. Volume 167. 105700. https://doi.org/10.1016/j.jaap.2022.105700

[165] Escalante, J., Chen, W., Tabatabaei, M., Hoang, A., Kwon, E., Lin, K., Saravanakumar, A., 2022. Pyrolysis of lignocellulosic, algal, plastic, and other biomass wastes for biofuel production and circular bioeconomy: A review of thermogravimetric analysis (TGA) approach. Renewable and Sustainable Energy Reviews. Volume 169. 112914. https://doi.org/10.1016/j.rser.2022.112914

[166] Corrêa, A., Silva, P., Gonçalves, M., Bastos, R., Filho, G., Conceição, L., 2023. Study of the activity and stability of sulfonated carbon catalyst from agroindustrial waste in biodiesel production: Influence of pyrolysis temperature on functionalization. Arabian Journal of Chemistry. Volume 16. Issue 8. 104964. https://doi.org/10.1016/j.arabjc.2023.104964

[167] Nassar, M., MacKay, G., 1984. Mechanism of Thermal Decomposition of Lignin. Wood and Fiber Science. Volume 16. Issue 3. https://wfs.swst.org/index.php/wfs/article/download/262/262/0

[168] Liu, Z., Liu, Z., 2020. Comparison of hydrochar- and pyrochar-based solid acid catalysts from cornstalk: Physiochemical properties, catalytic activity and deactivation behavior. Bioresource Technology. Volume 297. 122477. https://doi.org/10.1016/j.biortech.2019.122477

[169] NETZSCH Analyzing & Testing. TGA Measurements on Calcium Oxalate Monohydrate. Accessed on 14 of August 2024: https://analyzing-testing.netzsch.com/en/application-literature/tga-measurements-on-calcium-oxalate-monohydrate

[170] Tomczyk, A., Sokołowska, Z., Boguta, P., 2020. Biochar physicochemical properties: pyrolysis temperature and feedstock kind effects. Reviews in Environmental Science and Bio/Technology. Volume 19. Pages 191-215. https://doi.org/10.1007/s11157-020-09523-3

[171] Habil, R., Volker, R., Welton, N., Andrew, H., Peter, F., Kostas, P., 2016. (DE Patent No. 199 37 328 B4). Deutsches Patent - und Markenamt. Accessed on 10 of September 2024: https://patentimages.storage.googleapis.com/12/aa/d3/d36fc70c14a830/DE19937328B4.pdf

[172] Boakye, P., Sewu, D., Woo, H., Choi, J., Lee, C., Woo, S., 2017. Extraction of inorganic materials from fresh and dried alga Saccharina japônica. Journal of Environmental Chemical Engineering. Volume 5. Issue 5. Pages 4454-4461. https://doi.org/10.1016/j.jece.2017.08.030

[173] Gao, Y., Guo, X., Liu, Y., Fang, Z., Zhanh, M., Zhang, R., You, L., Li, T., Liu., 2018. A full utilization of rice husk to evaluate phytochemical bioactivities and prepare cellulose nanocrystals. Scientific Reports. Volume 8. 10482. https://doi.org/10.1038/s41598-018-27635-3

[174] Ahmed, S., Janaswamy, S., 2023. Strong and biodegradable films from avocado peel fiber. Industrial Crops and Products. Volume 201. 116926. https://doi.org/10.1016/j.indcrop.2023.116926

[175] Jayakumar, M., Hamda, A., Abo, L., Daba, B., Prabhu, S., Rangaraju, M., Jabesa, A., Periyasamy, S., Suresh, S., Baskar, G., 2023. Comprehensive review on lignocellulosic biomass derived biochar production, characterization, utilization and applications. Chemosphere. Volume 345. 140515. https://doi.org/10.1016/j.chemosphere.2023.140515

[176] Mofty, S., Elghazawy, N., Azzazy, H., 2023. A one-step facile process for extraction of cellulose from rice husk and its use for mechanical reinforcement of dental glass ionomer cement. RSC Sustainability. Volume 1. Pages 1743-1750. https://doi.org/10.1039/D3SU00230F

[177] Tan, X., Liu, Y., Zeng, G., Wang, X., Hu, X., Gu, Y., Yang, Z., 2015. Application of biochar for the removal of pollutants from aqueous solutions. Chemosphere. Volume 125. Pages 70-85. https://doi.org/10.1016/j.chemosphere.2014.12.058

[178] Severo, F., Silva, L., Moscoso, J., Sarfaraz, Q., Júnior, L., Lopes, A., Marzari, L., Molin, G., 2020. Chemical and physical characterization of rice husk biochar and ashes and their iron adsorption capacity. Discover Applied Sciences. Volume 2. 1286. https://doi.org/10.1007/s42452-020-3088-2

[179] Silva, G., Pimenta, L., Melo, J., Mendonça, H., Augusti, R., Takahashi, J., 2022. Phytochemicals of Avocado Residues as Potential Acetylcholinesterase Inhibitors, Antioxidants, and Neuroprotective Agents. Molecules. Volume 227. Issue 6. 1892. https://doi.org/10.3390/molecules27061892

[180] Dorhoi, E., Michiu, D., Pop, C., Rotar, A., Tofana, M., Pop, O., Socaci, S., Farcas, A., 2020. Macroalgae—A Sustainable Source of Chemical Compounds with Biological Activities. Nutrients. Volume 12. Issue 10. 3085. https://doi.org/10.3390/nu12103085

[181] Heuzé, V., Thiollet, H., Edouard, N., Bastianelli, D., Lebas, F., 2017. Peanut hulls. Feedipedia, a programme by INRAE, CIRAD, AFZ and FAO. https://feedipedia.org/node/696

[182] Zhao, Z., Zhou, H., Han, X., Han, L., Xu, Z., Wang, P., 2023. Rapid, Highly-Efficient and Selective Removal of Anionic and Cationic Dyes from Wastewater Using Hollow Polyelectrolyte Microcapsules. Molecules. Volume 28. Issue 7. 3010. https://doi.org/10.3390/molecules28073010

7. Appendix

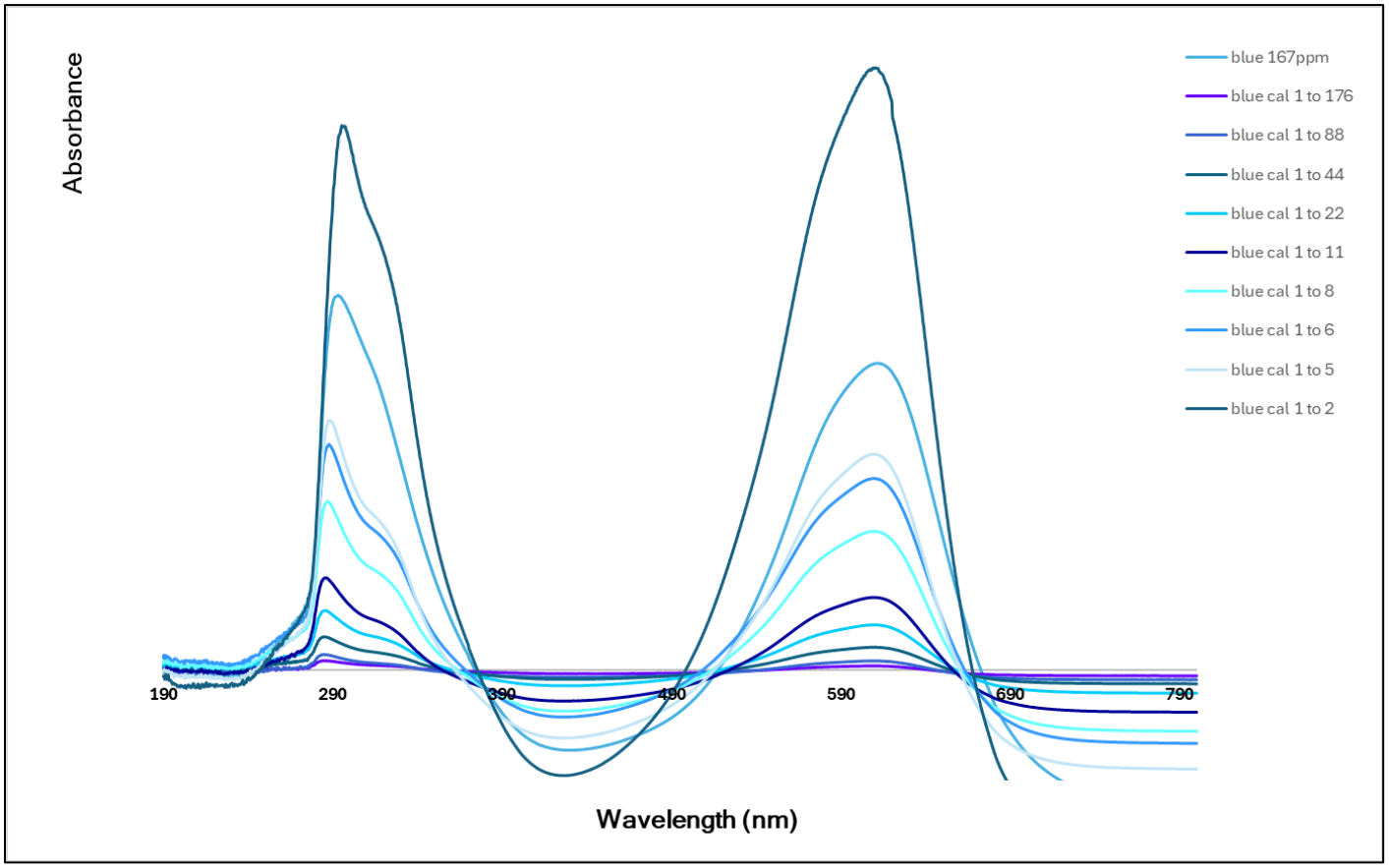

APG 1 - UV-VIS spectra of the Bezaktiv Blue Reactive Dye per different concentration

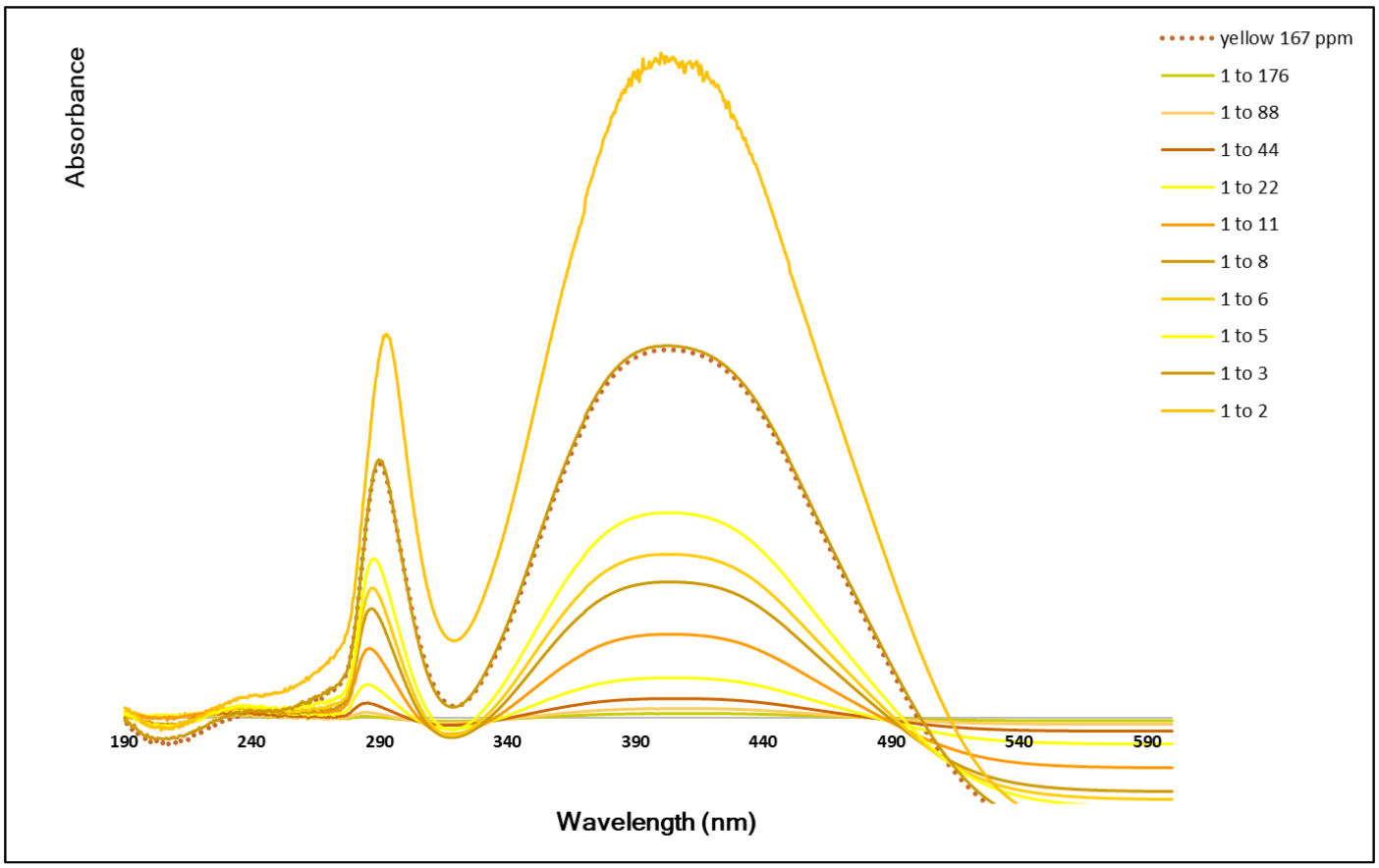

APG 2 - UV-VIS spectra of the Bezaktiv Yellow Reactive Dye per different concentration

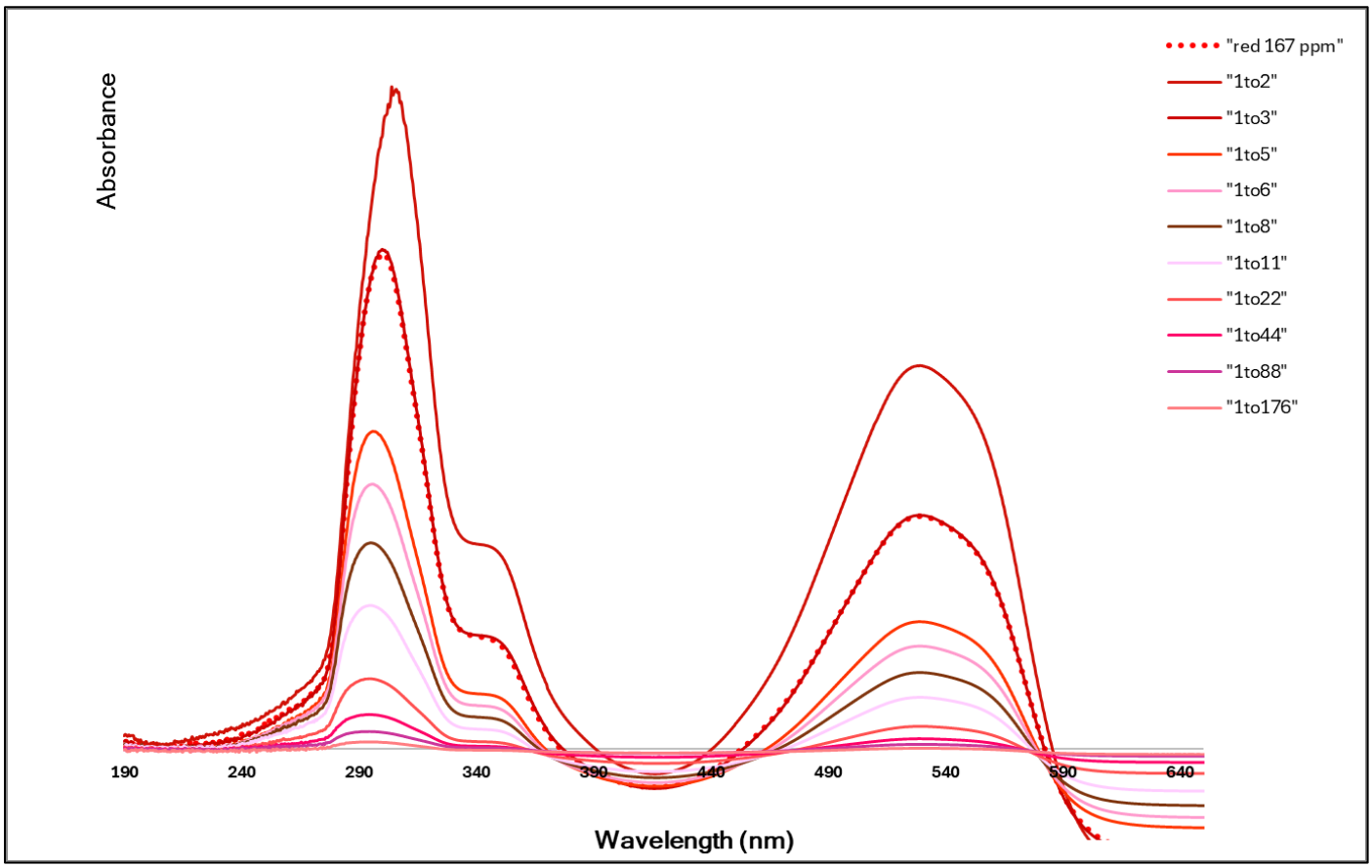

APG 3 - UV-VIS spectra of the Bezaktiv Red Reactive Dye per different concentration

Feedipedia Animal feed resources information system

Home | About Feedipedia | Team | Partners | Sponsoring | Contact us

Search Feedipedia Search

Did you find the information you were looking for? Is it valuable to you? Feedipedia is encountering funding shortage. We need your help to keep providing reference-based feeding recommendations for your animals. Would you consider donating? If yes, please click on the button Donate.
Any amount is the welcome. Even one cent is helpful to us!

Donate

Sponsored by

ADISSEO A Bluestar Company

Automatic translation

Selecionar idioma

Tecnologia do Google Tradutor

Feed categories

All feeds
Forage plants
- Cereal and grass forages
- Legume forages
- Forage trees
- Aquatic plants
- Other forage plants

Plant products/by-products
- Cereal grains and by-products
- Legume seeds and by-products
- Oil plants and by-products
- Fruits and by-products
- Roots, tubers and by-products
- Sugar processing by-products
- Plant oils and fats
- Other plant by-products

Feeds of animal origin
- Animal by-products
- Dairy products/by-products
- Animal fats and oils
- Insects

Other feeds
- Minerals
- Other products

Scientific names

Plant and animal families
Plant and animal species

Tools

FAO Ration Tool for dairy cows
FAO Laboratory Audit Tool

Resources

Broadening horizons
Literature search
Image search
Glossary
External resources
- Literature databases
- Feeds and plants databases
- Organisations & networks
- Books
- Journals

Seaweeds (marine macroalgae)

Description | Nutritional aspects | Nutritional tables | References

Tables of chemical composition and nutritional value

Rockweed (Ascophyllum nodosum), dried · Giant kelp (Macrocystis pyrifera), dried · Dulse (Palmaria palmata), dried · Sea lettuce (Ulva spp.), dried · Maerl (calcified seaweeds) · Laminaria and Saccharina seaweeds · Seaweeds (Sargassum spp.)

Avg: average or predicted value; SD: standard deviation; Min: minimum value; Max: maximum value; Nb: number of values (samples) used

Rockweed (Ascophyllum nodosum), dried

Main analysis	Unit	Avg	SD	Min	Max	Nb
Dry matter	% as fed	88.0	2.7	85.4	91.8	4
Crude protein	% DM	8.0	2.7	5.6	12.1	5
Crude fibre	% DM	5.5		4.1	6.8	2
NDF	% DM	20.9		19.8	22.0	2
ADF	% DM	13.1				1
Lignin	% DM	13.8		6.2	21.4	2
Ether extract	% DM	3.9	1.6	2.9	5.8	3
Ash	% DM	22.5	2.1	18.9	25.0	12
Gross energy	MJ/kg DM	14.7		14.5	14.7	2 *

Minerals	Unit	Avg	SD	Min	Max	Nb
Calcium	g/kg DM	20.0				1
Phosphorus	g/kg DM	1.0				1
Potassium	g/kg DM	24.0				1
Magnesium	g/kg DM	8.0				1
Manganese	mg/kg DM	12	3	7	17	8
Zinc	mg/kg DM	181	114	74	403	8
Copper	mg/kg DM	28	16	8	63	8
Iron	mg/kg DM	134	36	101	198	8

Amino acids	Unit	Avg	SD	Min	Max	Nb
Alanine	% protein	5.4		5.3	5.4	2
Arginine	% protein	6.0		4.0	8.0	2
Aspartic acid	% protein	8.4		6.9	9.8	2
Cystine	% protein	0.9		0.0	1.8	2
Glutamic acid	% protein	11.6		10.0	13.1	2
Glycine	% protein	4.8		4.5	5.0	2
Histidine	% protein	1.4		1.3	1.5	2
Isoleucine	% protein	3.1		2.8	3.4	2
Leucine	% protein	5.3		4.6	6.0	2
Lysine	% protein	4.6		4.3	4.9	2
Methionine	% protein	1.3		0.7	1.9	2
Phenylalanine	% protein	3.2		2.3	4.0	2
Proline	% protein	3.0		2.6	3.4	2
Serine	% protein	3.5		3.0	4.0	2
Threonine	% protein	3.6		2.8	4.3	2
Tyrosine	% protein	0.9				1
Valine	% protein	4.1		3.7	4.4	2

The asterisk * indicates that the average value was obtained by an equation.

References

Anderson et al., 2006; Applegate et al., 1995; Cruz-Suarez et al., 2008; Dierick et al., 2009; Erickson et al., 2012; Lunde, 1970

Last updated on 13/05/2015 17:13:12

Giant kelp (Macrocystis pyrifera), dried

Main analysis	Unit	Avg	SD	Min	Max	Nb

APT 1 - Chemical Composition of macroalgae

Dry matter	% as fed	92.5		92.3	92.6	2
Crude protein	% DM	10.1	2.3	6.6	13.2	7
Crude fibre	% DM	8.0	2.5	4.5	11.3	5
NDF	% DM	19.9				1
ADF	% DM	12.6				1
Lignin	% DM	3.6				1
Ether extract	% DM	0.6	0.2	0.2	0.8	7
Ash	% DM	32.0	9.5	10.8	38.6	7
Gross energy	MJ/kg DM	9.0	0.4	8.5	9.3	5

Minerals	Unit	Avg	SD	Min	Max	Nb
Calcium	g/kg DM	14.1	1.5	12.5	15.4	3
Phosphorus	g/kg DM	2.9		2.6	3.2	2
Potassium	g/kg DM	67.5	22.4	53.6	93.4	3
Sodium	g/kg DM	36.9	9.9	31.1	48.4	3
Magnesium	g/kg DM	39.0	22.8	12.9	55.0	3
Manganese	mg/kg DM	11				1
Zinc	mg/kg DM	12				1
Copper	mg/kg DM	2				1
Iron	mg/kg DM	117				1

Amino acids	Unit	Avg	SD	Min	Max	Nb
Alanine	% protein	10.9	1.8	8.1	13.0	5
Arginine	% protein	3.5	0.7	2.3	3.9	5
Aspartic acid	% protein	9.7	1.1	8.1	10.9	5
Cystine	% protein	2.5	0.8	1.4	3.2	5
Glutamic acid	% protein	14.3	2.4	12.6	18.4	5
Glycine	% protein	4.5	1.0	2.8	5.2	5
Histidine	% protein	1.3	0.3	0.9	1.7	4
Isoleucine	% protein	3.4	0.2	3.2	3.7	5
Leucine	% protein	5.8	0.4	5.3	6.4	5
Lysine	% protein	4.7	0.7	3.6	5.5	5
Methionine	% protein	1.9	0.4	1.5	2.4	5
Phenylalanine	% protein	3.8	0.4	3.3	4.2	5
Proline	% protein	3.6	0.2	3.2	3.8	5
Serine	% protein	4.2	0.6	3.2	4.8	5
Threonine	% protein	4.6	0.6	3.8	5.4	5
Tryptophan	% protein	0.9	0.1	0.9	1.0	4
Tyrosine	% protein	2.6	0.2	2.4	2.8	4
Valine	% protein	5.2	1.7	4.3	8.6	6

Secondary metabolites	Unit	Avg	SD	Min	Max	Nb
Tannins (eq. tannic acid)	g/kg DM	25.0	16.4	0.5	34.2	4

The asterisk * indicates that the average value was obtained by an equation.

References

Castro et al., 1991; Castro-Gonzalez et al., 1994; Cruz-Suarez et al., 2008; Mora-Castro et al., 2009; Ortiz et al., 2009

Last updated on 13/05/2015 17:15:23

Dulse (Palmaria palmata), dried

Main analysis	Unit	Avg	SD	Min	Max	Nb
Crude protein	% DM	19.1	6.1	9.9	26.5	12
Crude fibre	% DM	1.5				1
Ash	% DM	24.5		17.5	31.5	2

Minerals	Unit	Avg	SD	Min	Max	Nb
Manganese	mg/kg DM	11				1
Zinc	mg/kg DM	143				1
Copper	mg/kg DM	24				1
Iron	mg/kg DM	153				1

The asterisk * indicates that the average value was obtained by an equation.

References

Galland-Irmouli et al., 1999; Lunde, 1970; Mišurcová et al., 2010

Last updated on 11/10/2014 00:01:07

Sea lettuce (Ulva spp.), dried

Includes Ulva lactuca and Ulva rigida

Main analysis	Unit	Avg	SD	Min	Max	Nb
Dry matter	% as fed	88.6	3.0	83.6	92.9	8

APT 2 - Chemical Composition of macroalgae (Part 2)

Crude protein	% DM	18.6	7.3	8.0	29.5	14
Crude fibre	% DM	6.9	4.1	2.4	12.3	7
NDF	% DM	26.2	5.4	18.4	33.1	6
ADF	% DM	8.7	6.2	0.7	15.3	4
Lignin	% DM	3.5	2.1	1.9	6.0	3
Ether extract	% DM	1.2	0.8	0.1	2.5	14
Ash	% DM	23.0	7.4	10.1	39.1	13
Gross energy	MJ/kg DM	14.7	2.6	9.4	15.1	4 *

Minerals	Unit	Avg	SD	Min	Max	Nb
Calcium	g/kg DM	29.2	28.9	6.0	61.5	3
Phosphorus	g/kg DM	2.7	2.1	1.0	5.0	3
Potassium	g/kg DM	22.1		15.1	29.0	2
Sodium	g/kg DM	20.2		11.0	29.3	2
Magnesium	g/kg DM	16.7	3.2	13.0	19.0	3
Manganese	mg/kg DM	101				1
Zinc	mg/kg DM	45		28	61	2
Copper	mg/kg DM	12		7	17	2
Iron	mg/kg DM	1246		1052	1440	2

Amino acids	Unit	Avg	SD	Min	Max	Nb
Alanine	% protein	5.9		5.5	6.2	2
Arginine	% protein	4.5		3.2	5.7	2
Aspartic acid	% protein	7.9		7.3	8.4	2
Cystine	% protein	5.9				1
Glutamic acid	% protein	13.3		11.0	15.5	2
Glycine	% protein	5.4		4.9	5.9	2
Histidine	% protein	2.0		1.6	2.3	2
Isoleucine	% protein	2.6		2.2	2.9	2
Leucine	% protein	5.2		5.0	5.3	2
Lysine	% protein	3.8		3.7	3.9	2
Methionine	% protein	1.6		1.3	1.9	2
Phenylalanine	% protein	3.6		3.4	3.8	2
Proline	% protein	2.8				1
Serine	% protein	4.2		3.8	4.6	2
Threonine	% protein	3.8				1
Tyrosine	% protein	1.4				1
Valine	% protein	4.4		4.2	4.5	2

Ruminant nutritive values	Unit	Avg	SD	Min	Max	Nb
Energy digestibility, ruminants	%	60.0				1
DE ruminants	MJ/kg DM	8.8				*
ME ruminants	MJ/kg DM	7.1				*
a (N)	%	23.4		15.1	31.7	2
b (N)	%	31.9		22.0	41.8	2
c (N)	h-1	0.083		0.070	0.096	2
Nitrogen degradability (effective, k=4%)	%	45		45	46	2 *
Nitrogen degradability (effective, k=6%)	%	42		41	44	2 *

The asterisk * indicates that the average value was obtained by an equation.

References

Adubados et al., 2013; Arieli et al., 1993; Bindu et al., 2004; Cruz-Suarez et al., 2008; Diler et al., 2007; Gowda et al., 2004; Kut Guroy et al., 2007; Okab et al., 2013; Rai et al., 2008; Sebahattin et al., 2009; Valente et al., 2006; Ventura et al., 1994; Ventura et al., 1998; Zitouni et al., 2014

Last updated on 10/10/2014 23:49:35

Maerl (calcified seaweeds)

Main analysis	Unit	Avg	SD	Min	Max	Nb
Dry matter	% as fed	99.2	0.3	98.9	99.5	4
Ash	% DM	95.0	0.8	94.1	95.9	5

Minerals	Unit	Avg	SD	Min	Max	Nb
Calcium	g/kg DM	335.9	11.2	293.2	350.8	61
Sodium	g/kg DM	3.3	0.3	2.8	3.9	51
Magnesium	g/kg DM	32.7		32.2	33.2	2

The asterisk * indicates that the average value was obtained by an equation.

References

AFZ, 2011

Last updated on 11/10/2014 18:17:49

Laminaria and Saccharina seaweeds

Includes data for Laminara digitata, Laminaria hyperborea and Saccharina japonica

Main analysis	Unit	Avg	SD	Min	Max	Nb
Dry matter	% as fed	15.4	3.6	9.7	22.5	56
Crude protein	% DM	9.8	2.2	5.7	13.0	50
Crude fibre	% DM	6.6		5.5	7.7	2
NDF	% DM	16.6				1
Ether extract	% DM	0.8		0.5	1.0	2
Ash	% DM	31.5	7.6	19.3	44.0	79
Total sugars	% DM	8.5				1
Gross energy	MJ/kg DM	12.5				*

Minerals	Unit	Avg	SD	Min	Max	Nb
Calcium	g/kg DM	8.8				1
Phosphorus	g/kg DM	3.0				1
Potassium	g/kg DM	59.5				1
Sodium	g/kg DM	25.3				1
Magnesium	g/kg DM	5.5				1
Manganese	mg/kg DM	6	2	3	10	12
Zinc	mg/kg DM	111	70	9	276	12
Copper	mg/kg DM	14	9	2	34	12
Iron	mg/kg DM	196	233	12	865	12

Amino acids	Unit	Avg	SD	Min	Max	Nb
Alanine	% protein	6.5		5.7	7.3	2
Arginine	% protein	4.0		3.3	4.8	2
Aspartic acid	% protein	10.0		7.6	12.5	2
Cystine	% protein	2.2		1.2	3.2	2
Glutamic acid	% protein	15.0		6.2	23.8	2
Glycine	% protein	4.7		4.0	5.3	2
Histidine	% protein	3.0		2.2	3.8	2
Isoleucine	% protein	3.5		2.7	4.2	2
Leucine	% protein	6.0		4.9	7.2	2
Lysine	% protein	5.8		3.9	7.7	2
Methionine	% protein	1.7		0.9	2.4	2
Phenylalanine	% protein	3.9		3.2	4.5	2
Proline	% protein	3.1		3.1	3.1	2
Serine	% protein	3.6		3.3	4.0	2
Threonine	% protein	4.5		3.5	5.5	2
Tryptophan	% protein	0.4		0.3	0.5	2
Tyrosine	% protein	2.3		1.7	2.8	2
Valine	% protein	6.7		3.8	9.7	2

The asterisk * indicates that the average value was obtained by an equation.

References

Black, 1950; Dawczynski et al., 2007; Kolb et al., 2004; Lunde, 1970; Marsham et al., 2007; Mišurcová et al., 2010; Rupérez et al., 2001

Last updated on 20/05/2015 16:57:36

Seaweeds (Sargassum spp.)

Main analysis	Unit	Avg	SD	Min	Max	Nb
Dry matter	% as fed	92.1	2.4	88.8	94.7	7
Crude protein	% DM	8.5	1.8	6.0	11.6	10
Crude fibre	% DM	10.1	2.4	6.4	13.3	9
NDF	% DM	29.5	3.4	23.7	32.0	5
ADF	% DM	21.3	4.4	14.8	24.9	4
Lignin	% DM	4.5		1.0	7.9	2
Ether extract	% DM	1.2	0.9	0.4	2.8	9
Ash	% DM	35.9	12.8	18.4	51.2	9
Starch (polarimetry)	% DM	0.0	0.0	0.0	0.0	3
Total sugars	% DM	1.9	0.1	1.8	2.0	3
Gross energy	MJ/kg DM	9.1		8.9	9.2	2

Minerals	Unit	Avg	SD	Min	Max	Nb
Calcium	g/kg DM	3.8	2.6	1.5	6.4	4
Phosphorus	g/kg DM	2.2	1.0	0.5	2.7	5
Potassium	g/kg DM	46.2		15.9	76.6	2
Sodium	g/kg DM	36.0	9.4	23.3	42.8	5
Magnesium	g/kg DM	7.7		7.5	7.9	2
Manganese	mg/kg DM	214	106	60	286	4
Zinc	mg/kg DM	214	151	11	364	5
Copper	mg/kg DM	7	4	5	14	5
Iron	mg/kg DM	7291	6327	263	12177	5

Amino acids	Unit	Avg	SD	Min	Max	Nb

Alanine	% protein	4.6		4.3	5.0	2
Arginine	% protein	4.9		4.5	5.4	2
Aspartic acid	% protein	7.6		6.1	9.1	2
Cystine	% protein	0.9		0.8	0.9	2
Glutamic acid	% protein	14.5		10.2	18.7	2
Glycine	% protein	4.0		3.3	4.8	2
Histidine	% protein	2.0		1.3	2.6	2
Isoleucine	% protein	3.9		3.7	4.0	2
Leucine	% protein	6.0		5.3	6.7	2
Lysine	% protein	3.5		3.1	3.9	2
Methionine	% protein	1.6		1.5	1.6	2
Phenylalanine	% protein	3.7		2.7	4.6	2
Proline	% protein	3.2		2.6	3.8	2
Serine	% protein	3.3		2.8	3.7	2
Threonine	% protein	3.5		3.0	4.1	2
Tryptophan	% protein	0.4				1
Tyrosine	% protein	2.9		2.8	3.0	2
Valine	% protein	4.6		4.2	4.9	2

Secondary metabolites	Unit	Avg	SD	Min	Max	Nb
Tannins (eq. tannic acid)	g/kg DM	22.0				1

The asterisk * indicates that the average value was obtained by an equation.

References

Bindu et al., 2004; Casas-Valdez et al., 2006; Dawczynski et al., 2007; El-Deek et al., 2009; Gojon-Baez et al., 1998; Marin et al., 2009; Mišurcová et al., 2010; Rai et al., 2008

Last updated on 20/05/2015 17:03:13

Datasheet citation

Heuzé V., Tran G., Giger-Reverdin S., Lessire M., Lebas F., 2017. *Seaweeds (marine macroalgae)*. Feedipedia, a programme by INRAE, CIRAD, AFZ and FAO. https://www.feedipedia.org/node/78 *Last updated on May 29, 2017, 16:46*

English correction by Tim Smith (Animal Science consultant) and Hélène Thiollet (AFZ)

Image credits

Claire Fackler / CINMS, NOAA • Dozens • Eric Moody • Cwmhiraeth • Teun Spaans • Emkaer • Stemonitis • Graça Gaspar

Peanut hulls

Description | Nutritional aspects | Nutritional tables | References

Tables of chemical composition and nutritional value

Peanut hulls

Avg: average or predicted value; SD: standard deviation; Min: minimum value; Max: maximum value; Nb: number of values (samples) used

Peanut hulls

Main analysis	Unit	Avg	SD	Min	Max	Nb
Dry matter	% as fed	91.6	2.6	87.2	96.1	26
Crude protein	% DM	7.0	1.6	4.0	10.5	33
Crude fibre	% DM	65.9	9.6	43.9	80.5	27
NDF	% DM	66.4	17.9	27.6	87.0	13
ADF	% DM	56.4	18.7	13.1	76.2	12
Lignin	% DM	22.4	11.8	5.8	45.2	15
Ether extract	% DM	2.0	1.8	0.2	7.3	15
Ash	% DM	5.2	2.4	2.0	11.6	33
Gross energy	MJ/kg DM	19.8	1.9	17.8	22.0	4 *

Minerals	Unit	Avg	SD	Min	Max	Nb
Calcium	g/kg DM	2.4	1.6	1.3	7.0	19
Phosphorus	g/kg DM	0.7	0.5	0.3	2.2	19
Potassium	g/kg DM	6.9	2.3	1.7	9.1	8
Sodium	g/kg DM	0.1	0.1	0.0	0.2	12
Magnesium	g/kg DM	1.2	0.3	0.9	1.8	9
Manganese	mg/kg DM	38	11	29	50	3
Zinc	mg/kg DM	64	70	23	145	3
Copper	mg/kg DM	15	8	9	27	4
Iron	mg/kg DM	210	92	109	295	4

Amino acids	Unit	Avg	SD	Min	Max	Nb
Alanine	% protein	4.4				1
Arginine	% protein	3.0				1
Aspartic acid	% protein	13.6				1
Glutamic acid	% protein	10.8				1
Glycine	% protein	4.7				1
Histidine	% protein	2.4				1
Isoleucine	% protein	3.7				1
Leucine	% protein	6.3				1
Lysine	% protein	4.6				1
Phenylalanine	% protein	3.9				1
Proline	% protein	8.9				1
Serine	% protein	4.4				1
Threonine	% protein	3.3				1
Tyrosine	% protein	1.3				1
Valine	% protein	4.9				1

Ruminant nutritive values	Unit	Avg	SD	Min	Max	Nb
OM digestibility, ruminants	%	20.1		20.0	20.1	2
OM digestibility, ruminants (gas production)	%	8				1
Energy digestibility, ruminants	%	17.3				*
DE ruminants	MJ/kg DM	3.4				*
ME ruminants	MJ/kg DM	2.7				*
ME ruminants (gas production)	MJ/kg DM	4.5				1
Nitrogen digestibility, ruminants	%	18.7		0.0	37.4	2

Pig nutritive values	Unit	Avg	SD	Min	Max	Nb
Energy digestibility, growing pig	%	32.5				1
DE growing pig	MJ/kg DM	6.4				*
Nitrogen digestibility, growing pig	%	29.6				1

The asterisk * indicates that the average value was obtained by an equation.

References

AFZ, 2011; Alibes et al., 1990; Aregheore, 2001; Blancou et al., 1978; Chumpawadee et al., 2007; CIRAD, 1991; Enueme et al., 1987; Felix et al., 1993; FUSAGx/CRAW, 2009; Gowda et al., 2004; Lindemann et al., 1986; Maglad et al., 1986; Ohlde et al., 1982; Onwuka et al., 1997; Oyenuga, 1968; Parigi-Bini et al., 1991; Richard et al., 1989; Sunvold et al., 1995

Last updated on 02/10/2016 02:11:01

Datasheet citation

Heuzé V., Thiollet H., Tran G., Edouard N., Bastianelli D., Lebas F., 2017. *Peanut hulls*. Feedipedia, a programme by INRAE, CIRAD, AFZ and FAO. https://feedipedia.org/node/696 *Last updated on February 1, 2017, 11:31*

English correction by Tim Smith (Animal Science consultant)

Image credits

- IITA
- Nicole Köhler
- Denis Bastianelli, CIRAD
- Denis Bastianelli, CIRAD

APT 1;2;3;4;5 - Heuzé V., Tran G., Giger-Reverdin S., Lessire M., Lebas F., 2017. *Seaweeds (marine macroalgae)*. Feedipedia, a programme by INRAE, CIRAD, AFZ and FAO. https://www.feedipedia.org/node/78 *Last updated on May 29, 2017, 16:46*

APT 6;7 - Heuzé V., Thiollet H., Tran G., Edouard N., Bastianelli D., Lebas F., 2017. Peanut hulls. Feedipedia, a programme by INRAE, CIRAD, AFZ and FAO. https://feedipedia.org/node/696 Last updated on February 1, 2017, 11:31